AD-A044 235 MCDONNELL DOUGLAS RESEARCH LABS ST LOUIS MO F/G 11/6
INFLUENCE OF RARE-EARTH ADDITIONS ON PROPERTIES OF TITANIUM ALL--ETC(U)
MAY 77 C R WHITSETT, S M SASTRY, J E O'NEAL N00014-76-C-0626
UNCLASSIFIED MDC-Q10627 NL

OF 2
AD
A044235

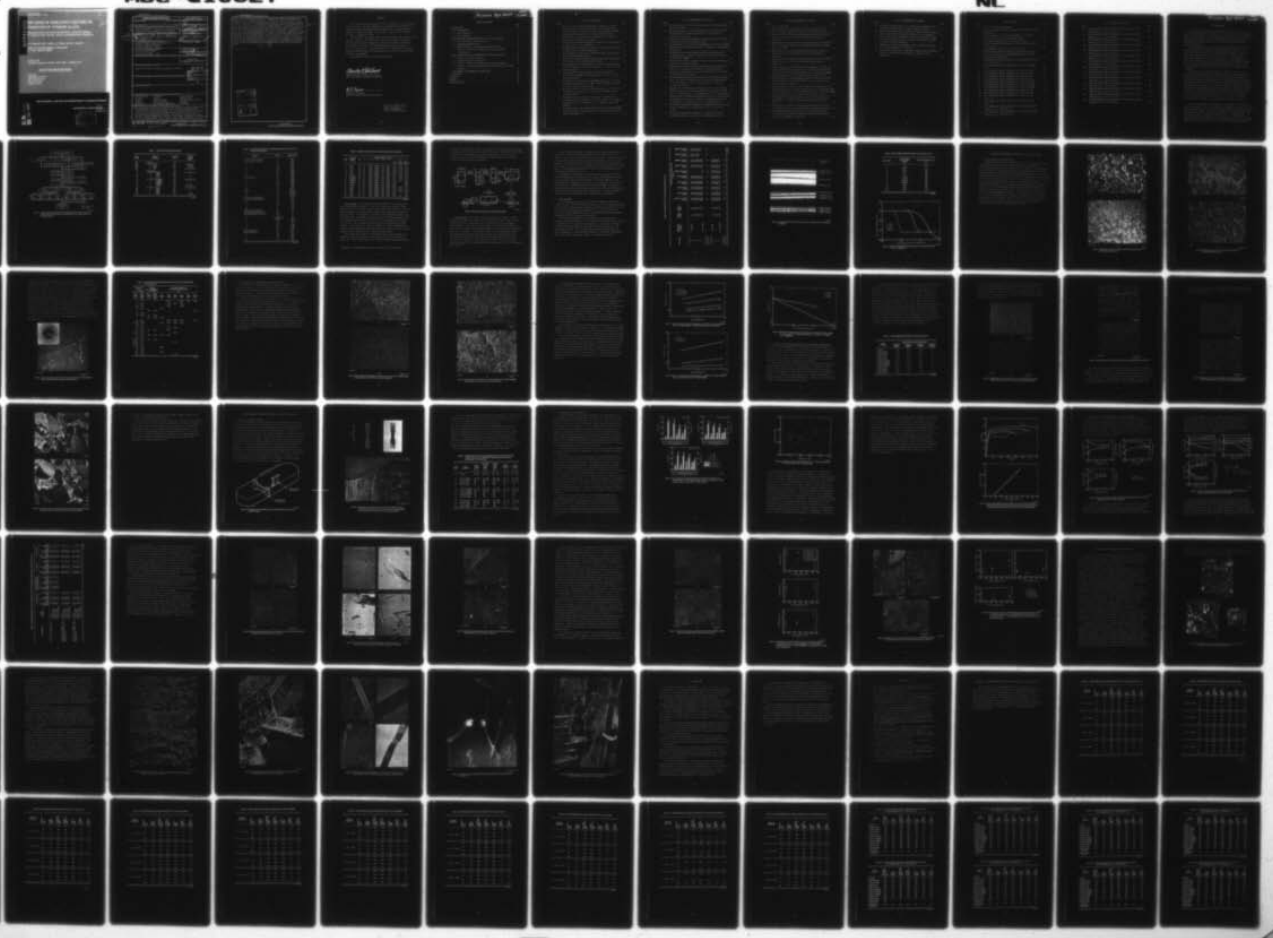

Report MDC Q0627
Contract No. N00014-76-C-0626

(12)

INFLUENCE OF RARE-EARTH ADDITIONS ON PROPERTIES OF TITANIUM ALLOYS

Microstructures and Room-Temperature Tensile Properties of Ti-6Al-4V with Yttrium, Erbium, and Mischmetal Additions

C.R. Whitsett, S.M.L. Sastry, J.E. O'Neal, and R.J. Lederich

McDonnell Douglas Research Laboratories
St. Louis, Missouri 63166

31 May 1977
Technical Report for period 1 April 1976 - 31 March 1977

Prepared for:
DEPARTMENT OF THE NAVY
Office of Naval Research
800 N. Quincy Street
Arlington, VA 22217

MCDONNELL DOUGLAS RESEARCH LABORATORIES

MCDONNELL DOUGLAS CORPORATION

UNCLASSIFIED

SECURITY CLASSIFICATION OF THIS PAGE *(When Data Entered)*

REPORT DOCUMENTATION PAGE

READ INSTRUCTIONS BEFORE COMPLETING FORM

1. REPORT NUMBER
2. GOVT ACCESSION NO. —
3. RECIPIENT'S CATALOG NUMBER (9)

4. TITLE *(and Subtitle)*: INFLUENCE OF RARE-EARTH ADDITIONS ON PROPERTIES OF TITANIUM ALLOYS Microstructures and Room-Temperature Tensile Properties of Ti-6Al-4V with Yttrium, Erbium, and Mischmetal Additions.
5. TYPE OF REPORT & PERIOD COVERED: Technical Report. 1 Apr [illegible]76-31 Mar [illegible]77,
6. PERFORMING ORG. REPORT NUMBER: (14) MDC-Q0627

7. AUTHOR(s): (10) Charles R. Whitsett, Shankar M. L. Sastry, James E. O'Neal, Richard J. Lederich
8. CONTRACT OR GRANT NUMBER(s): N00014-76-C-0626 new (15)

9. PERFORMING ORGANIZATION NAME AND ADDRESS
McDonnell Douglas Research Laboratories
McDonnell Douglas Corporation
St. Louis, Missouri 63166

10. PROGRAM ELEMENT, PROJECT, TASK AREA & WORK UNIT NUMBERS

11. CONTROLLING OFFICE NAME AND ADDRESS
Office of Naval Research
800 N. Quincy Street
Arlington, Virginia 22217

12. REPORT DATE: (11) 31 May [illegible]77
13. NUMBER OF PAGES: ~~103~~ (12) 100p.

14. MONITORING AGENCY NAME & ADDRESS *(if different from Controlling Office)*

15. SECURITY CLASS. *(of this report)*: Unclassified

15a. DECLASSIFICATION/DOWNGRADING SCHEDULE

16. DISTRIBUTION STATEMENT *(of this Report)*

Approved for public release; distribution unlimited.

17. DISTRIBUTION STATEMENT *(of the abstract entered in Block 20, if different from Report)*

18. SUPPLEMENTARY NOTES

19. KEY WORDS *(Continue on reverse side if necessary and identify by block number)*

Titanium alloy	Lanthanum	Elastic modulus
Ti-6Al-4V	Cerium	Yield stress
Yttrium	Microstructure	Ultimate tensile stress
Erbium	Grain refinement	Elongation
Mischmetal	Second-phase dispersion	Ductility

20. ABSTRACT *(Continue on reverse side if necessary and identify by block number)*

The influence of different concentrations of metallic yttrium, erbium, and mischmetal (MM) on the microstructure and room-temperature mechanical properties of Ti-6Al-4V was studied. Alloy ingots containing 0.02-0.3 wt% Y, 0.1-2.0 wt% Er, and 0.01-0.2 wt% MM were cast, forged, hot-rolled, and mill-annealed in the α-β and β fields. The metallic rare-earth additions produce a uniform dispersion of small (< 70 nm diam) second-phase precipitates in the Ti-6Al-4V matrix. Both Y and Er effect grain refinement and microstructural homogeneity and retard grain growth; mischmetal is less effective

DD FORM 1 JAN 73 1473 EDITION OF 1 NOV 65 IS OBSOLETE

alpha-beta 405315

beta UNCLASSIFIED

SECURITY CLASSIFICATION OF THIS PAGE *(When Data Entered)*

than Y or Er. Yttrium and erbium act slightly as β-phase stabilizers and mischmetal is an α-phase stabilizer. The roller pressures required for hot-rolling are less for rare-earth-modified Ti-6Al-4V, and edge-cracking during rolling is reduced for Y concentrations ≤ 0.05 wt% and Er concentrations ≤ 0.1 wt%. The transverse and longitudinal elastic modulus, yield stress, and ultimate tensile stress are not adversely affected by Y and Er concentrations ≤ 0.1 wt%, and the room-temperature ductility is increased. Mischmetal in 0.1-0.2 wt% concentrations degrades the tensile properties. Rare-earth second-phase precipitation-strengthening is a factor in the room-temperature tensile properties for only α-β annealed Ti-6Al-4V in which the volume fraction of equiaxed α is significant. Slight (< 5%) reductions of yield stress observed for Y- and Er-containing Ti-6Al-4V are likely due to scavenging of interstitial oxygen by the rare-earth precipitates. Pronounced improvement of ductility is due to grain refinement and slip homogenization by the rare-earth dispersoids.

PREFACE

This report presents the results of the first phase of an investigation of the effects of rare-earth additives on titanium alloys performed by the McDonnell Douglas Research Laboratories under Office of Naval Research Contract No. N00014-76-C-0626. The scientific officer for the contract is Dr. Bruce A. MacDonald of ONR.

The principal investigator until 31 October 1976 was Dr. Bhakta B. Rath, who was succeeded as principal investigator by Dr. Charles R. Whitsett. Co-investigators are Dr. Shankar M. L. Sastry, Mr. James E. O'Neal and Mr. Richard J. Lederich. The cooperation and attention to detail of Dr. F. H. Froes, Mr. V. C. Peterson, and Mr. C. F. Yolton of the Crucible Materials Research Center in the preparation of alloys for this study are gratefully acknowledged.

This report has been reviewed and is approved.

Charles R. Whitsett
Chief Scientist - Solid State Sciences
McDonnell Douglas Research Laboratories

D. P. Ames
Donald P. Ames
Staff Vice President
McDonnell Douglas Research Laboratories

B. A. MacDonald
Bruce A. MacDonald
Office of Naval Research

TABLE OF CONTENTS

LIST OF ILLUSTRATIONS

LIST OF ILLUSTRATIONS (continued)

LIST OF ILLUSTRATIONS (continued)

LIST OF ILLUSTRATIONS (continued)

LIST OF TABLES

LIST OF TABLES (Continued)

1. INTRODUCTION

A systematic investigation is being conducted of the effects of rare-earth (RE) additions to Ti-6Al-4V. The first phase of this investigation, which is reported here, is the determination of the influence of different concentrations of erbium, yttrium, and mischmetal on the microstructure and room-temperature tensile properties of Ti-6Al-4V subjected to various annealing procedures.

A near-term objective of this research is to demonstrate that metallic rare-earth additives can improve the high-temperature formability, and thus reduce fabrication costs, of Ti-6Al-4V without adversely affecting the strength and toughness of the alloy. Moreover, previous studies of rare-earth additives to α-Ti[1-3] form the basis for expecting that appropriate combinations of rare-earth additives and processing conditions will be effective for improving other characteristics of Ti-6Al-4V, such as high-temperature strength, corrosion resistance, and low-temperature formability.

The mechanical and fracture-mechanics properties, as well as the formability, of most materials are directly related to the size and distribution of grains, cells, and phases in the polycrystalline aggregate. Refining the polycrystalline structure not only improves both the physical and chemical properties but also assures uniformity throughout the structure. Microstructural refinement in Ti alloys is frequently achieved by repeated cold-reduction and annealing, hot rolling at moderate temperatures, thermal cycling at the allotropic temperature, and addition of alloying elements. While most of these processes have been moderately successful they have not been proved to be either cost effective or desirable for welding, stress-corrosion resistance, or prolonged high-temperature exposure.

In this investigation, the approach is to introduce into Ti-6Al-4V a uniform dispersion of fine (<70 nm diam), second-phase, rare-earth particles, which are particularly effective for refining the alloy microstructure and retarding grain growth. Specifically, metallic Er, Y, and mischmetal (MM) were added in small concentrations (0.01-0.2 wt%) to Ti-6Al-4V melts. Mischmetal, which is a mixture of La, Ce, and Nd, was selected as a possibly lower-cost alternative to Y or Er. All of the rare-earth metals used are

miscible in all proportions with Ti in the liquid state.[4] Er has negligible solubility in solid Ti at all temperatures. The maximum solubilities in β-Ti, at 1360-1500°C, of Y, La, and Ce are approximately 3, 4, and 5 wt%, respectively. The maximum solubilities in α-Ti, at about 900°C, of Y, La, and Ce are approximately 0.1, 4, and 4 wt%, respectively. At room temperature, Er and Y have negligible solubility in Ti, but approximately 1 wt% La or Ce is soluble. When added to Ti-alloys in concentrations less than 1 wt%, Er and Y should precipitate as second-phase dispersoids as an alloy is cooled, whereas metallic MM should remain in solution. An important practical consideration is the difficulty of preventing the formation of stable rare-earth oxides in MM before it is dissolved in molten Ti during normal alloy-casting procedures. Thus, of the amount of MM added to an alloy, only a fraction will be dissolved and the remainder will be in the form of oxide-particle inclusions.

A recent study[5] showed that Y_2O_3-additive is a beta-grain refiner in Ti-6Al-4V and, according to one producer, decreases the cost of ingot reduction by at least 6%. However, in contrast to Y and other rare-earth metals, Y_2O_3 is practically insoluble in molten Ti at temperatures usually achieved in alloy production and remains as large (1-10 μm) inclusions. Furthermore, the Y_2O_3 particles tend to agglomerate in Ti-6Al-4V and can degrade the tensile strength and fracture toughness, particularly in the short transverse direction.

The results presented in this report show that metallic rare-earth additives effectively refine the microstructure and increase the ductility of Ti-6Al-4V without significantly affecting the room-temperature mechanical properties. The qualitative improvement in formability observed during the hot rolling of small, 5.4-kg Ti-6Al-4V-RE ingots supports the contention that metallic rare-earth additives can reduce the cost of alloy fabrication.

2. ALLOY PREPARATIONS*

2.1 Ingot Preparation

0.1-kg Button Ingots: For preliminary assessment of the melting characteristics and the microstructural changes effected by the addition of Er, Y, and MM to Ti-6Al-4V, 0.1-kg button ingots of Ti-6Al-4V (reference alloy), Ti-6Al-4V-1.0Er, Ti-6Al-4V-0.48Y, and Ti-6Al-4V-0.10MM were prepared by vacuum-arc-melting the alloys in a water-chilled copper hearth. Each button was prepared from a mixture of Ti-6Al-4V and metallic rare-earth. An additional Ti-6Al-4V-1.0Er alloy was prepared by adding the appropriate quantity of Al-Er master alloy instead of metallic Er. The button ingots confirmed that the rare-earths refine the microstructure of Ti-6Al-4V and proved the feasibility of utilizing a master alloy containing rare-earth metal for the casting of Ti-6Al-4V-RE alloys.

5.4-kg Ingots: Figure 1 is an outline of the alloy preparations and heat-treatments for most of this study. Fifteen 5.4-kg Ti-6Al-4V ingots with various rare-earth additions were prepared to determine the effects of varying the concentrations of Er, Y, and MM. The nominal compositions of the 0.1-kg and 5.4-kg ingots are given in Table 1 together with the form of the rare-earth addition for each ingot. All of the 5.4-kg ingots were prepared with the same lots of Ti sponge and Al-V master alloy. The chemical analyses of the starting materials are given in Table 2, and the chemical analyses of the as-cast ingots are given in Table 3.

Ingot Melting: The ingots were melted in vacuum by the consumable-electrode arc-melting method. Each 5.4-kg charge consisted of five 76-mm diam pressed-briquettes of blended Ti-sponge, Al-V master alloy, and Al-RE master alloy. The briquettes were welded together in tandem to form the consumable electrode, which was melted into a water-cooled, 120-mm diam, copper mold. Each molten ingot was conditioned, inverted, and melted a second time to achieve compositional homogeneity.

*Ingots for this investigation were cast, forged, and rolled by Crucible Materials Research Center, Colt Industries, Inc., Pittsburgh, PA.

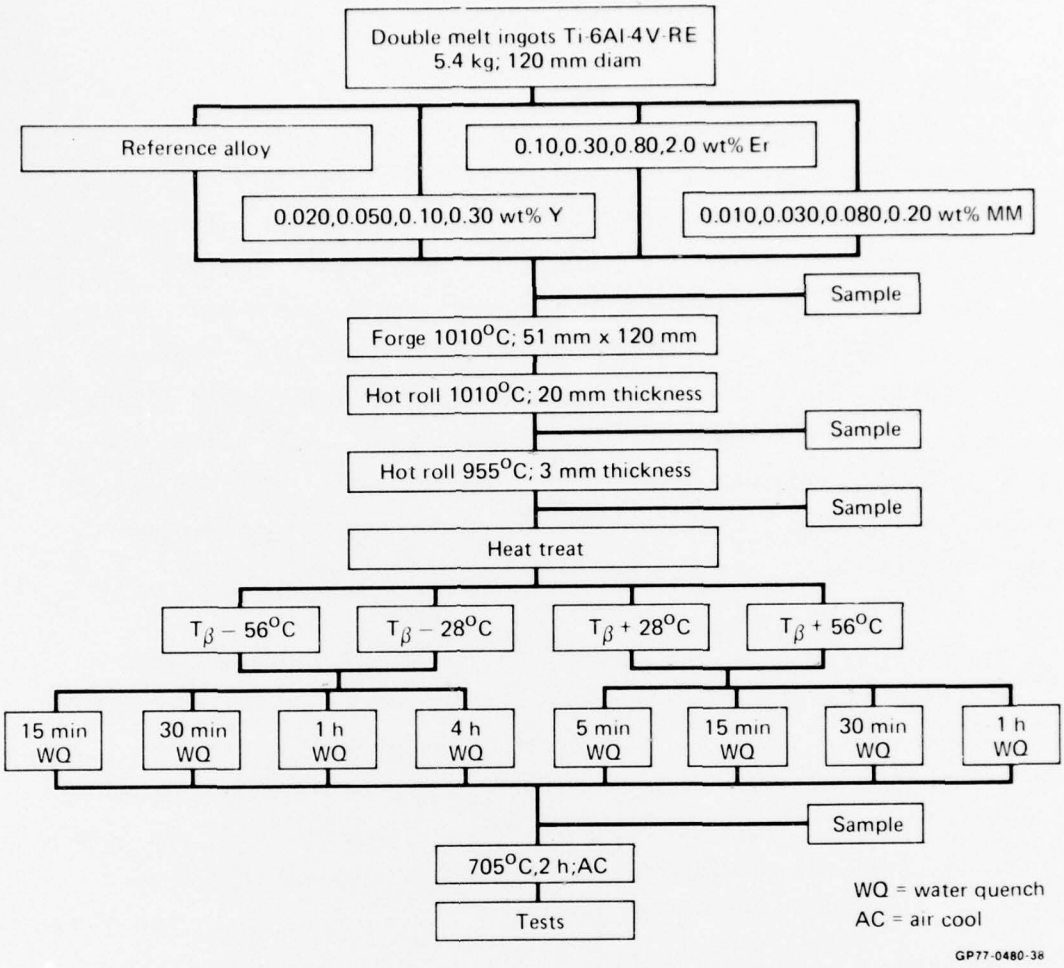

Figure 1. Outline of alloy preparations and heat treatments for study of microstructures and room-temperature tensile properties of Ti-6Al-4V alloys with erbium, yttrium, and mischmetal additions.

TABLE 1. Ti-6Al-4V-RE INGOT PREPARATIONS

Ingot number	Nominal composition	Ingot mass (kg)	Form of rare-earth additive
614	Ti-6Al-4V	0.1	–
615	Ti-6Al-4V-0.10MM	0.1	MM granules
616	-1.0Er	0.1	Er metal
617	-0.48Y	0.1	Y metal
660	-1.0Er	0.1	Al-Er master alloy
14	Ti-6.15Al-4.1V	5.4	–
4	Ti-6.15Al-4.1V-0.020Y	5.4	Al-Y master alloy
5	-0.050Y	5.4	↓
15	-0.10Y	5.4	↓
16	-0.30Y	5.4	↓
8	Ti-6.15Al-4.1V-0.010MM	5.4	Al-MM master alloy
9	-0.030MM	5.4	↓
10	-0.080MM	5.4	↓
11	-0.20MM	5.4	↓
12	-0.20MM	5.4	MM granules
25	Ti-6.15Al-4.1V-0.10Er	5.4	Al-Er master alloy
26	-0.30Er	5.4	↓
27	-0.80Er	5.4	↓
28	-2.0Er	5.4	↓
29	-0.80Er	5.4	Er metal

GP77-0480-1

TABLE 2. CHEMICAL ANALYSIS OF STARTING MATERIALS FOR Ti-6Al-4V-RE INGOT PREPARATIONS

Material	Element	Weight percent
Ti sponge, Mg reduced, Brinell hardness number = 140 (max)	Ti	99.8
	C	0.02
	Cl	0.09
	H	0.002
	Fe	0.02
	Mg	0.04
	Mn	0.001
	N	0.008
	O	0.09
	Si	0.004
Al-V master alloy	Al	45.9
	V	53.8
	B	0.0003
	Fe	0.28
	Mo	0.08
	O	0.03
	Si	0.32
Al shot	Al	99.0 min
	Fe	0.40 max
	O	0.10 max
	S	0.25 max
Al-Y master alloy (supplied by Molycorp, Inc., White Plains, NY)	Al	23.5
	Y	76.5
	C	0.13
	Cu	0.12
	Fe	0.10
	O	1.0
	V	0.05
Mischmetal, 13-mm diam rod (procured as Ceralloy 100X from Ronson Metals Corp., Phoenix, AR)	Ce	53
	Gd	2
	Nd	16
	Pr	5
	La and other RE	24
	total RE	99.9
	Al	0.01
	Ca	0.01
	Fe	0.05
	Mg	0.025
	Si	0.01
Erbium (procured from Research Chemicals)	Er	99.9+
	Ca	0.01
	Fe	0.02
	Mg	0.01
	Si	0.01
	Ta	0.01

GP77-0480-2

TABLE 3. CHEMICAL ANALYSES OF Ti-6Al-4V/RARE-EARTH 5.5 kg INGOTS

Ingot no.	Rare-earth addition (wt %)	Chemical composition (wt %)								
		Al	V	C	H	Fe	N	O		
								Top	Center	Bottom
14	None	6.1	3.8	0.029	0.0056	0.14	0.044	0.173	0.181	0.177
4	0.02Y	5.9	3.7	0.033	0.0050	0.13	0.041	0.160	0.148	0.159
5	0.05Y	5.9	3.8	0.032	0.0054	0.09	0.037	0.160	0.176	0.155
15	0.10Y	6.2	3.8	0.026	0.0050	0.11	0.040	0.165	0.172	0.171
16	0.30Y	6.3	4.0	0.029	0.0058	0.11	0.040	0.172	0.185	0.173
8	0.010MM	6.0	3.7	0.025	0.0051	0.19	0.026	0.137	0.143	0.138
9	0.030MM	6.1	3.7	0.025	0.0046	0.09	0.033	0.191	0.142	0.147
10	0.080MM	6.1	3.8	0.026	0.0071	0.11	0.039	0.171	0.157	0.150
11	0.20MM	6.1	3.8	0.023	0.0068	0.07	0.028	0.155		0.162
12	0.20MM	6.3	3.8	0.028	0.0062	0.07	0.038	0.160		0.157
25	0.10Er	6.1	3.9	0.047	0.0061	0.09	0.034	0.169	0.158	0.151
26	0.30Er	6.2	3.9	0.025	0.0055	0.09	0.029	0.142	0.146	0.140
27	0.80Er	6.4	3.9	0.036	0.0046	0.08	0.029	0.153	0.149	0.151
28	2.0Er	6.4	3.9	0.041	0.0044	0.08	0.033	0.164		0.170
29	0.80Er	6.4	3.9	0.038	0.0056	0.08	0.034	0.158	0.147	0.167

GP77-0480-3

Ingot-Forging: The forging and rolling reductions of the ingots are shown schematically in Figure 2. Before the ingots were forged, a 20-mm thick slice was cut from the bottom of each ingot for studies of the as-cast microstructures. In preparation for forging, the ingots were coated with Metlseel RA-537*. The ingots were heated to 1010°C (1850°F) and drawn into octagonal prisms (approximately 180 mm long and 90 mm between parallel sides) on a 1800-kN (200 ton) press in three steps, with reheating of the ingots at each step. The octagonal prisms were then upset-forged 30% at 1010°C (1850°F). Ti-6Al-4V-2.0Er, Ti-6Al-4V-0.20MM, and Ti-6Al-4V-0.80MM ingots exhibited severe cracking during initial forging at 1010°C and were therefore forged at 1120°C (2050°F) for the remaining forging steps.

After being upset-forged, the ingots were grit-blasted, ground, and pickled to remove all cracks from the original sides. The ends were not ground, but severe end-cracking of the Ti-6Al-4V-0.20MM ingots necessitated

*Tradename of Glidden-Durkee Division of SCM Corp., Cleveland, OH.

cropping the ends of these ingots. The ingots were conditioned, coated again with Metlseel RA-537, heated to 1010°C (1120°C in the case of Ti-6Al-4V-0.20MM), and drawn into approximately 51 x 100 x 120 mm plates. During this last forging step, the Ti-6Al-4V-0.20MM ingots again developed severe surface cracks, which were removed by grinding.

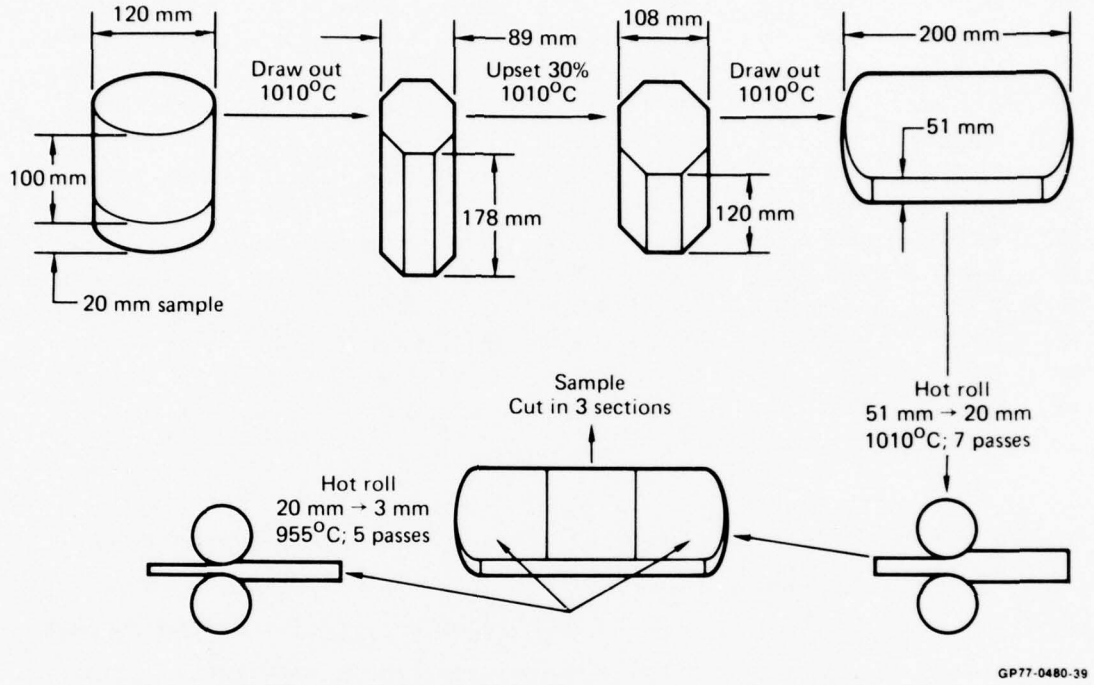

Figure 2. Forging and rolling steps for 5.4-kg Ti-6Al-4V-RE ingots.

Ingot Rolling: The forged, 51-mm thick plates were heated to 1010°C (1850°F) and rolled in seven passes to a thickness of 20 mm. This rolling required 24-50 s for each plate, and the sheets cooled to approximately 800°C (1400°F) by the time of the final pass. The Ti-6Al-4V-0.20MM ingots developed gross surface tears during rolling, but the other alloy compositions were free of cracking. A 100-mm long section for short-transverse tensile test specimens was cut from the center region of each rolled plate, and the remaining two pieces of each plate were heated to 955°C (1750°F) and rolled in five passes to a final thickness of 3 mm. This final rolling procedure required 17-35 s during which time the sheets cooled to approximately 700°C (1300°F).

For the Ti-6Al-4V reference, Ti-6Al-4V-Y, and Ti-6Al-4V-MM ingots, the rolling force for each pass was measured, and the results are given in Table 4. Because the roller-forces for the small plates could not be measured accurately and, further, because the temperatures during rolling were not measured, the rolling-force data in Table 4 only qualitatively measure the hot-formability of the alloys. Nevertheless, the trend towards lower rolling forces as the temperature decreases is clear for the RE-containing alloys compared with the reference alloy.

Photographs of the edges of 3-mm rolled plates are shown in Figure 3; these photographs show qualitatively the relative cracking during rolling for the various types and concentrations of rare-earth additives. The edge-cracking is comparable in the cases of the Ti-6Al-4V reference alloy, Ti-6Al-4V-0.10Y, Ti-6Al-4V-0.30Er, and Ti-6Al-4V-0.030MM. For smaller rare-earth concentrations, the edge cracking of the alloys with RE additives is less than that of the Ti-6Al-4V reference alloy. The edge-cracking in Ti-6Al-4V-0.02Y and Ti-6Al-4V-0.10Er, in particular, was negligible.

2.2 Heat Treatment

The rolled sheets were each cut into 60-mm lengths for anneals at T_β-56°C, T_β-28°C, T_β+28°C, and T_β+56°C, where T_β is the β-transus temperature for each alloy. Specimens were annealed at T_β-56°C and T_β-28°C for 15, 30, 60, and 240 min and at T_β+28°C and T_β+56°C for 5, 15, 30, and 60 min. Following the high-temperature anneals, the specimens were water-quenched, annealed at 705°C for 120 min, and air-cooled.

The β-transus temperature of each alloy was determined prior to annealing by heating samples in 14°C increments (6°C in some cases), holding at temperature for 15 min, and water-quenching. The samples were then polished and metallographically examined for relative amounts of α and transformed-β phases. The β-transus temperature was designated as the lowest temperature at which the microstructure is completely transformed-β phase. The results are listed in Table 5 and plotted in Figure 4.

TABLE 4. ROLLING DATA FOR Ti-6Al-4V/RARE-EARTH ALLOYS

Pass number	Roller entry temperature °C (°F)	Initial thickness (mm)	Final thickness (mm)	Roller force per unit width of plate ($N \cdot m^{-1}$)									
				Ingot 14 Ti-6Al-4V (reference)	Ingot 4 Ti-6Al-4V-0.02Y	Ingot 5 Ti-6Al-4V-0.05Y	Ingot 15 Ti-6Al-4V-0.10Y	Ingot 16 Ti-6Al-4V-0.30Y	Ingot 8 Ti-6Al-4V-0.01MM	Ingot 9 Ti-6Al-4V-0.03MM	Ingot 10 Ti-6Al-4V-0.08MM	Ingot 11 Ti-6Al-4V-0.20MM	Ingot 12 Ti-6Al-4V-0.20MM
First cycle													
1	1010 (1850)	51	43	790	790	670	820	760	–	720	690	280	620
2		43	36	970	980	790	970	880	–	800	820	850	850
3		36	30	1050	610	850	930	950	–	800	820	810	930
4		30	28	1180	1200	820	880	1010	–	720	820	680	790
5		28	25	1470	1590	1490	1360	1250	–	1140	980	1020	1300
6		25	20	2490	1940	1990	1890	2010	–	1970	1590	–	1700
7	≈ 760 (≈1400)	20	19	2360	2420	1700	1750	1910	1910	1860	1590	–	–
Total time for first cycle (s)				45	45	45	45	45	45	50	50	30	30
Second cycle													
1	955 (1750)	19	13	2090	1980	1890	1940	1930	2010	2180	2350	–	–
2		13	9.4	1920	1970	1710	1950	1910	1900	2120	2200	–	–
3		9.4	6.4	2780	2800	2600	2790	2680	2710	2920	2940	–	–
4		6.4	3.8	4940	4380	4110	4380	4200	4270	4370	4580	–	–
5	≈ 705 (≈1300)	3.8	3.3	5030	4680	4450	4730	4620	4550	4680	4700	–	–
Total time for second cycle (s)				35	30	25	25	25	25	25	25	–	–

GP77-0480-4

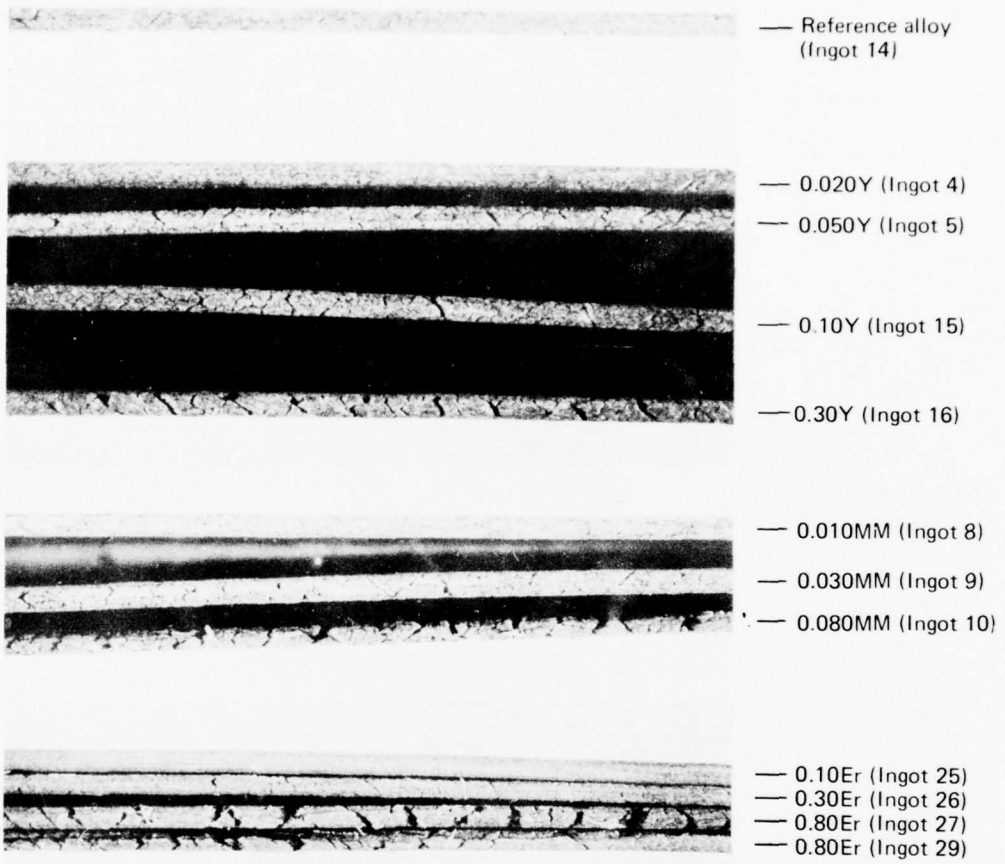

GP77-0480-41

Figure 3. Photographs of 3.2-mm thick, hot-rolled sheets of Ti-6Al-4V with rare-earth additives as indicated.

TABLE 5. BETA TRANSUS TEMPERATURES OF Ti-6Al-4V-RE ALLOYS

Ingot number	Rare earth added to Ti-6Al-4V (wt %)	Beta transus temperature, T_β (^oC)
14	none	1010
4	0.020Y	1010
5	0.050Y	988
15	0.10Y	988
16	0.30Y	988
8	0.010MM	988
9	0.030MM	988
10	0.080MM	988
25	0.10Er	1004
26	0.30Er	988
27,29	0.80Er	982

GP77-0480-5

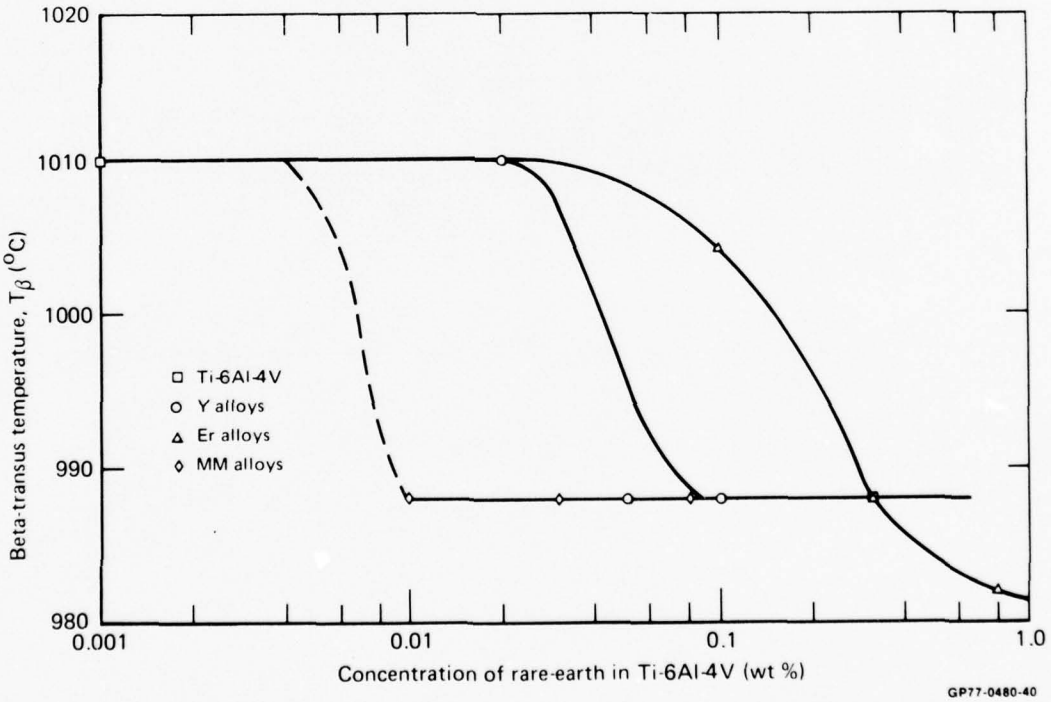

Figure 4. Ti-6Al-4V beta-transus temperature as function of concentrations of added Y (○), Er (△), and MM (◇).

3. MICROSTRUCTURAL CHARACTERIZATIONS OF Ti-6Al-4V-RE ALLOYS

3.1 Microstructures of As-Cast Alloys

A 20-mm thick slice was cut from the bottom of each 5.4-kg alloy ingot for characterization of the as-cast microstructures. Specimens for metallographic examination were prepared from the centers of the 20-mm thick slices. Figures 5 and 6 show the typical microstructures observed in the Ti-6Al-4V reference alloy and the rare-earth containing alloys. The as-cast microstructure of the reference alloy consists of large grains with extensive coarse-α formed during cooling at the prior-β grain boundaries. In contrast, the Y- and Er-containing alloys exhibit a more homogeneous structure. The mischmetal-containing alloys do not show any pronounced grain refinement (Figure 6b), and the transformed microstructures in Ti-6Al-4V-MM alloys are similar to that in the reference alloy. The preferential α-nucleation at the prior-β grain boundaries observed in the reference alloy is absent in the Y- and Er-containing alloys, in which the α-phase nucleates uniformly. The grain size is considerably smaller in the Y- and Er-containing alloys than in the reference alloy, and the prior-β grain size significantly decreases with increasing concentrations of Y and Er.

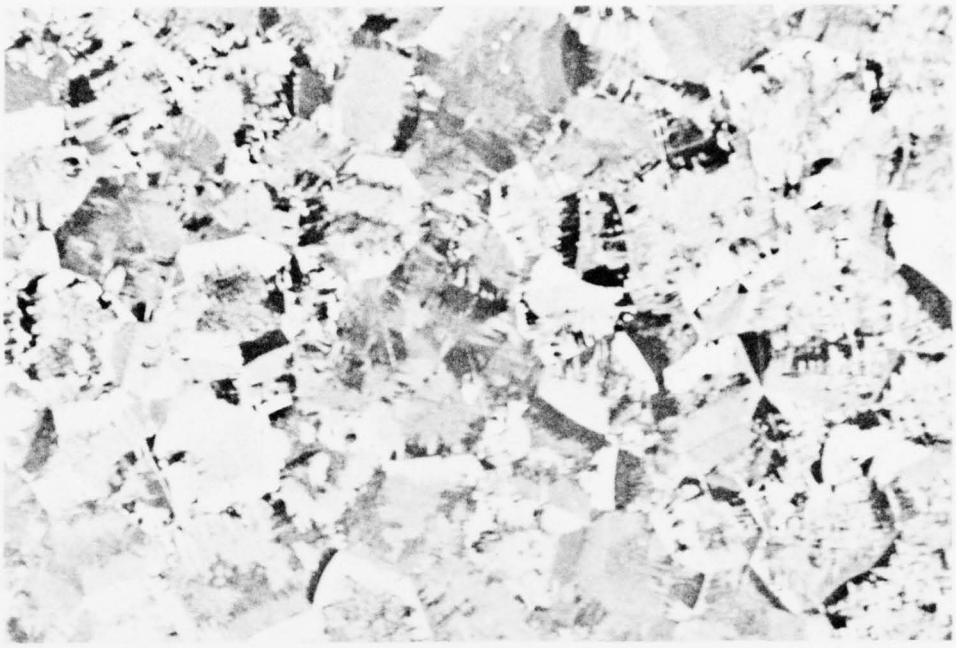

(a)

0.5 cm

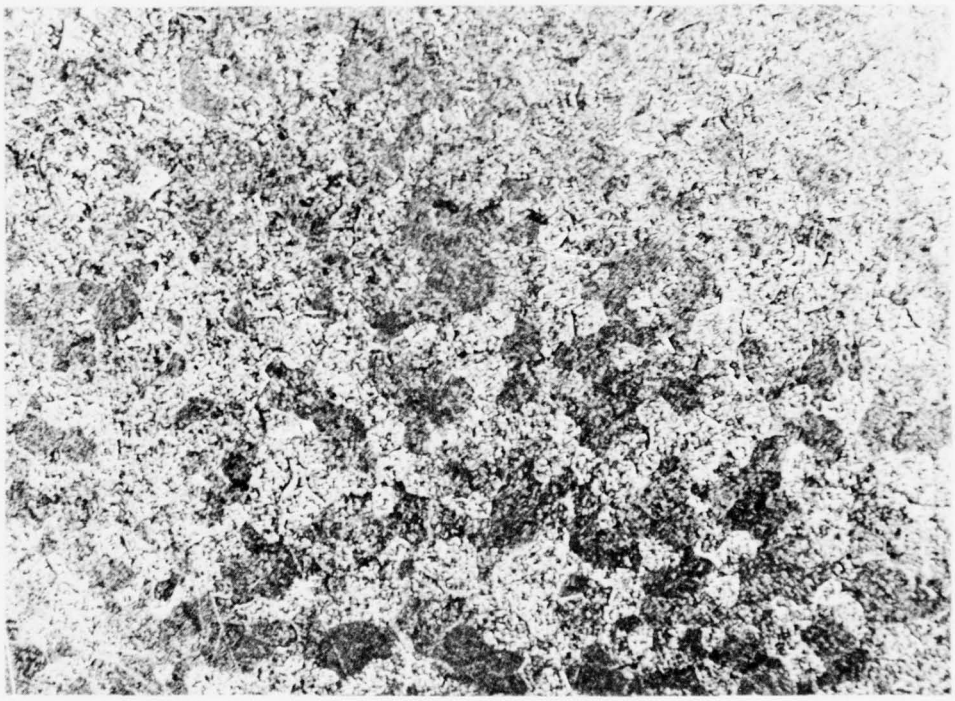

GP77-0480-42

(b)

0.5 cm

Figure 5. Microstructures of as-cast (a) Ti-6Al-4V reference alloy (Ingot 14) and (b) Ti-6Al-4V-0.30Y (Ingot 16).

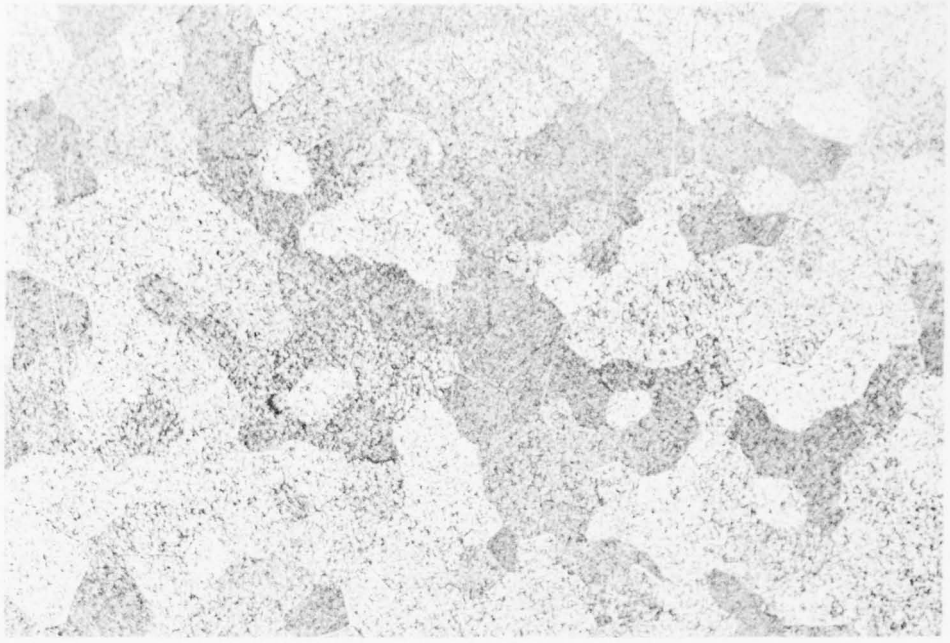

(a)

0.5 cm

GP77-0480-43

(b)

0.5 cm

Figure 6. Microstructures of as-cast (a) Ti-6Al-4V-0.30Er (Ingot 26) and (b) Ti-6Al-4V-0.010MM (Ingot 8).

3.2 Dispersoid Characteristics

The nature of the dispersoids in selected rare-earth-containing alloys was studied by electron microscopy of thin foils and extraction replicas.

Figures 7a and 7b are thin-foil electron micrographs showing dispersoids in Ti-6Al-4V-0.16Y and Ti-6Al-4V-1.0Er alloys. The dispersoids are spherical, 20-70 nm in diam, and incoherent with the matrix. Examination of foils prepared from several alloys revealed that the density of dispersoids varied considerably for the same alloy composition, and in some foils very few dispersoids could be seen. This could be due to leaching of the dispersoids during electrolytic thinning of the foils as well as inhomogeneous mixing of the rare-earth additives during melting.

The small size and uniform distribution of the Er and Y dispersoids observed in Ti-6Al-4V implies that they precipitated during cooling of the alloy. Both Er and Y are soluble in all proportions in molten Ti, and the initial-reaction step in the preparation of the ingots for this study was the dissolution of the metallic rare-earths in the alloy melts. Because the negative free-energies of formation of Er_2O_3 and Y_2O_3 are higher than those of TiO_2 and Al_2O_3[6], the dissolved rare-earths will scavenge oxygen in the melt and to a lesser extent scavenge interstitial oxygen during high-temperature processing of the solid alloy. Rare-earth oxides formed in the melt will form fine, stable particles before the alloy is solidified, and it is quite probable that many of the observed dispersoids are oxide precipitates. The compositions of the dispersoids is not a factor in their direct influence on the alloy behavior; the important factors are the small size of the dispersoid particles that are formed from the metallic rare-earths dissolved in the Ti-alloy melt and their stability at the temperatures for which the dispersoid influence is sought for modifying the alloy behavior.

The dispersoid phase was also studied by transmission electron microscopic examination of carbon extraction replicas prepared from the alloys. Specimens were first polished and etched in Kroll's etchant*. A carbon film was evaporated onto the surface of a specimen and then floated off by dipping the specimen in dilute Kroll's reagent. The replicas were collected on copper grids and examined in the transmission electron microscope.

*Kroll's etchant contains 1-3 ml HF and 2-6 HNO_3 in 1000 ml water.

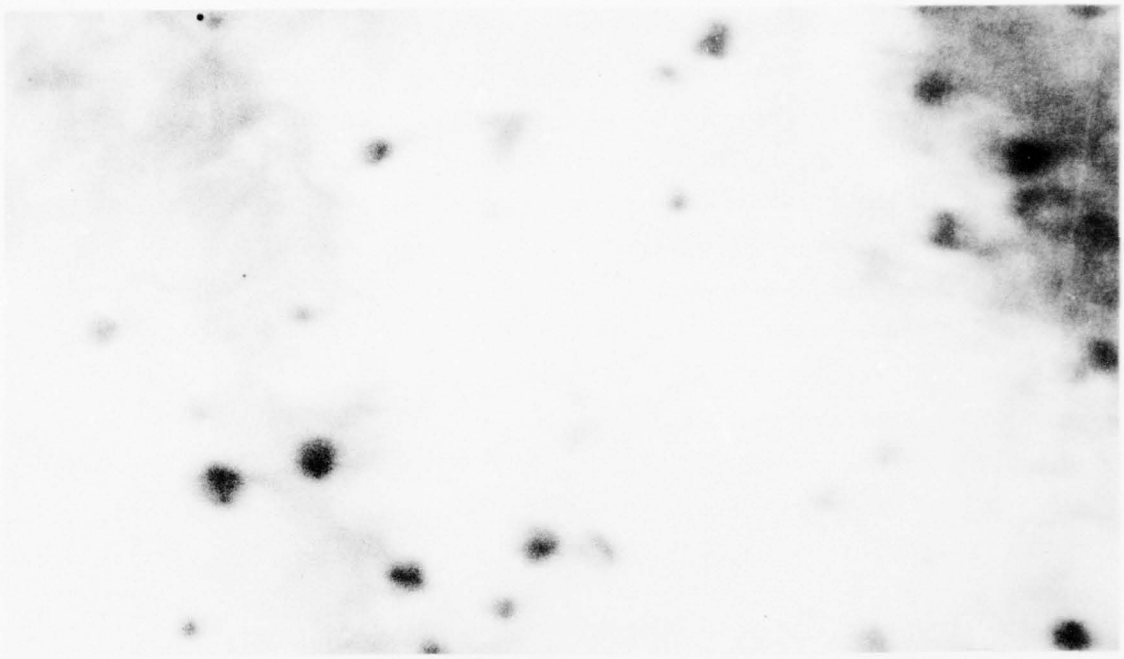

(a)

250 nm

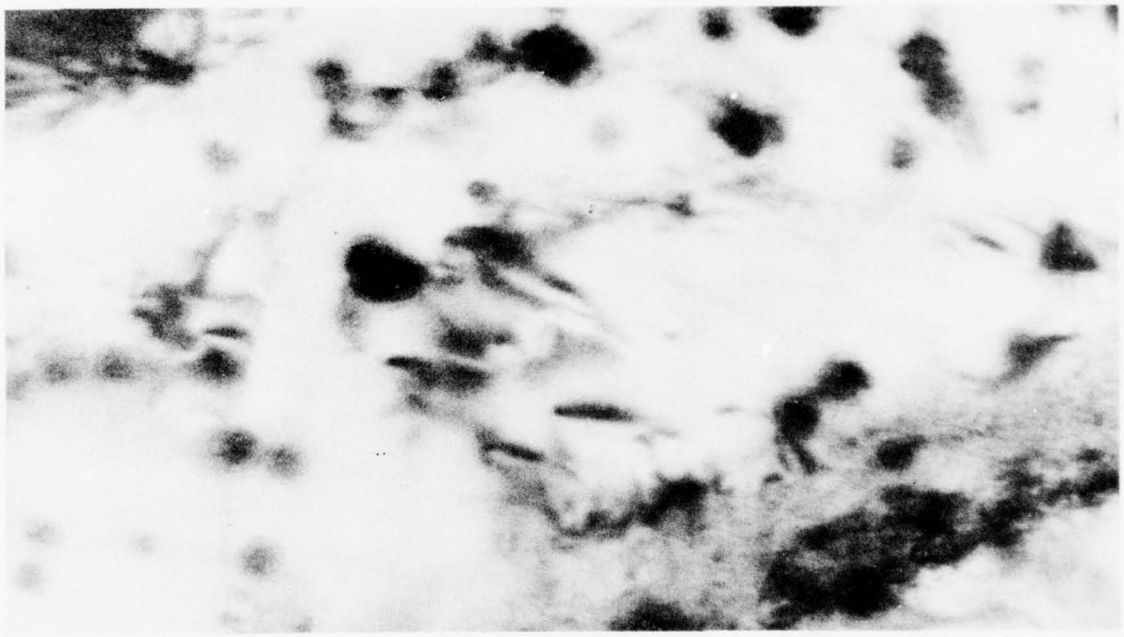

GP77-0480-44

(b)

250 nm

Figure 7. Thin-foil electron micrographs showing rare-earth dispersoids in (a) Ti-6Al-4V-0.16Y and (b) Ti-6Al-4V-1.0Er.

Figure 8 is an electron micrograph of a replica showing the dispersoids in a Ti-6Al-4V-0.30Y alloy. Selected-area diffraction (SAD) patterns were obtained from different regions of the replicas. The most commonly observed patterns were either incomplete ring patterns, characteristic of polycrystalline particles with preferred orientations, or single-crystal spot patterns; the inset in Figure 8 shows a typical pattern. Interplanar spacings were computed from several SAD patterns, and these are listed in Table 6 together with the interplanar spacings of Y and Y_2O_3. Although no unambiguous inferences can be made, the observed interplanar spacings possibly are those of Y_2O_3 particles. However, the SAD patterns do not exclude the possibility that the dispersoids are neither Y_2O_3 nor Y, and they may be intermetallic compounds of Al and Y. Even if the particles in the replica are Y_2O_3, no conclusion can be made as to whether the particles were present in the alloy matrix as Y_2O_3 or as Y that oxidized during the replica forming and stripping.

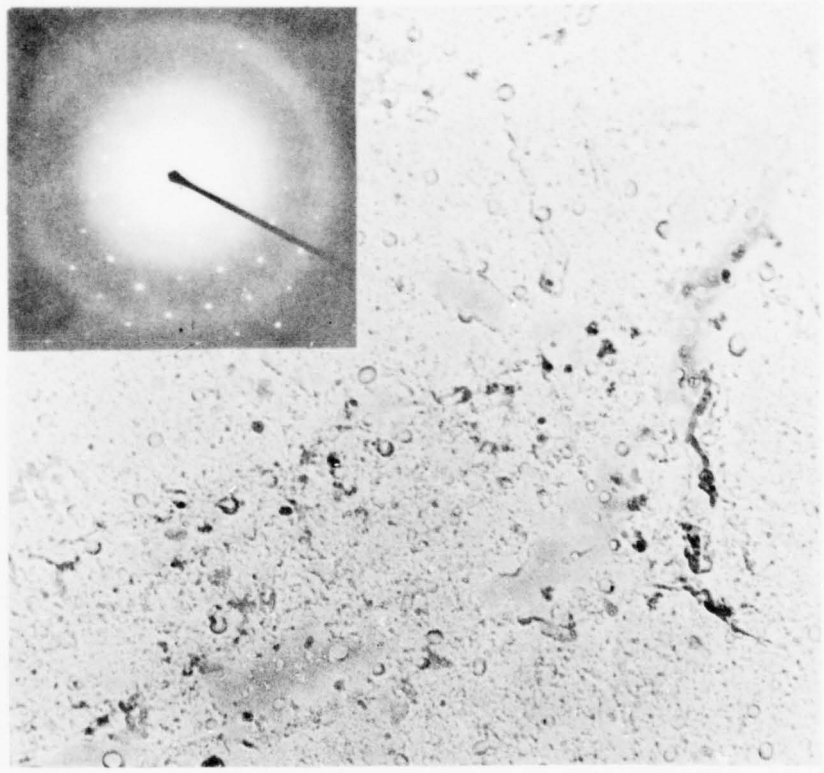

Figure 8. Electron micrograph of carbon-extraction replica of dispersoids in Ti-6Al-4V-0.30Y; inset shows electron diffraction pattern of single dispersoid.

TABLE 6. ELECTRON-DIFFRACTION INTERPLANAR SPACINGS FOR DISPERSOIDS IN Ti-6Al-4V-0.30Y

Yttrium oxide, Y_2O_3 b.c.c., a_o=1.0604 nm		Yttrium, Y hex., a=0.36474 nm, c=0.57306 nm		Interplanar spacings of dispersoids in Ti-6Al-4V-0.30Y (nm)					
Miller indices h,k,ℓ	Interplanar distance, d (nm)	Miller indices h,k,ℓ	Interplanar distance, d (nm)	Plate 4001	Plate 4024	Plate 4033	Plate 4025	Plate 4027	Plate 4026
					0.451		0.455	0.451	0.456
211	0.434				0.430	0.427	0.429		
220	0.375				0.358		0.356		
310	0.335			0.323					
		100	0.315						0.314
222	0.306								
321	0.283	002	0.286						
		101	0.275	0.270					
400	0.265				0.261	0.266	0.258		0.261
411,330	0.250			0.251	0.250	0.243	0.247		
420	0.237								
332	0.226				0.227	0.220			
422	0.217	102	0.212		0.215				
510,431	0.208					0.203			
521	0.194	003	0.191	0.194	0.193				
440	0.187								
530,433	0.182	110	0.182						
600,442	0.177					0.175			
611,532	0.172								
620	0.168			0.166					
541	0.164								
622	0.160			0.159					
631	0.156					0.155			

GP77-0480-6

3.3 Microstructures of Hot-Worked and Annealed Alloys

The influence of β-annealing and α-β annealing treatments on the microstructural changes of alloys hot-rolled under mill conditions was studied. The alloys were hot-worked and heat-treated according to the schedule outlined in Figure 1. Following the high-temperature heat treatments, the alloy sheets were annealed at 705°C for 2 h and air cooled.

Figures 9 and 10 show the microstructures of alloys annealed in the β-field, water quenched, and then annealed for 2 h at 705°C. Water quenching from the β field results in the needle-like martensitic α' structure, a nonequilibrium, supersaturated, α structure produced by diffusionless transformation of the β phase. Upon annealing the martensitic structure at 705°C, the α' transforms to equilibrium α+β. Thus, the microstructures shown in Figures 9 and 10 are the transformed-β structures consisting of α and β plates. Grain boundaries outlining the prior-β grains can be seen. Under identical β-annealing conditions, Y- and Er-containing alloys exhibit a smaller prior-β grain size than the reference alloy and mischmetal-containing alloys, and this is true for all β-annealing times of the schedule shown in Figure 1.

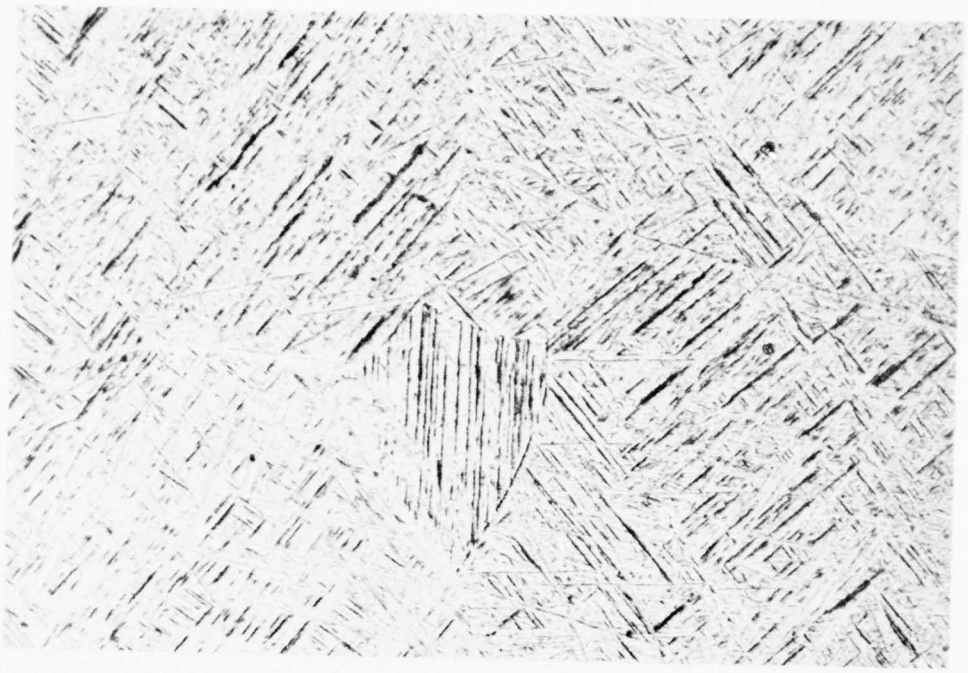

(a)

100 μm

GP77-0480-46

(b)

100 μm

Figure 9. *Microstructures of beta-annealed (a) Ti-6Al-4V reference alloy and (b) Ti-6Al-4V-0.30Y; alloys annealed at $T_\beta + 56^oC$ for 5 min and water-quenched.*

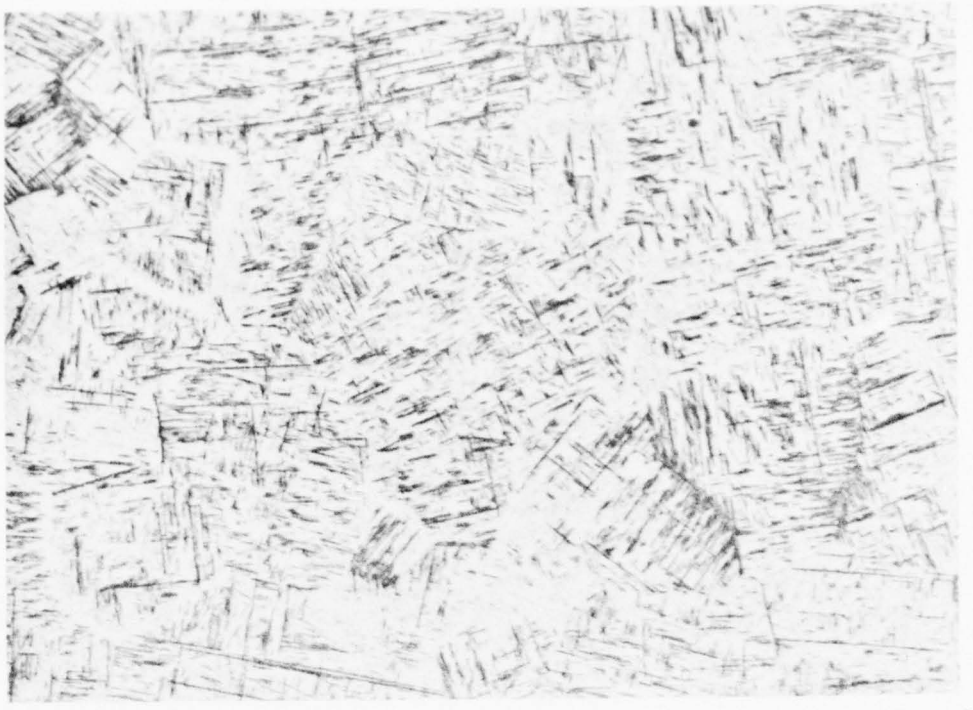

(a)

100 μm

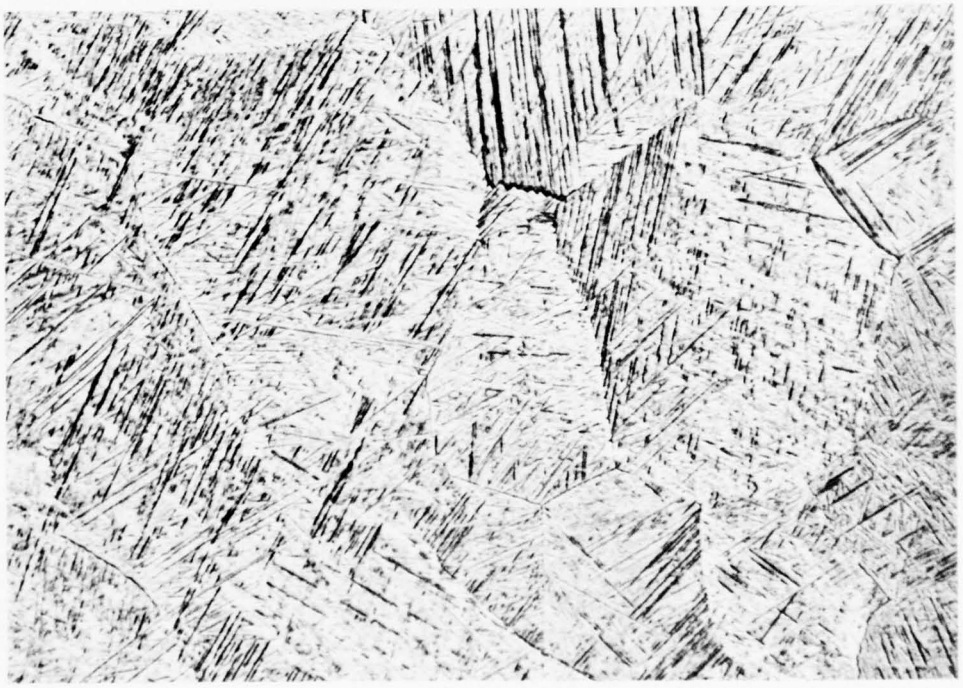

GP77-0480-47

(b)

100 μm

Figure 10. Microstructures of beta-annealed (a) Ti-6Al-4V-0.80Er and (b) Ti-6Al-4V-0.080MM; alloys annealed at T_β + 56°C for 5 min and water-quenched.

The time-dependent β-grain growth was studied at two temperatures, T_β+56°C and T_β+28°C. The average grain-size of each annealed alloy was computed from a statistical analysis of at least 300 grain-size measurements. Grain size was measured by the standard linear-intercept method. Figures 11 and 12 show the β-grain size as a function of annealing time at T_β+56°C for Ti-6Al-4V-Y and Ti-6Al-4V-Er alloys; similar results were obtained for alloys annealed at T_β+28°C. The grain growth follows a relationship of the form $D = kt^n$, where D is the average grain size, t is the isothermal annealing time, and k and n are time invariants which depend on temperature and material parameters. Increasing amounts of Y and Er result in a significant decrease of the grain-growth exponent, n. A grain refinement of nearly an order of magnitude is observed in alloys containing the highest concentrations of Er and Y. The results clearly establish that Y and Er not only effectively refine β grains but also retard grain growth at elevated temperatures.

The influence of rare-earth concentration on the β-grain size of alloys annealed at T_β+56°C for 1 h is shown in Figure 13. Of the three rare-earth additives, Y and Er are more effective grain refiners than mischmetal, with as little as 0.05 wt% Y or 0.1 wt% Er effecting significant grain refinement.

The net grain-refinement observed in Ti-6Al-4V-Er and Ti-6Al-4V-Y alloys is a consequence of the influence of Er and Y dispersoids on both recrystallization and grain growth. The influence of second-phase particles on the formation of recrystallization nuclei depends on the size of the particles. Fine particles inhibit grain nucleation by the Zener drag[7] they exert on the deformed substructure, but coarse particles stimulate nucleation by acting as nucleation sites. Recrystallization is retarded by fine second-phase particles because of the drag they exert on freshly-formed grain boundaries.

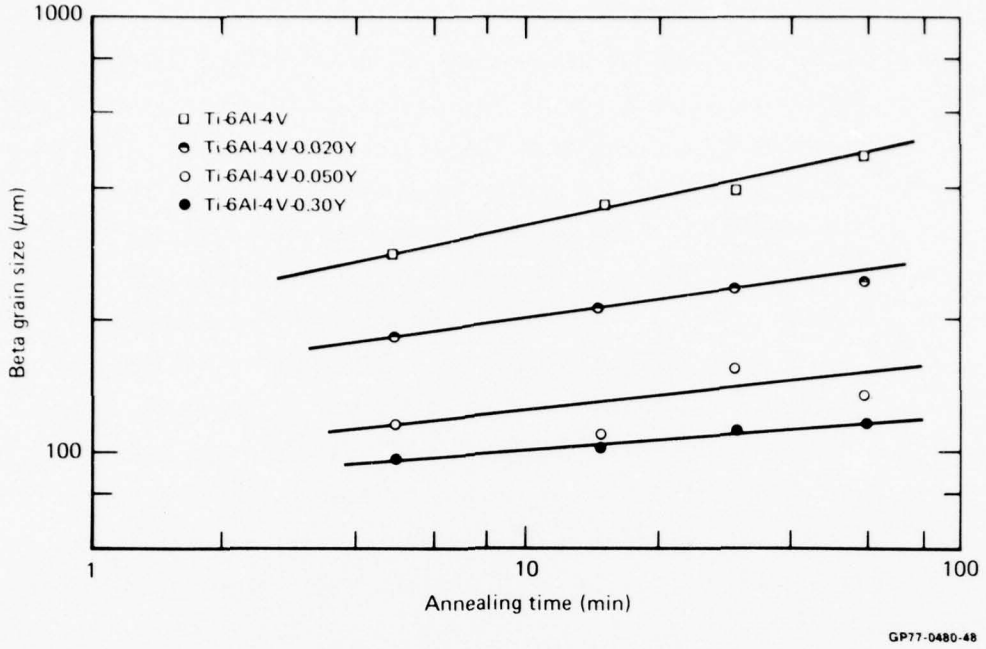

Figure 11. Beta grain size as function of annealing time at T_β + 56°C for (□) Ti-6Al-4V reference alloy, (⊖) Ti-6Al-4V-0.020Y, (○) Ti-6Al-4V-0.05Y, and (●) Ti-6Al-4V-0.30Y.

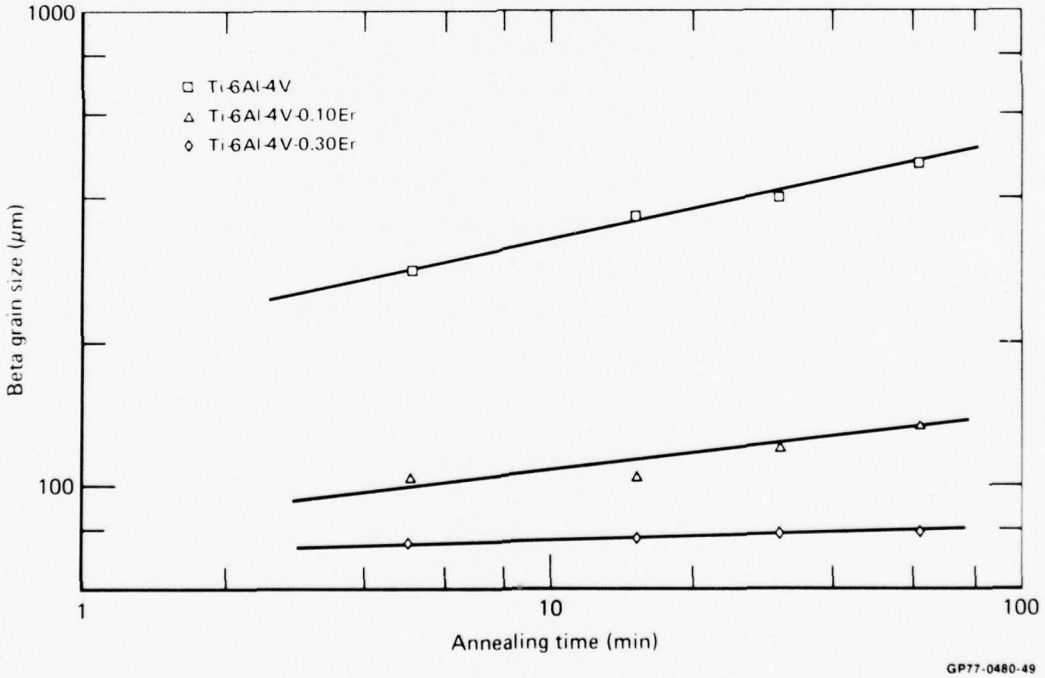

Figure 12. Beta grain size as function of annealing time at T_β + 56°C for (□) Ti-6Al-4V reference alloy, (△) Ti-6Al-4V-0.10Er, and (◇) Ti-6Al-4V-0.30Er.

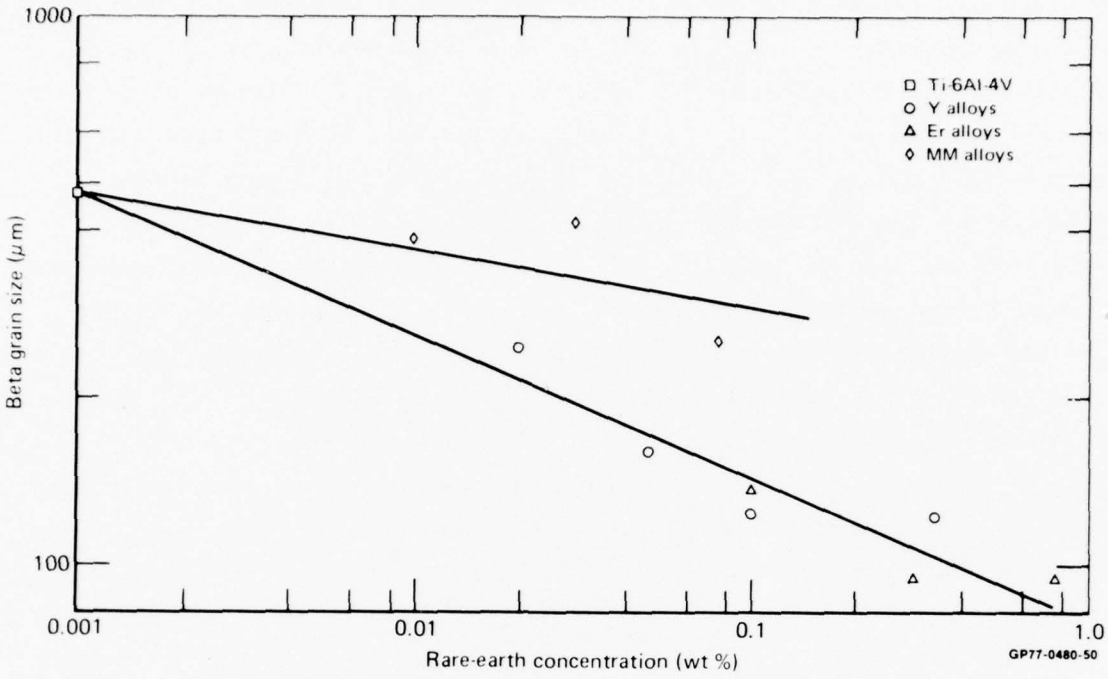

Figure 13. Beta-grain size as function of rare-earth concentration in Ti-6Al-4V-RE alloys annealed for 1 h at $T_\beta + 56^oC$; (□) Ti-6Al-4V reference alloy, (○) Y additive, (△) Er additive, and (◇) MM additive.

3.4 Influence of Rare-Earth Additions on the Beta-Transus Temperature

The β-transus temperatures of Ti-6Al-4V-RE alloys determined at the beginning of this investigation were discussed in Section 2. Because the microstructures of some of the hot-worked and beta-annealed alloys indicated that not all alloys were in the β field when water-quenched in accordance with the Figure 1 schedule, the question of the influence of rare-earth additions on the β-transus temperature was reexamined.

The annealing times (15 min) used earlier for beta-transus temperature determinations were too short for equilibrium to be obtained. A second series of alloy samples was encapsulated in quartz tubes under vacuum, annealed at temperatures of 985, 995, 1010, and 1020°C for 24 h, and water quenched. The samples were metallographically examined to determine the relative amounts of α and transformed-β phases. Selected alloy samples were examined by transmission-electron microscopy.

The high-temperature phases observed in specimens annealed at different temperatures are listed in Table 7. The β-transus temperature for most of the alloys is between 1010°C and 1020°C. The β-transus temperature is lowered by Y and Er concentrations greater than 0.1 wt%. Mischmetal in concentrations up to 0.08 wt% does not alter the β-transus temperature. Relative to T_β values listed in Table 5, Table 7 implies higher β-transus temperatures. The discrepancy may be due to the short annealing times used before and also to increases of the oxygen content during mill annealing. The entire question of the relative influences of small concentrations of dissolved rare-earth metals, interstitial-oxygen, and oxygen scavenging by the rare-earth dispersoids needs to be examined carefully in specimens for which both the rare-earth and oxygen concentrations are well characterized. Inasmuch as the reference and RE-containing alloys were subjected to identical treatments in the present study, conclusions about the comparative influences of the rare-earths on T_β are valid.

TABLE 7. HIGH-TEMPERATURE PHASES IN Ti-6Al-4V-RE ALLOYS

Alloy composition	Phases observed in water-quenched alloy			
	Annealed at 985°C	Annealed at 995°C	Annealed at 1010°C	Annealed at 1020°C
Ti-6Al-4V	α + β	α + β	α + β	β
Ti-6Al-4V-0.020Y	α + β	α + β	α + β	β
Ti-6Al-4V-0.050Y	α + β	α + β	α + β	β
Ti-6Al-4V-0.10Y	α + β	α + β	α + β	β
Ti-6Al-4V-0.30Y	α + β	α + β	β	β
Ti-6Al-4V-0.010 MM	α + β	α + β	α + β	β
Ti-6Al-4V-0.030 MM	α + β	α + β	α + β	β
Ti-6Al-4V-0.080 MM	α + β	α + β	α + β	β
Ti-6Al-4V-0.10 Er	α + β	α + β	α + β	β
Ti-6Al-4V-0.30 Er	α + β	α + β	β	β
Ti-6Al-4V-0.80 Er	α + β	β	β	β

GP77-0480-7

The influence of increasing Er-concentration on the stabilization of β is shown in Figures 14a and 14b, which show the microstructures of two Er-containing alloys annealed at 996°C and water quenched. The alloy with 0.1 wt% Er exhibits an α+β microstructure (consisting of primary-α and transformed-β). A similar effect is seen in Ti-6Al-4V-Er alloys quenched from 1010°C (Figures 15a and 15b).

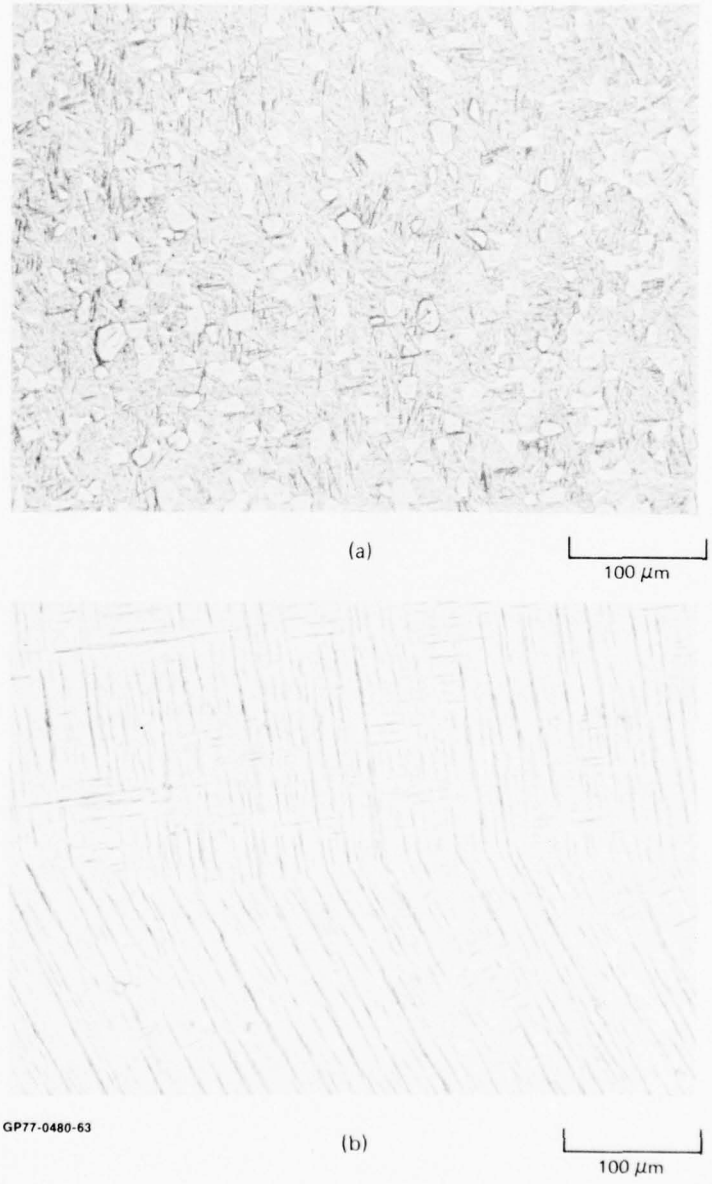

Figure 14. Microstructures of (a) Ti-6Al-4V-0.10Er and (b) Ti-6Al-4V-0.80Er annealed at 995°C, showing influence of Er concentration on beta-phase stabilization.

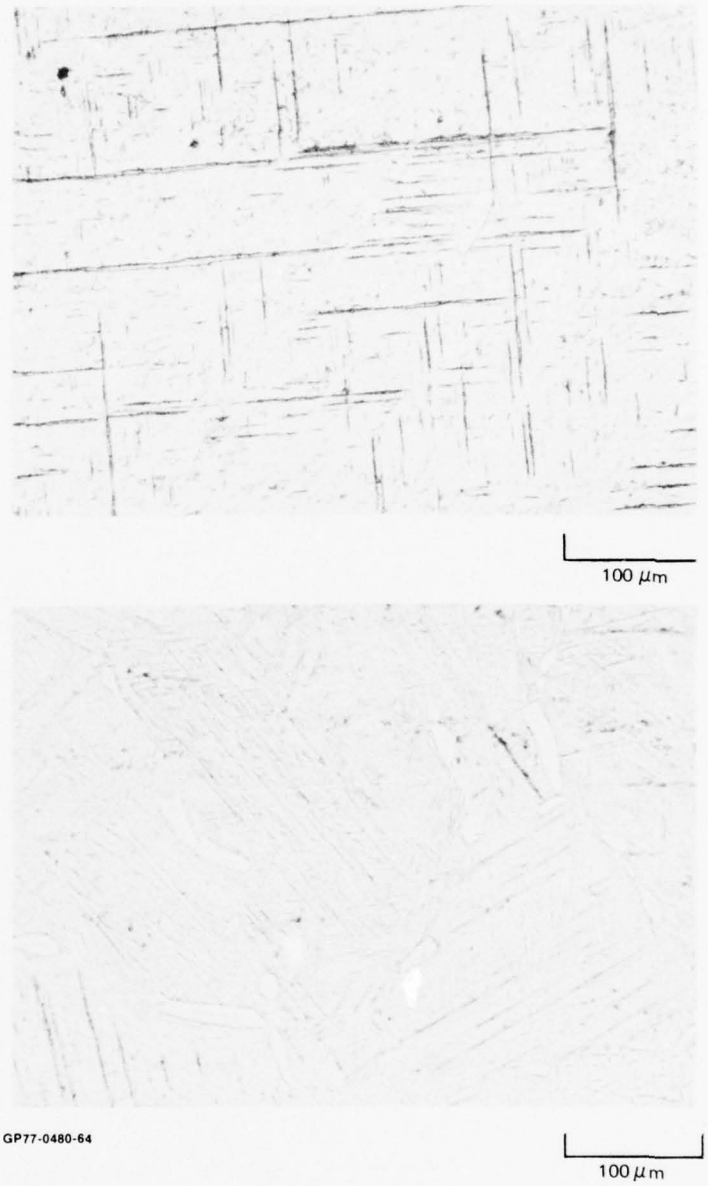

Figure 15. Microstructures of (a) Ti-6Al-4V-0.10Er and (b) Ti-6Al-4V-0.80Er annealed at 1010°C.

The influence of Y on beta-phase stabilization at 995°C is shown in Figure 16. With an increase in Y content, the volume fraction of primary-α decreases. At 1010°C, the alloy containing 0.30 wt% Y is completely β phase.

The details of typical transformed-β structures observed in the alloys are shown in Figure 17. The structures shown in Figure 17 result from β annealing and water quenching followed by stabilization annealing in the

α+β field and air cooling to room temperature. The martensite structure formed upon quenching from the β field decomposes into fine acicular α+β on aging in the α-β field.

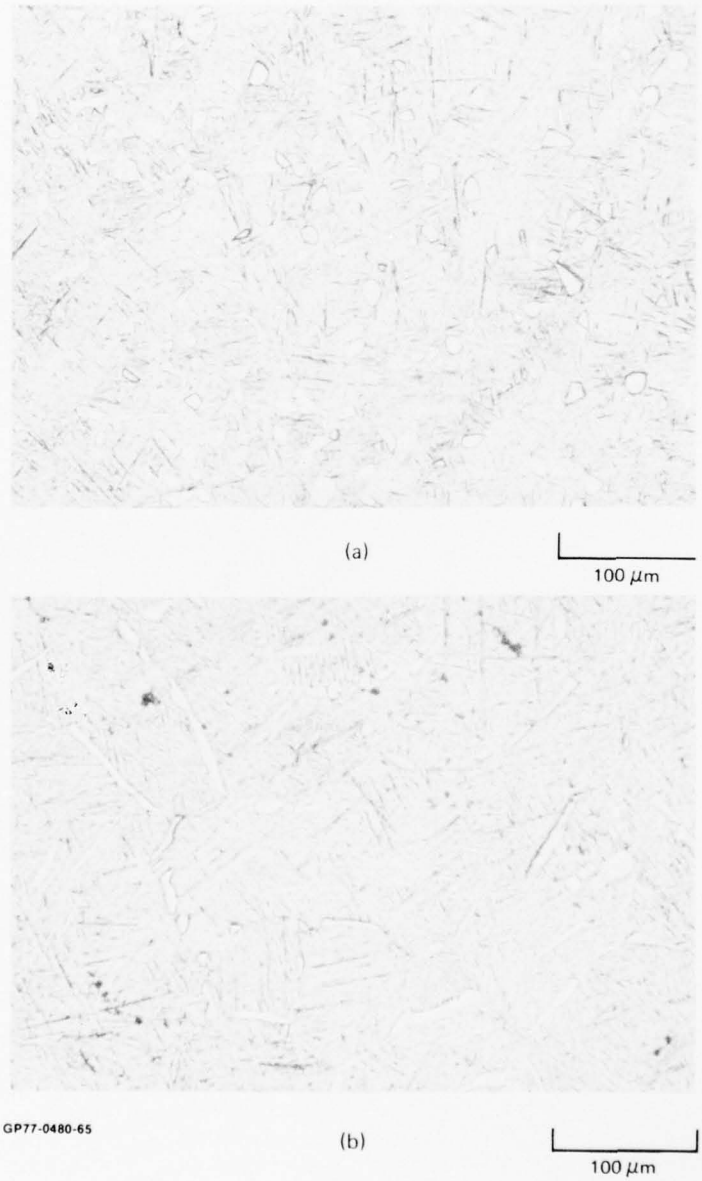

Figure 16. Microstructures of (a) Ti-6Al-4V-0.020Y and (b) Ti-6Al-4V-0.30Y annealed at 995°C, showing influence of Y concentration on beta-phase stabilization.

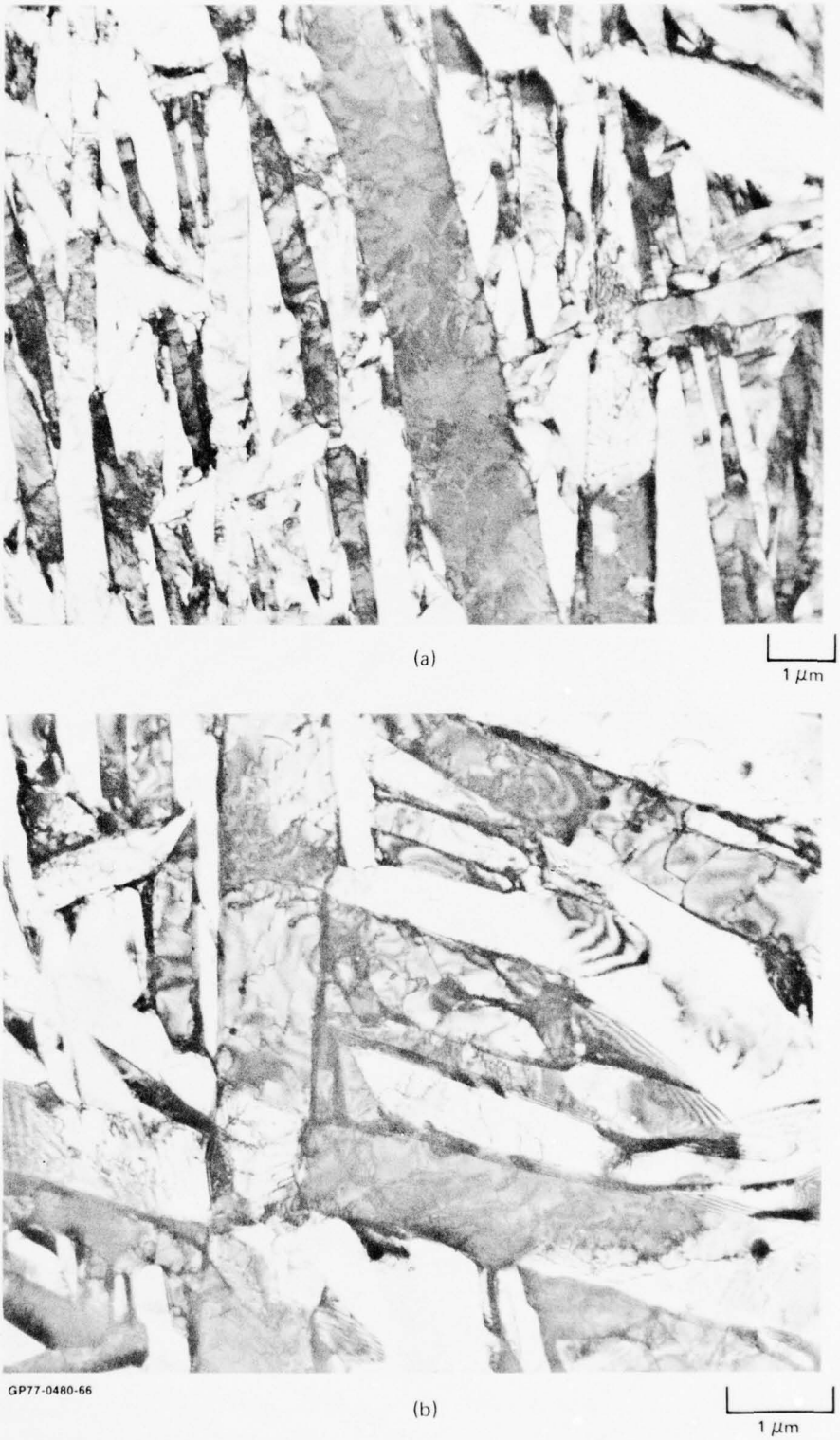

Figure 17. Transmission electron micrographs of beta-annealed (a) Ti-6Al-4V reference alloy and (b) Ti-6Al-4V-0.050Y.

In contrast to the beta-stabilizing influence of Y and Er, mischmetal is an alpha stabilizer. This effect is illustrated in Figure 18. In mischmetal-containing alloys annealed at 995°C, the volume fraction of primary-α is higher in the higher mischmetal alloy. Figures 19a and 19b show a comparison of the $\alpha+\beta$ structures observed in Ti-6Al-4V-0.050Y and Ti-6Al-4V-0.080MM alloys annealed at the same temperature (955°C) in the

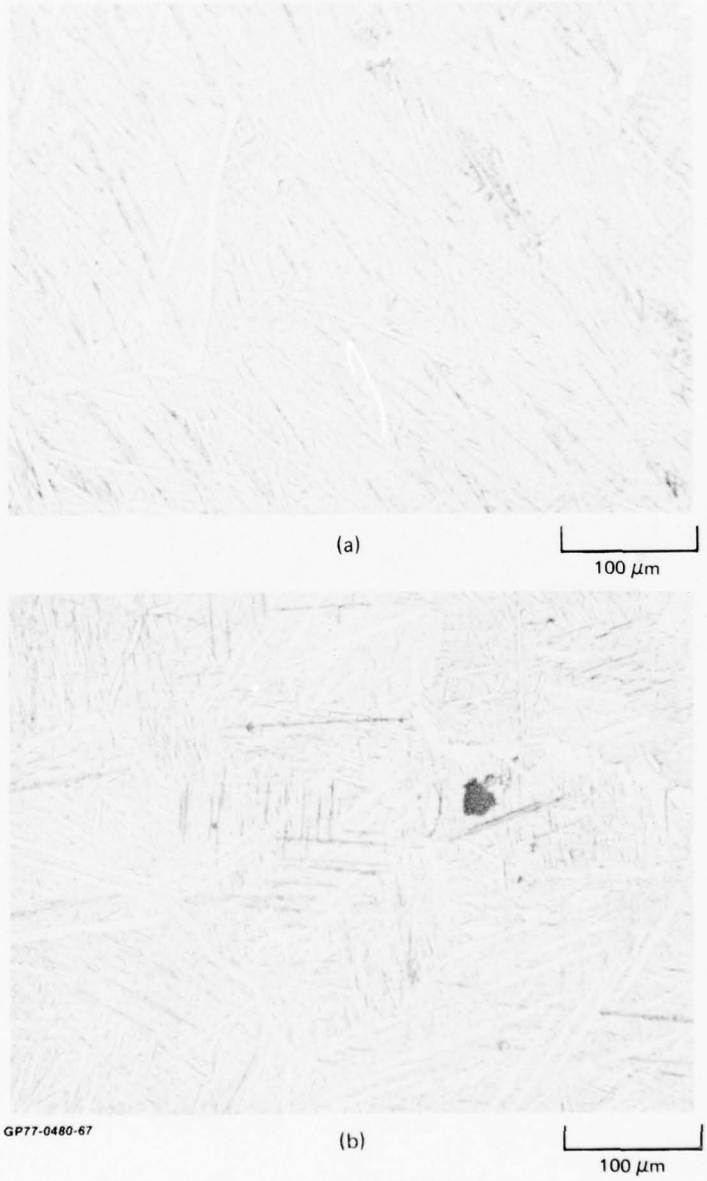

Figure 18 Microstructures of (a) Ti-6Al-4V-0.010MM and (b) Ti-6Al-4V-0.080MM annealed at 955°C, showing influence of mischmetal on alpha-phase stabilization.

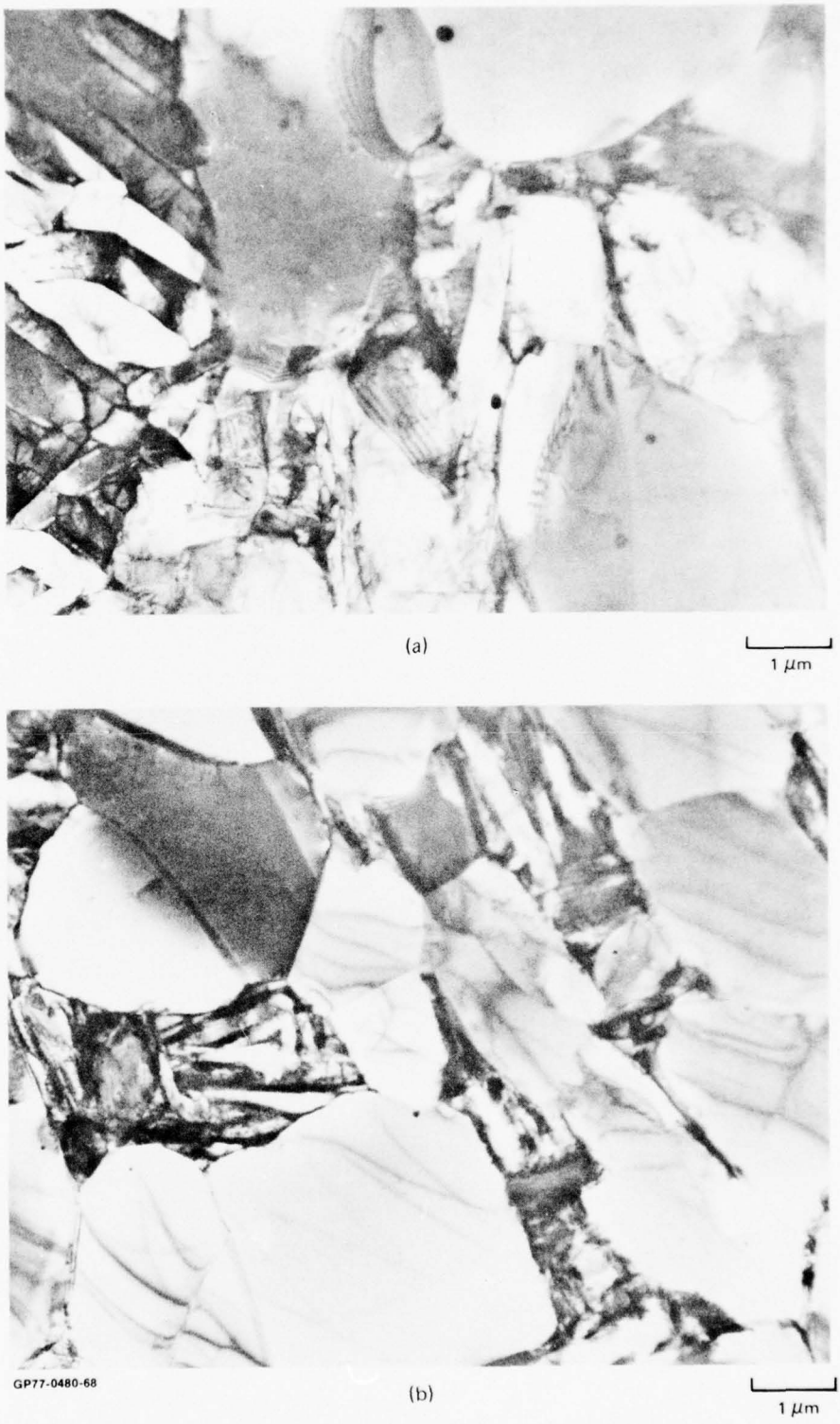

Figure 19. Transmission electron micrographs showing equiaxed alpha and transformed beta in alpha-beta annealed (a) Ti-6Al-4V-0.05Y and (b) Ti-6Al-4V-0.080MM.

α-β field. The mischmetal-containing alloy shows a higher volume fraction of primary α than the Y-containing alloy.

The metallographic studies indicate that only Y and Er in concentrations greater than 0.1 wt% lower the β-transus temperature of Ti-6Al-4V; mischmetal up to 0.08 wt% does not significantly alter the beta-transus temperature. The observed influence of Y on β-phase stabilization and of MM on α-phase stabilization is in agreement with the phase diagrams of Ti-Y, Ti-Ce, and Ti-La alloys. The phase diagrams show a decrease in β-transus temperature of Ti with increasing Y concentration and an increase in beta-transus temperature for Ti-Ce and Ti-La alloys[4].

4. ROOM-TEMPERATURE TENSILE PROPERTIES OF Ti-6Al-4V-RE ALLOYS

4.1 Transverse Tensile Properties

The room-temperature tensile properties of the Ti-6Al-4V-RE alloys in the short-transverse (ST) and long-transverse (LT) directions were measured to determine the influence of rare-earth additives on the tensile properties in the transverse directions of relatively thick sheets. A 100-mm long sheet was cut from the center of each alloy plate when it had been hot-rolled to a 20-mm thickness according to the Figure 1 schedule, and tensile specimens were prepared from these sheets. Figure 20 shows the orientation of tensile specimens relative to the rolling direction. The LT tensile specimens were machined to the final configuration from the alloy sheets as illustrated in Figure 21a. To provide for gripping the ST tensile specimens in the test instrument, Ti-6Al-4V end-tabs were electron-beam welded to the ST specimens (Figure 21b). The weld zone was examined by optical microscopy, which showed the heat-affected zone to be confined to the end tabs. Figure 21c shows the microstructure of the weld region of a ST specimen; the microstructure in the gauge section was not affected by the welding.

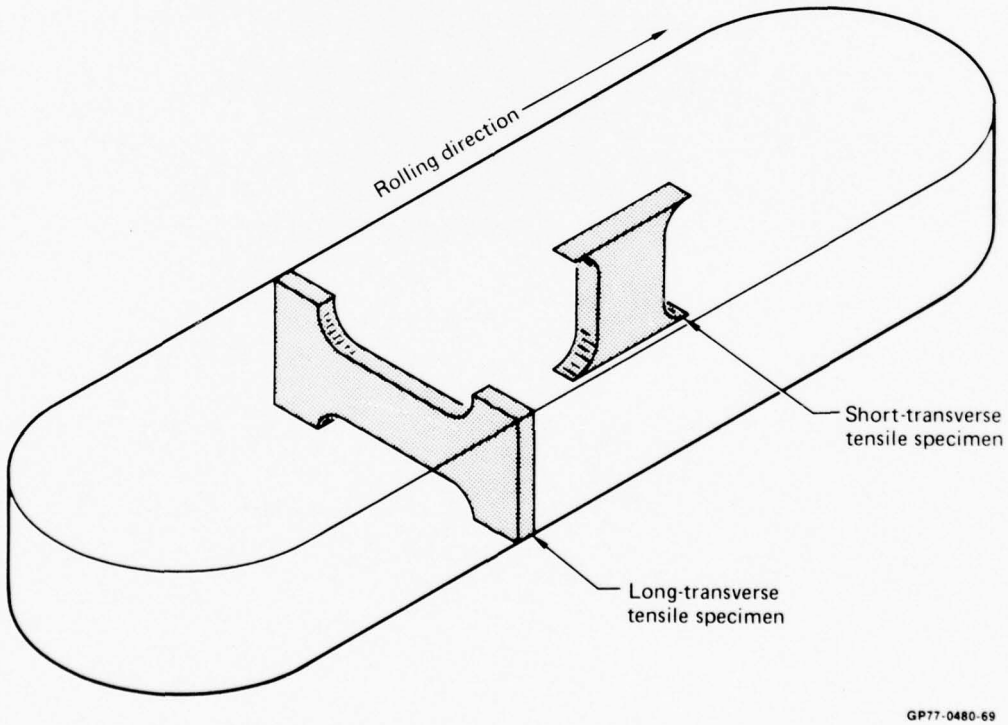

Figure 20. Orientation of tensile specimens relative to rolling direction in 20-mm thick Ti-6Al-4V-RE plates.

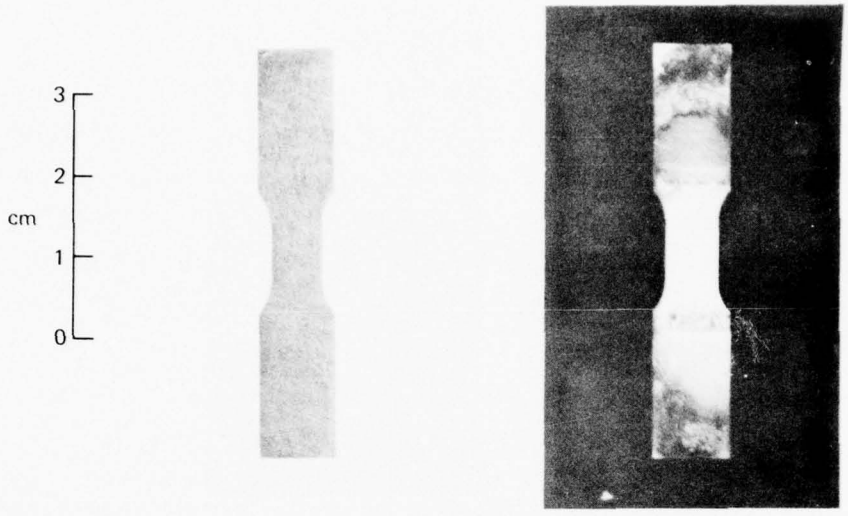

(a) (b)

(c)

Figure 21. Photographs of tensile specimens from 20-mm thick Ti-6Al-4V-RE plates; (a) long-transverse specimen, (b) short-transverse specimen with welded tabs, and (c) microstructure of weld region of short-transverse specimen.

The tensile specimens were polished with 240-grit paper to remove surface irregularities. The gauge section of each tensile specimens was 8.0 x 6.0 x 3.1 mm. The specimens were tested in uniaxial tension at a strain rate of 0.005/min to yield and 0.02/min from yield to fracture.

The tensile properties of the alloys in the long-transverse and short-transverse directions are listed in Table 8. Both the yield stress and ultimate tensile-stress are lower in the short-transverse direction than in the long-transverse direction for all alloys including the Ti-6Al-4V reference. A slight decrease in strength with rare-earth additions is observed in the ST and LT directions, and ductility is affected little by small concentrations of Y and Er. Alloys containing 0.02Y, 0.05Y, and 0.1Er exhibit excellent ductility with little loss in strength. The ductility of the alloys decreases significantly with mischmetal additions.

TABLE 8. ROOM-TEMPERATURE TENSILE PROPERTIES OF HOT-ROLLED (1010°C) Ti-6Al-4V-RE ALLOYS IN THE SHORT-TRANSVERSE (ST) AND LONG-TRANSVERSE (LT) DIRECTIONS

Ingot number	Alloy composition	Elastic modulus (GPa)		Yield stress at 0.2% offset (MPa)		Ultimate tensile stress (MPa)		Uniform elongation (%)		Total elongation (%)	
		ST	LT	ST	LT	ST	LT	ST	LT	ST	LT
14	Ti-6Al-4V	80	109	903	1010	1057	1117	4.4	5.0	21.3	20.8
4	Ti-6Al-4V-0.020Y	98	108	852	985	994	1082	4.8	4.7	23.1	25.0
5	Ti-6Al-4V-0.050Y	88	111	850	961	1005	1056	4.6	5.0	20.2	23.8
15	Ti-6Al-4V-0.10Y	99		886		1022		4.3		11.4	
16	Ti-6Al-4V-0.30Y	95		820		980		3.5		7.6	
8	Ti-6Al-4V-0.010MM	101	109	820	912	982	1004	4.8	4.3	16.5	19.2
9	Ti-6Al-4V-0.030MM	88	119	819	962	986	1051	5.0	4.2	14.2	20.1
10	Ti-6Al-4V-0.080MM	103		844		1002		4.5		11.5	
11	Ti-6Al-4V-0.20MM	86		852		1011		3.4		11.5	
12	Ti-6Al-4V-0.20MM	99		870		1033		3.1		6.7	
25	Ti-6Al-4V-0.10Er	104	111	906	982	1018	1062	4.3	4.7	13.2	21.6
26	Ti-6Al-4V-0.30Er	103	108	824	985	978	1060	4.2	4.0	15.7	20.9
27	Ti-6Al-4V-0.80Er	98		835		960		3.7		9.8	
29	Ti-6Al-4V-0.80Er	99		821		952		4.2		7.2	

GP77-0480-8

4.2 Longitudinal Tensile Properties

A detailed study of the mechanical properties of Ti-6Al-4V-RE alloys as functions of annealing temperatures and time in the single-phase β field and the two-phase α+β field was made. The alloys were annealed at T_β+56°C, T_β+28°C, T_β-28°C, and T_β-56°C; alloy sheets 60-mm long and 3-mm thick were heat treated in the β field for 5, 15, 30, and 60 min and in the α+β field for 15, 30, 60, and 240 min and were water quenched. The sheets were subsequently annealed at 705°C for 2 h and air cooled to room temperature. Samples were grit blasted after heat treatment and acid-pickled 0.2 mm per side to remove oxygen-contaminated metal. Tensile specimens 50 mm long having a 3 x 6 mm reduced-area gauge section, with tensile axes parallel to the rolling direction, were machined from the heat-treated sheets. Tensile tests were performed at a strain rate of 0.01/min.

The tensile properties of the alloys after various annealing treatments are listed in Tables A1-A28 in Appendix A. Some of the general trends are summarized below.

The yield stress, ultimate tensile-stress, and uniform elongation for selected alloys annealed at different temperatures are plotted in Figure 22. The β-annealed alloys exhibit higher yield stresses and ultimate tensile stresses and lower ductility than the α-β annealed alloys, but a change in the β-annealing temperature does not significantly alter the mechanical properties. The influence of annealing time on the properties of β-annealed alloys is shown in Tables A21-A28 in Appendix A. With the exception of alloys annealed for 5 min, which are not representative of β-annealed alloys because the 5-min annealing time is too short for attainment of equilibrium, the alloys do not show any significant variation of yield stress and ultimate tensile stress with time in the β field. The yield stress of β-annealed alloys is nearly independent of prior-β grain size, as is shown in Figure 23. However, as seen from Figure 22, ductility is inversely related to prior-β grain size.

In the case of β-annealed alloys, the starting microstructure is transformed-β consisting of plate-like α+β. Alloys quenched from the β field and subsequently stabilization annealed at 705°C exhibit larger prior-β grain sizes for longer-duration β anneals but have essentially no difference in the morphology and size of α-β plates. The yield stress in such alloys is probably governed by individual plate thickness rather than the grain size because the slip length is limited by the individual plates.

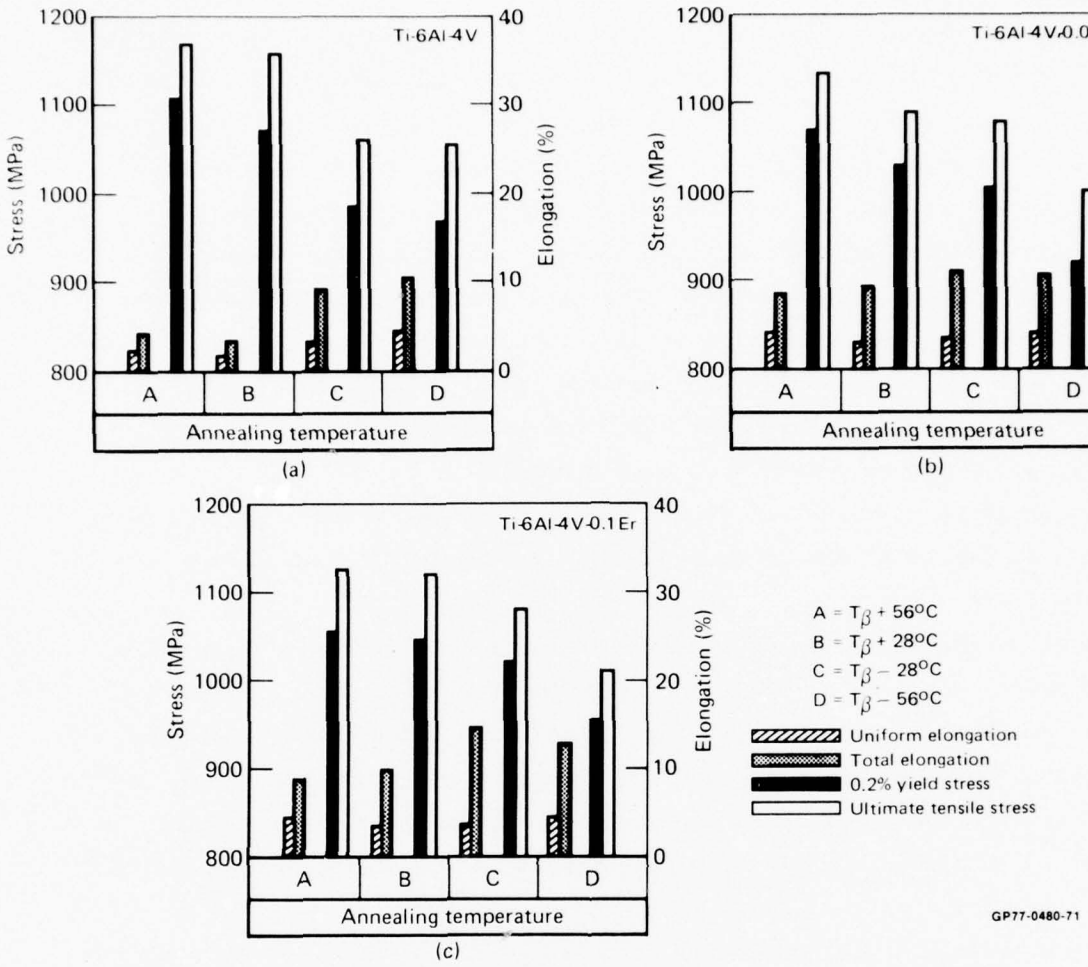

Figure 22. Room-temperature mechanical properties of (a) Ti-6Al-4V reference alloy, (b) Ti-6Al-4V-0.020Y, and (c) Ti-6Al-4V-0.10Er annealed at T_β + 28°C and T_β + 56°C for 60 min and at T_β − 28°C and T_β − 56°C for 180 min.

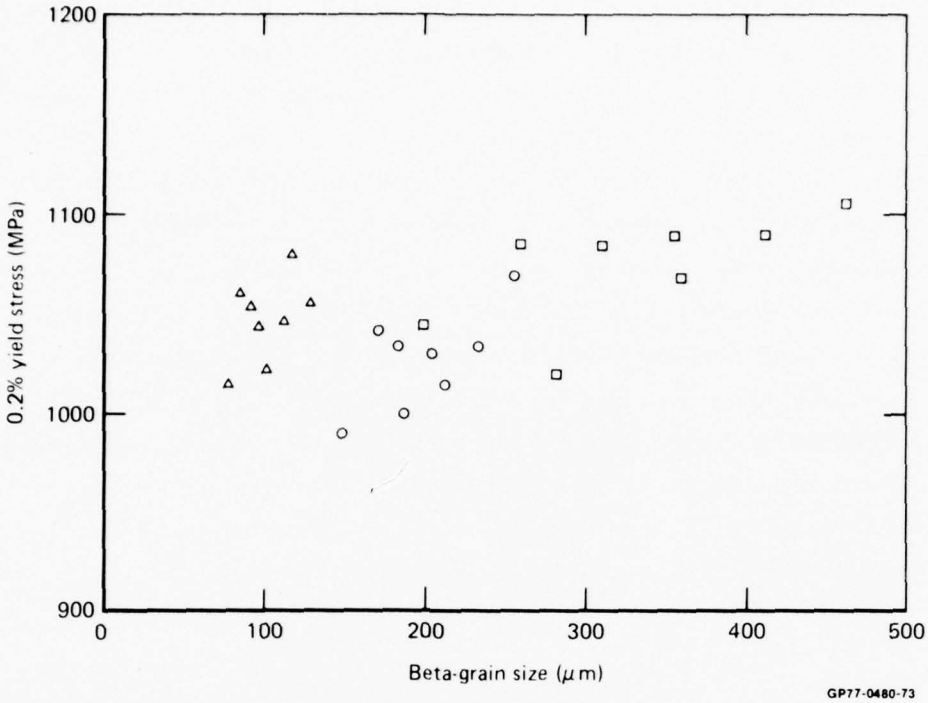

Figure 23. Dependence of yield stress on beta-grain size for (□) Ti-6Al-4V reference alloy, (○) Ti-6Al-4V-0.020Y, and (△) Ti-6Al-4V-0.10Er.

When the alloys are annealed in the α+β field, the properties are markedly altered by a change in annealing temperature. In general, a lower α-β annealing temperature results in a lower yield stress and ultimate tensile stress and a slightly higher ductility (Figure 22). No systematic trend of the effects of annealing time on strength and ductility of α-β annealed alloys is observed. The values reported in Tables A13-A20 show considerable scatter, which can be explained by random variations of the volume-fraction of transformed-β. This was confirmed by a detailed microstructural examination of several α-β annealed alloys, which showed that the expected volume fraction of transformed-β did not vary systematically with temperature and time of α-β annealing. The observed random variations in the amounts of α and transformed-β phases are believed to be due to small differences in the mill processing of the different alloys. A correlation between the yield stress and volume fraction of transformed-β was observed for α-β annealed alloys. Figure 24 shows the stress-strain curves of three alloys with varying amounts of transformed-β. Figure 24b

shows the linear variation of yield stress with the amount of transformed-β, which is expected if a simple rule of mixtures is invoked to explain the deformation behavior of α-β annealed alloys. The microstructure of α-β annealed alloys consists of primary equiaxed-α grains and Widmanstätten transformed-β. The yield stress of such alloys is governed by some form of superposition of the flow stress of equiaxed-α and the composite flow stress of transformed-β. A linear extrapolation of the plot in Figure 24b to 100% transformed-β gives a yield stress higher than that observed experimentally, which implies that the yield stress must depart from a linear behavior for transformed-β volumes > 60%. The rule of mixtures is a simplified approximation to the flow stress for the complex transformed-β structure, and a more rigorous treatment should take into account the grain sizes of the α and transformed-β and the relative sizes of α and β plates in transformed-β.

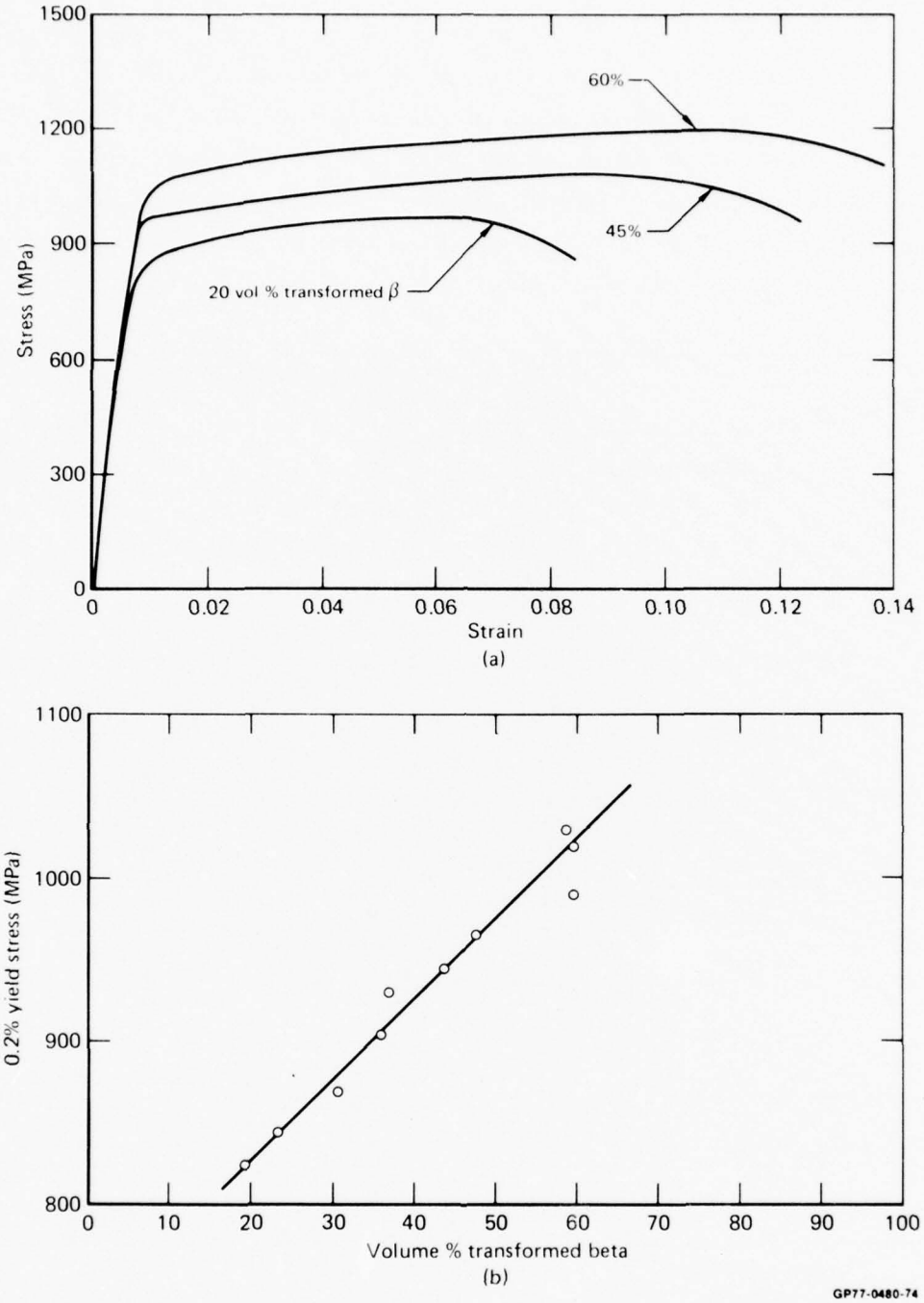

Figure 24. Effect of volume percent of transformed beta on the stress-strain characteristic of alpha-beta annealed Ti-6Al-4V; (a) stress-strain characteristics for 20, 45, and 60 vol % transformed beta and (b) dependence of yield stress on vol % transformed beta.

4.3 Influence of Rare-Earth Additives on Tensile Properties

The influence of rare-earth additives on the mechanical properties of β-annealed alloys is shown in Figure 25, in which the data points are the average values for all annealing conditions listed in Tables A21-A28. With increasing rare-earth concentration, the yield stress decreases slightly and the ductility increases. However, the decrease in yield stress is small (< 5%) for up to 0.1 wt% Er or Y. Mischmetal, even in small concentrations, reduces the yield stress significantly.

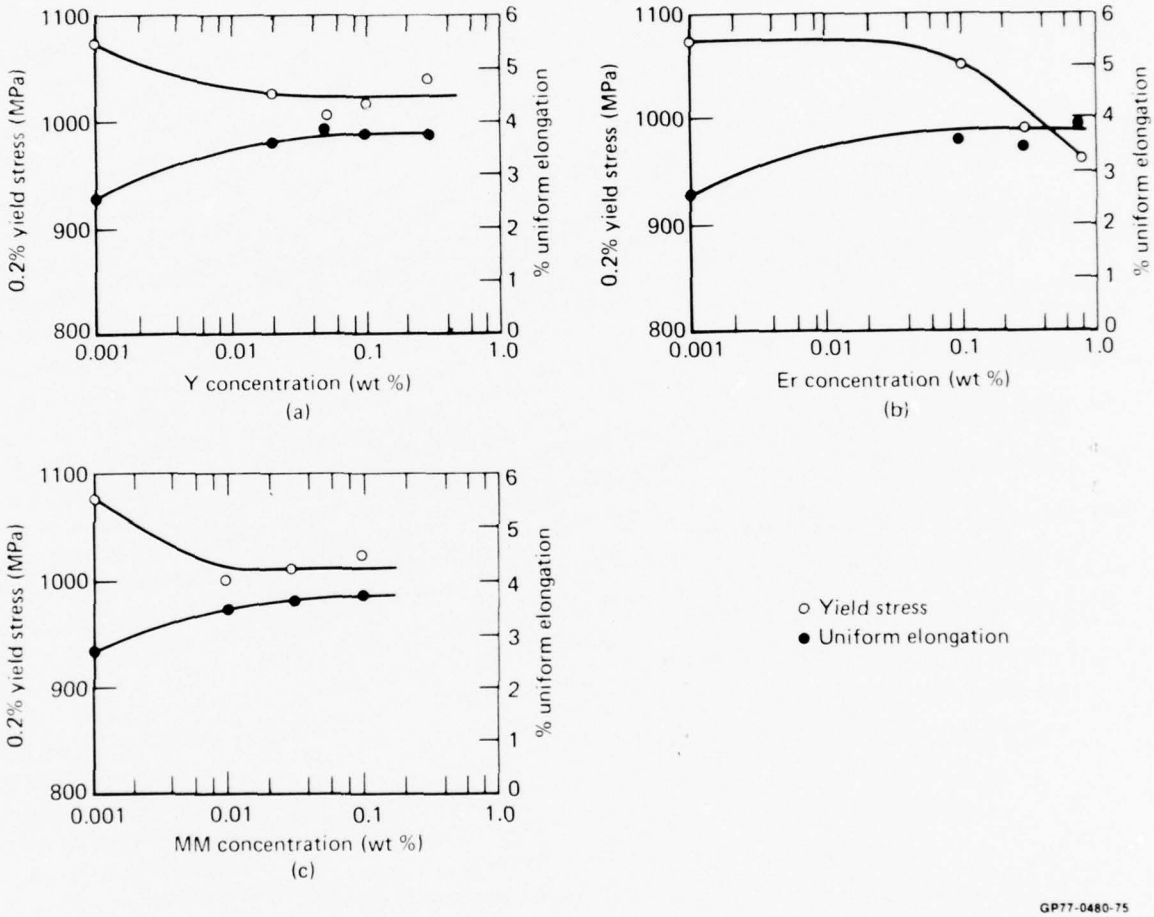

Figure 25. Yield-stress and uniform elongation of beta-annealed Ti-6Al-4V-RE alloys as functions of concentrations of (a) Y, (b) Er, and (c) MM.

The influence of rare-earth additives on the yield stress and uniform elongation of α-β annealed alloys is shown in Figure 26, in which the data points are the average values for all annealing times listed in Tables A13-A20. In the α-β annealed alloys, the rare-earth influence is dependent

on the annealing temperatures. For Y- and Er-containing alloys annealed at a temperature near T_β, the yield stress decreases slightly with the addition of rare earths, similar to the β-annealed alloys. However, for the alloys annealed at the lower α-β temperature, the reduction of yield stress with the addition of Er and Y is less. Mischmetal significantly reduces the yield stress of α-β annealed alloys.

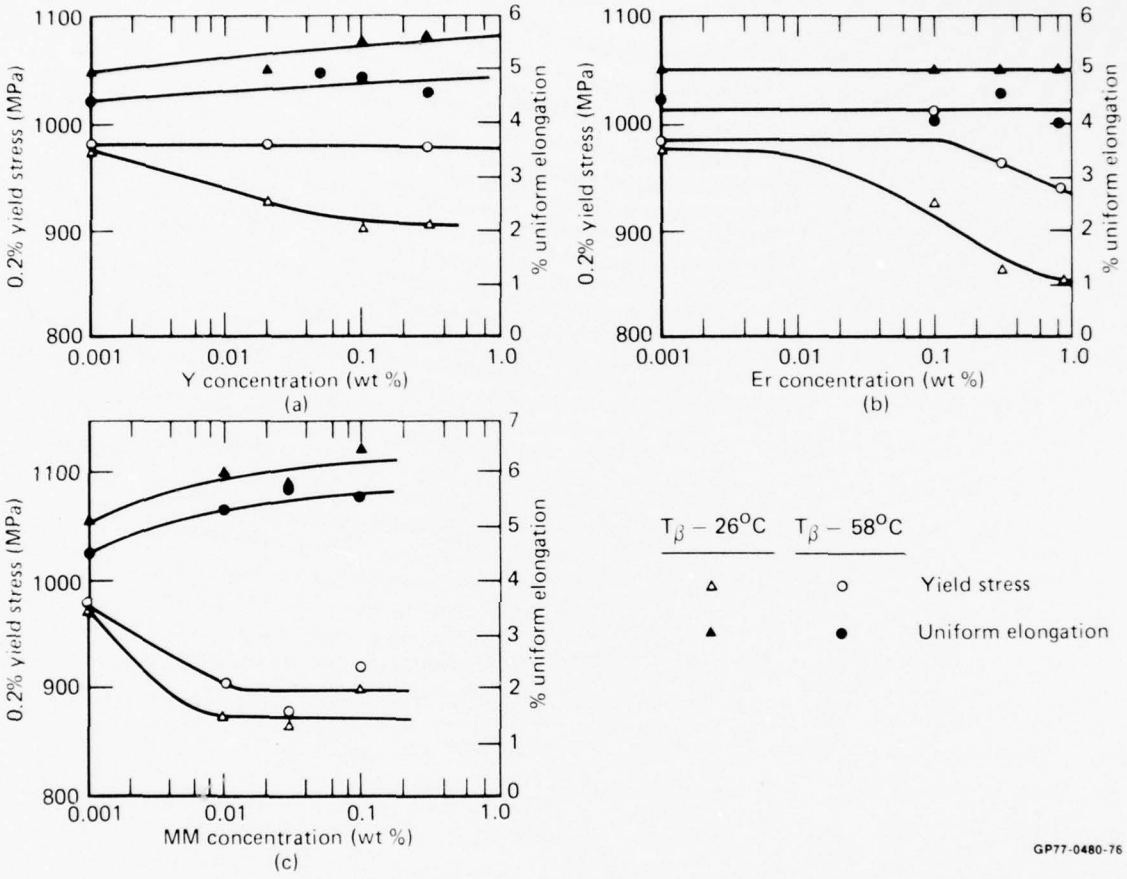

Figure 26. Yield stress and uniform elongation of alpha-beta annealed Ti-6Al-4V-RE alloys as functions of concentrations of (a) Y, (b) Er, and (c) MM.

The results presented in Figures 25 and 26 show that when the microstructure is predominantly transformed-β, the yield stress is controlled by the Widmanstätten α+β structure. The rare-earth additives do not contribute any strengthening because of the overriding influence of the transformed-β structure. The slight reduction in strength observed in rare-earth-containing alloys is likely due to a lower interstitial oxygen content of the Ti-6Al-4V-RE

alloys; the rare earths because of their greater affinity for oxygen can scavenge part of the dissolved oxygen from the alloy matrix. As the volume fraction of primary-α is increased by annealing at lower α-β temperatures, a strengthening influence of the Y and Er additives is evident that largely compensates the oxygen-scavenging effect. The Ti-6Al-4V-MM alloys under all annealing conditions, however, exhibit a significantly lower strength than the reference alloy.

4.4 Influence of Annealing Temperature and Cooling Rate on Tensile Properties

Because metallographic examinations of the mill-annealed alloys revealed that not all specimens had been annealed in the β field as specified, selected alloy compositions were re-annealed in accordance with the schedule shown in Figure 27. The compositions of the alloys, annealing temperatures, and cooling rates were selected to study the combined influences of rare-earth additives and various modifications of transformed-β and $\alpha+\beta$ microstructures on the mechanical properties. The heat treatments shown in Figure 27 produce (1) different types of transformed-β, (2) morphological differences in α and β, and (3) differences in the relative volume-fractions of α and β. In addition, the low-temperature aging treatment can possibly produce either short-range-ordered regions of Ti and Al atoms or Ti_3Al (α_2) precipitates in the alloy matrix[8].

The room-temperature tensile properties of the alloys subjected to the Figure 27 heat treatments are listed in Table 9. Because the properties result from combined effects of complex Ti-6Al-4V microstructures and the rare-earth dispersoids, the tensile-property changes cannot in most cases be attributed to specific variables. The microstructures prior to the heat treatments shown in Figure 27 were not the same for all the alloys; consequently, the tensile property changes to be discussed in this section also reflect to a certain extent the prior history of the alloys.

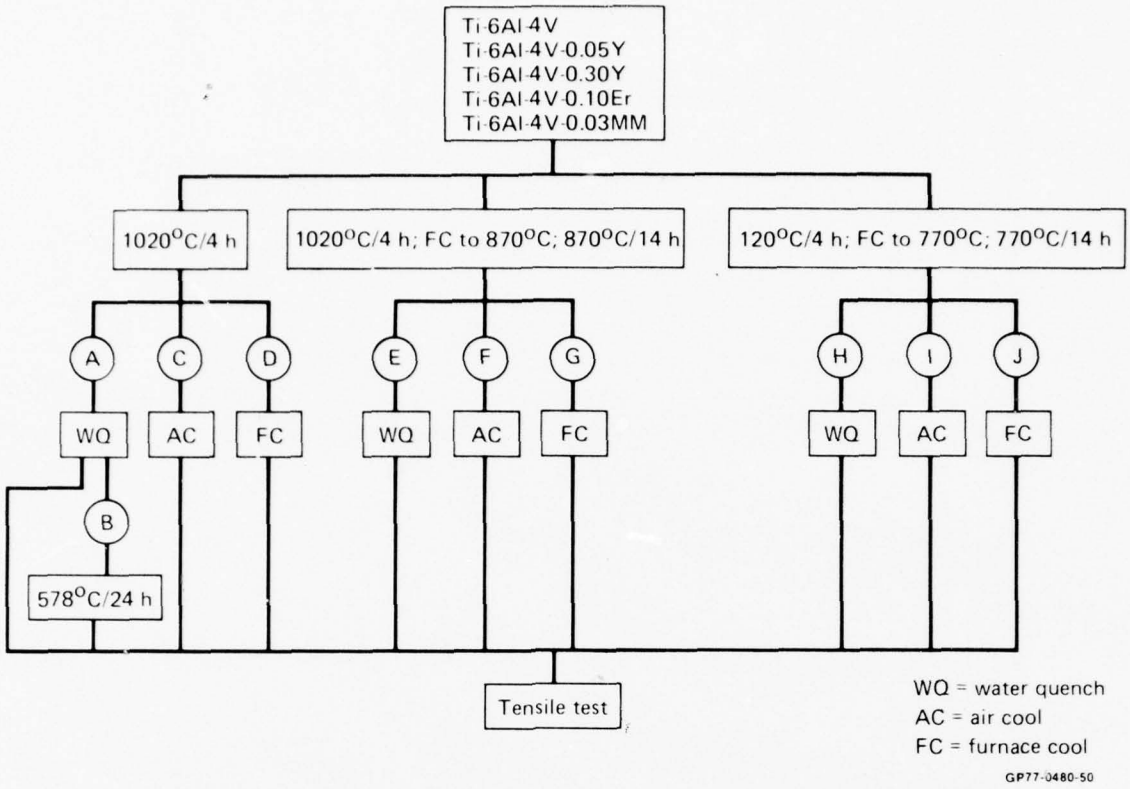

Figure 27. Heat treatments to vary relative fractions of alpha and beta phases and transformed-beta structure in Ti-6Al-4V-RE alloys.

TABLE 9. ROOM TEMPERATURE TENSILE PROPERTIES OF BETA-ANNEALED AND AGED Ti-6Al-4V-RE ALLOYS

Heat treatment	Alloy composition	Water-quenched			Water-quenched and aged at 570°C for 24 h			Air-cooled			Furnace-cooled		
		Yield stress at 0.2% offset (MPa)	Ultimate tensile stress (MPa)	Total elongation (%)	Yield stress at 0.2% offset (MPa)	Ultimate tensile stress (MPa)	Total elongation (%)	Yield stress at 0.2% offset (MPa)	Ultimate tensile stress (MPa)	Total elongation (%)	Yield stress at 0.2% offset (MPa)	Ultimate tensile stress (MPa)	Total elongation (%)
Beta annealed at 1020°C for 4 h	Ti-6Al-4V	1012	1132	2.0	1110	1192	2.6	915	994	4.2	900	982	4.1
	Ti-6Al-4V-0.050Y	900	1062	2.6	1050	1125	3.8	848	1005	11.5	892	990	12.0
	Ti-6Al-4V-0.30Y	990	1140	3.7	848	910	2.5	862	1020	10.7	840	975	12.5
	Ti-6Al-4V-0.10Er	997	1222	5.9	1065	1192	3.2	877	1050	11.7	900	1042	6.8
	Ti-6Al-4V-0.030MM	877	1050	2.7	1020	1140	3.7	840	1020	7.4	840	937	4.6
Beta annealed at 1020°C for 4 h, furnace cooled to 870°C, annealed at 870°C for 14 h	Ti-6Al-4V	847	1035	5.9				880	960	4.2	885	1005	6.4
	Ti-6Al-4V-0.050Y	922	1031	13.0				855	960	9.0	855	958	8.2
	Ti-6Al-4V-0.30Y	810	1020	13.3				840	949	8.0	825	930	6.2
	Ti-6Al-4V-0.10Er	840	1050	9.2				877	1020	11.1	862	990	7.9
	Ti-6Al-4V-0.030MM	802	967	8.3				840	949	5.8	832	930	5.7
Beta annealed at 1020°C for 4 h, furnace cooled to 770°C, annealed at 770°C for 14 h	Ti-6Al-4V	855	1020	11.7				885	997	5.5	900	1005	3.7
	Ti-6Al-4V-0.050Y	810	975	16.0				900	994	10.2	877	971	3.1
	Ti-6Al-4V-0.30Y	750	968	13.7				863	980	9.6	790	902	6.8
	Ti-6Al-4V-0.10Er	780	1005	12.9				855	1012	10.7	862	1020	7.8
	Ti-6Al-4V-0.030MM	780	975	11.3				877	990	7.5	832	937	6.1

GP77-0480-9

Alloys quenched from the β field exhibit high strength and low ductility. The high strength results from the acicular martensitic structure, which contains a high density of internal-dislocation substructures, and the prior-β grain size has no significant effect. For example, the Ti-6Al-4V-0.10Er alloy, although it has a finer prior-β grain size than the reference alloy (Figure 28), does not exhibit the increased yield stress expected from the Hall-Petch relationship between yield stress and grain size. However, a finer grain size imparts a higher ductility. Of the three rare-earth additives, mischmetal considerably reduces the yield stress and ultimate tensile-stress; Y improves the ductility but decreases the strength slightly; and Er improves the ultimate tensile-stress and ductility.

Alloys quenched from the β field and aged at 570°C have higher strengths than quenched β-annealed alloys with the exception of Ti-6Al-4V-0.30Y. The increased strength results from the decomposition of martensite into α+β. The β-phase nucleates as small precipitates (Figure 29) and acts as a precipitation-strengthening phase; consequently, the yield stress is increased. The ultimate tensile stress, however, is not increased.

Air cooling and furnace cooling of the alloys from the β field result in slightly lower strength and higher ductility, characteristic of the Widmanstätten α+β structure of the alloys. The β-annealed rare-earth-containing alloys exhibit a significantly higher ductility than the reference alloys in the air-cooled and furnace-cooled conditions. The improved ductility is attributed to the finer colony size in Ti-6Al-4V-RE alloys than in the reference alloy (compare Figures 30a and 30b). Thus, in the β-annealed alloys, the yield stress and ultimate tensile stress are related to the individual plate sizes, whereas ductility is related to colony size.

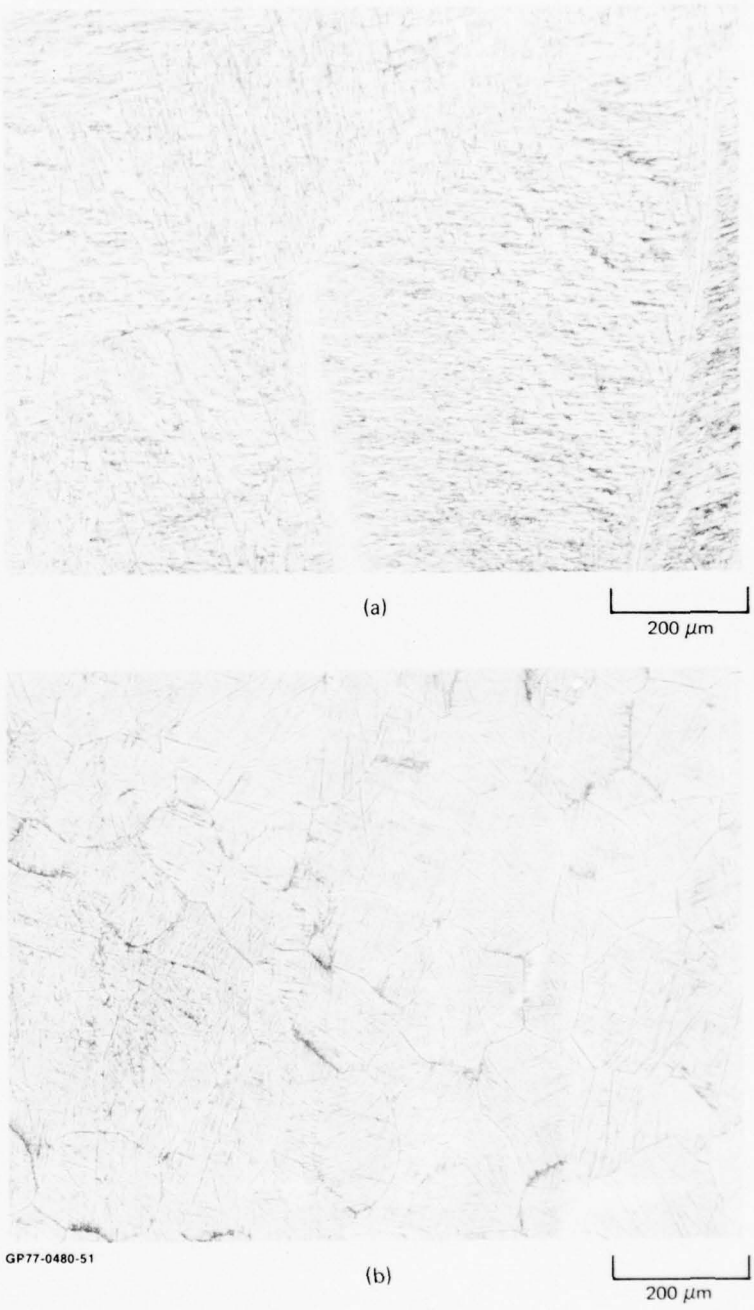

Figure 28. Microstructures of beta-annealed and water-quenched (a) Ti-6Al-4V reference alloy and (b) Ti-6Al-4V-0.10Er (heat treatment A, Figure 14).

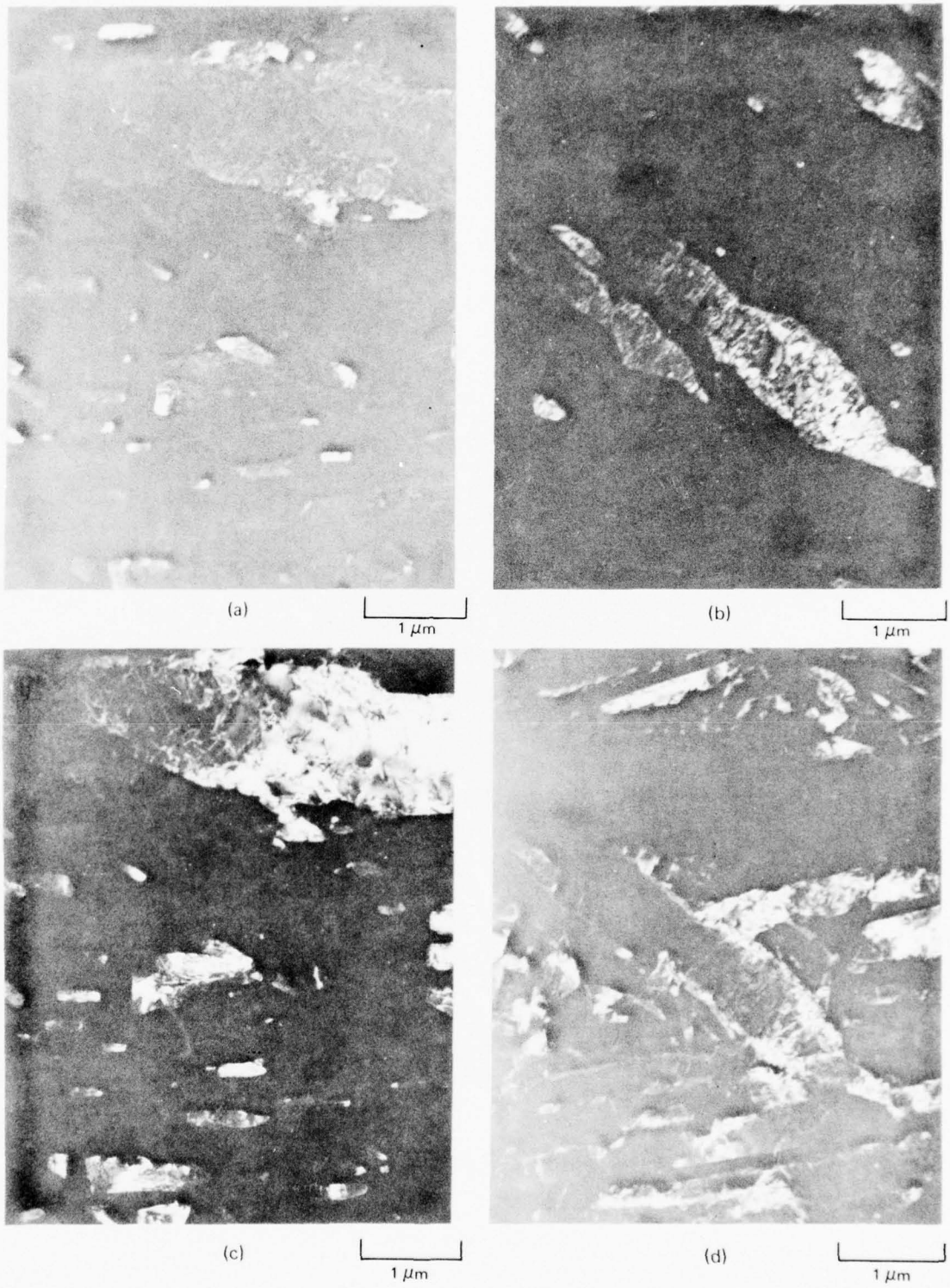

Figure 29. Dark-field electron micrograph of beta precipitates in alpha-prime phase of Ti-6Al-4V reference alloy quenched from 1020°C and aged for 24 h at 550°C. GP77-0480-62

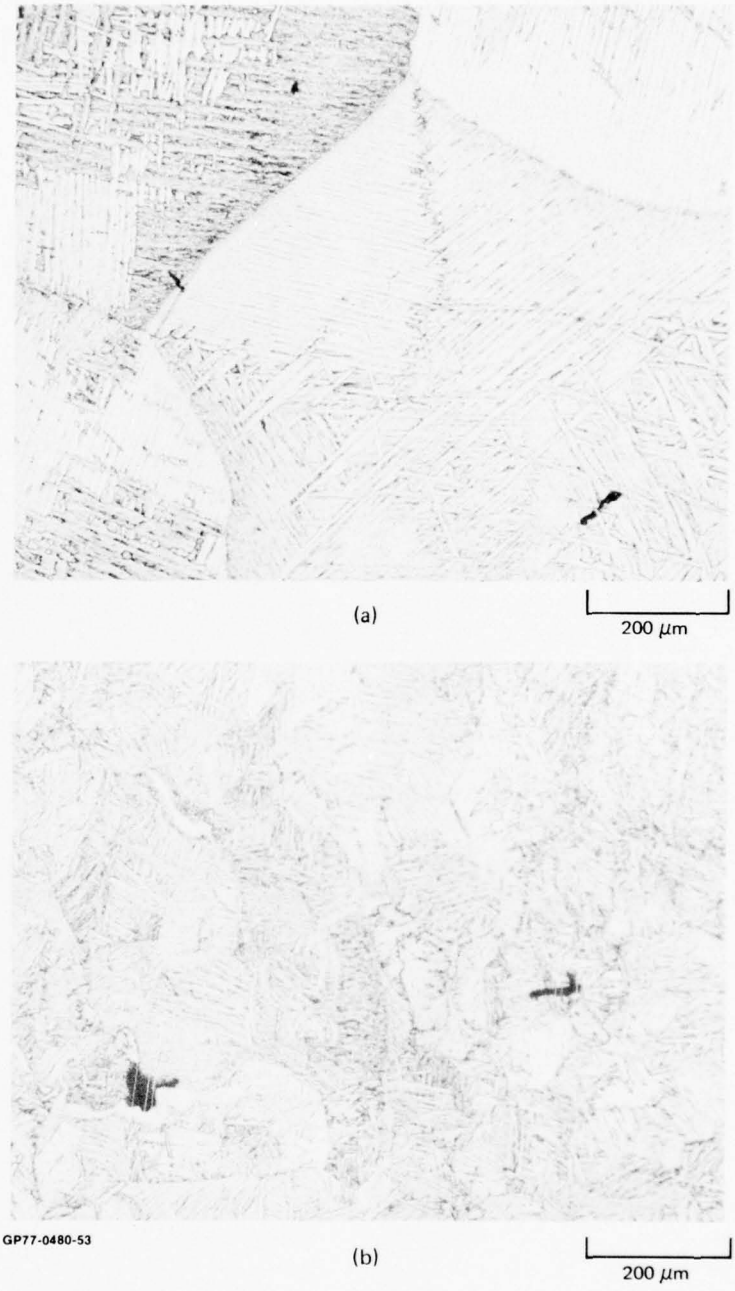

Figure 30. Microstructures of beta-annealed and air-cooled (a) Ti-6Al-4V reference alloy and (b) Ti-6Al-4V-0.05Y (heat treatment C , Figure 14).

Duplex annealing at two α-β temperatures, 870°C and 770°C, was performed to produce different volume fractions of α phase. Beta-annealed alloys, furnace cooled and subsequently annealed in the α-β field, exhibit the plate-like α+β morphology as shown in Figure 31. The relative sizes and amounts of α and β depend on the α-β annealing temperature. Depending on the cooling rate from the α-β annealing temperature, the high-temperature β-phase transforms to either metastable retained-β (in the case of water quenching) or transformed-β (in the case of air cooling). The α-β annealed alloys have lower yield stresses, lower ultimate tensile stresses, and higher ductility (Table 9) than β-annealed alloys. Alloys water-quenched from the α-β field exhibit higher ductility than the air-cooled and furnace-cooled alloys, whereas the yield stress and ultimate tensile stress are not significantly altered by varying the cooling rates. The highest ductility values are obtained for the alloys quenched from the lower temperature in the α-β field. Thus, the microstructure conducive to high ductility is that containing a high volume-fraction of α and retained β. Possible reasons for the decrease of ductility with slower cooling-rate are (1) a coarser α-β microstructure and (2) possible precipitation of α_2 during cooling.

The effect of rare-earth additives on the ductility is prominent in the α-β annealed alloys. The ductility is increased considerably with the addition of Y and Er. The influence of annealing temperature and cooling rate on the ductility of the alloys is shown in Figure 32. Water-quenched alloys show a strong dependence of ductility on annealing temperature, but the ductility of air-cooled alloys does not vary significantly with changes in annealing temperatures. In the furnace-cooled alloys, only the Y-containing alloys show a dependence of ductility on annealing temperature. The increased ductility of Ti-6Al-4V-0.050Y and Ti-6Al-4V-0.30Y furnace-cooled from 1020°C results from the finer colony size in these alloys (Figure 33). Under all conditions of annealing temperature and cooling rate, the rare-earth-bearing alloys exhibit higher ductility than the reference alloy.

The variation of ultimate tensile stress with annealing temperature and cooling rate is shown in Figure 34. Only the water-quenched alloys show a strong dependence of ultimate tensile stress on annealing temperature.

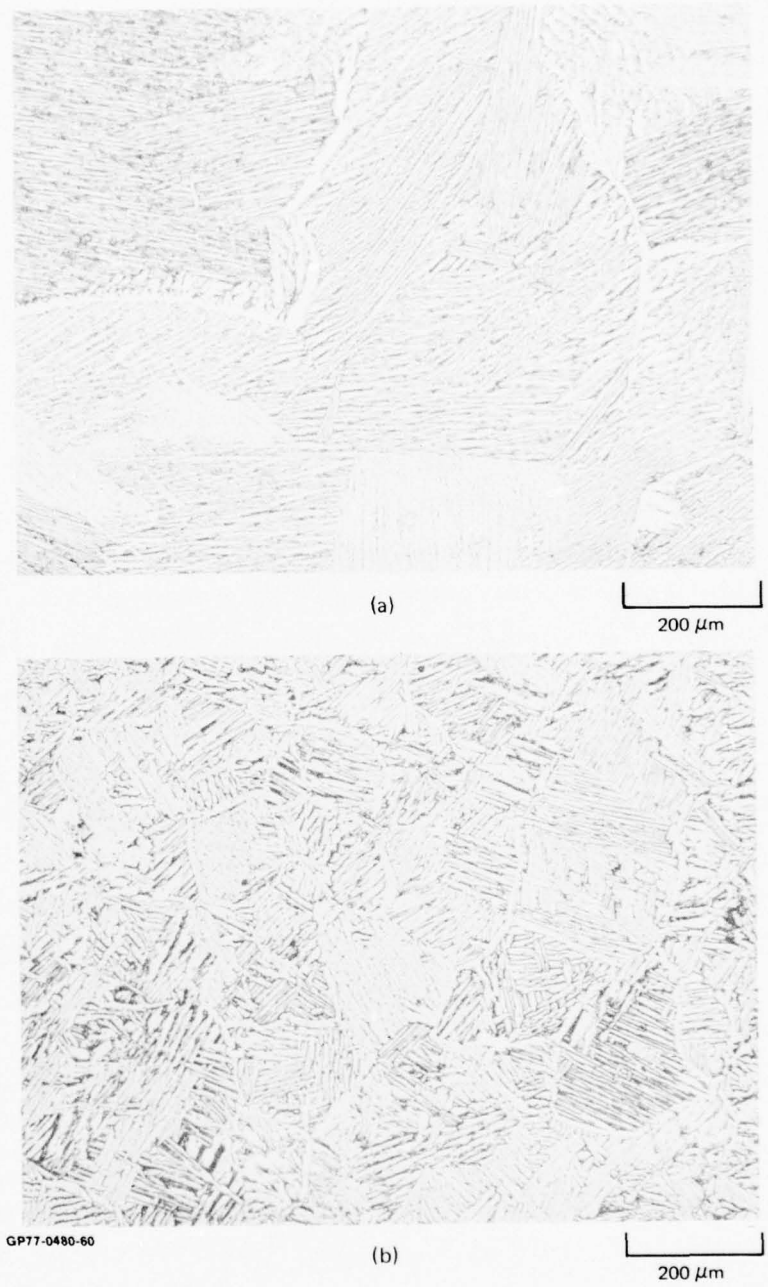

Figure 31. Microstructures of alpha beta annealed and air-cooled (a) Ti-6Al-4V reference alloy and (b) Ti-6Al-4V-0.050Y (heat treatment I, Figure 14).

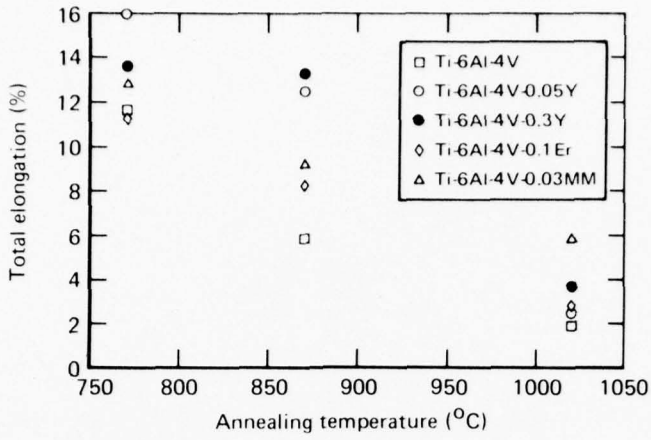

(a)

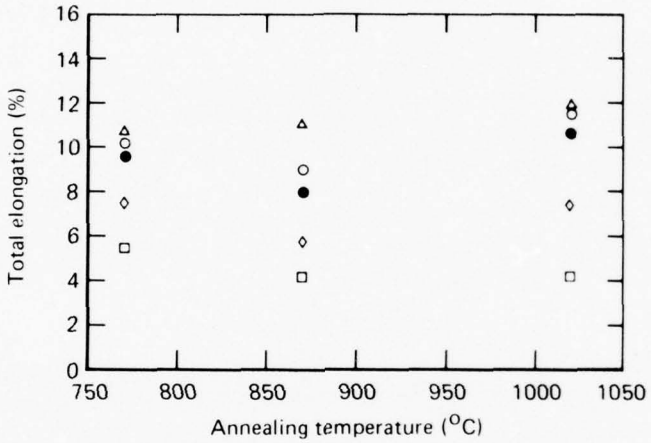

(b)

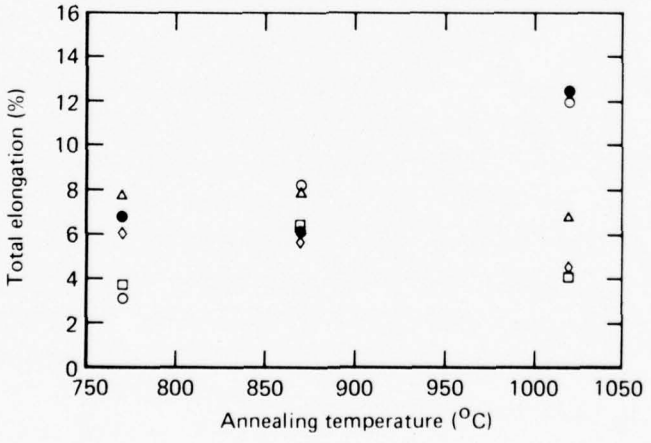

(c)

GP77-0480-77

Figure 32. Total elongation of Ti-6Al-4V-RE alloys annealed at 770, 870, and 1020°C; (□) Ti-6Al-4V reference alloy, (○) Ti-6Al-4V-0.050Y, (●) Ti-6Al-4V-0.30Y, (◇) Ti-6Al-4V-0.10Er, and (△) Ti-6Al-4V-0.030MM; (a) water quenched, (b) air cooled, and (c) furnace cooled.

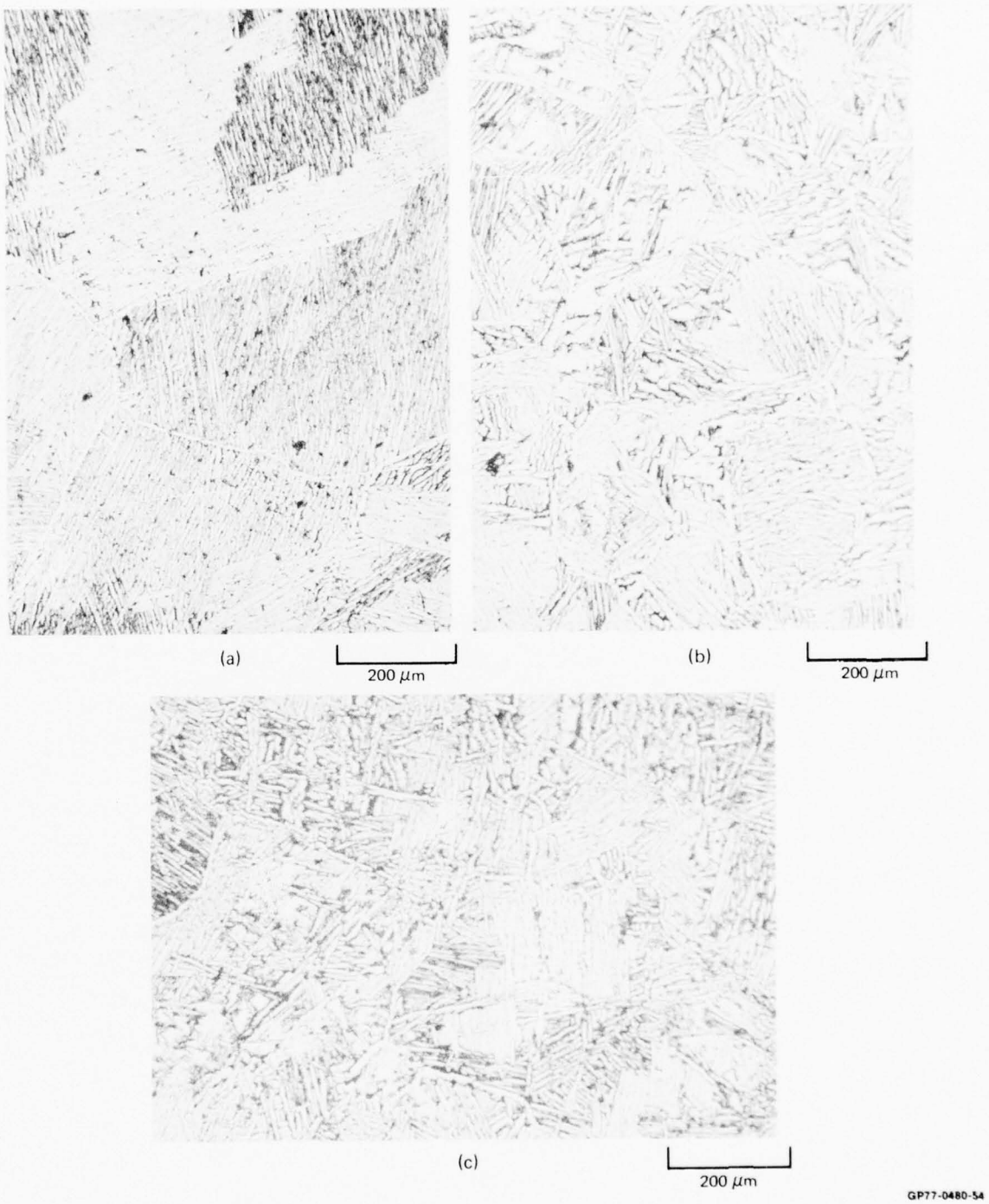

Figure 33. Microstructures of beta-annealed and furnace-cooled (a) Ti-6Al-4V reference alloy, (b) Ti-6Al-4V-0.050Y, and (c) Ti-6Al-4V-0.30Y (heat treatment D, Figure 14).

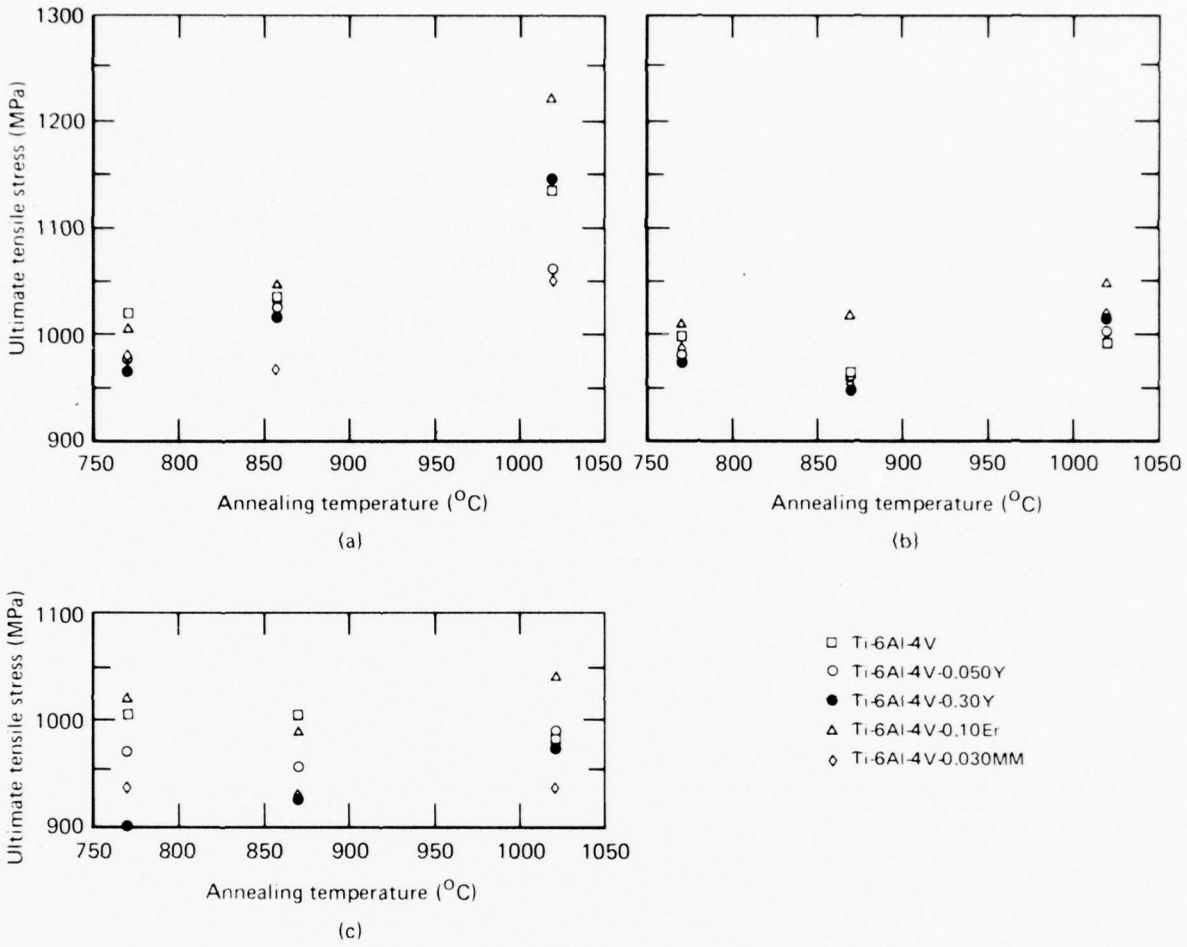

Figure 34. Ultimate tensile strength of Ti-6Al-4V-RE alloys annealed at 770, 870, and 1020°C; (□) Ti-6Al-4V reference alloy, (○) Ti-6Al-4V-0.050Y, (●) Ti-6Al-4V-0.30Y, (△) Ti-6Al-4V-0.10Er, and (◇) Ti-6Al-4V-0.030MM; (a) water quenched, (b) air cooled, and (c) furnace cooled.

5. FRACTOGRAPHY AND DEFORMATION SUBSTRUCTURES

The surfaces of specimens fractured in uniaxial tension were examined by scanning electron microscopy to determine the fracture modes and distribution of rare-earth dispersoids. The dislocation substructure in deformed specimens was studied by transmission electron microscopy of thin foils prepared from gauge sections of tensile specimens.

Figures 35a and 35b are scanning electron micrographs of fracture surfaces of reference alloy and Ti-6Al-4V-0.10Er, respectively, which were β-annealed, water-quenched, α-β annealed at 705°C for 2 h, and air cooled to room temperature. The microstructure resulting from this treatment consists of the fine-scale α+β structure similar to that shown in Figure 18. The dimple fracture observed in the alloys shows that the fracture occurred by classical void nucleation, growth, and coalescence processes. The dimple sizes in the β-annealed reference alloy range from 0.1 μm to 0.5 μm, and the plate width in the microstructure (Figure 18) varies from 0.2 μm to 2 μm. A large number of dimples smaller in size than the α-β plate width were observed. The dimple size in the Ti-6Al-4V-0.10Er alloy (Figure 35b) is smaller than in the reference alloy. The dispersoids are distributed homogeneously, as the right-hand photomicrograph in Figure 35b shows.

A comparison of the fracture appearances of β-annealed and α-β annealed alloys is given in Figures 36a and 36b, which are fractographs of Ti-6Al-4V-0.10Er. The general fractographic features are similar in all alloys that had corresponding heat treatments. In the β-annealed condition, the alloys show uniform dimples throughout the fracture surface, but the fractographic features in α-β annealed alloys consist of a mixture of dimples, which result from transformed-β, and facets, which are produced by α-phase.

The dislocation substructures in deformed specimens with different types of microstructures were examined to correlate microstructure and substructure with strength and ductility. Figures 37a and 37b show the dislocation substructures in two alloys having martensitic microstructures, which were produced by β-annealing and water-quenching. This heat treatment produces a fine α' martensite with extensive internal substructure. Because the initial dislocation density is large in these specimens and the mean slip-length is small, the alloys work-harden rapidly; stress concentrations build up early in the deformation process, and such alloys therefore fracture

after small amounts of plastic strain. Thus, all the alloys given a β-anneal and water-quench treatment (heat treatment A in Figure 27) exhibit high ultimate tensile strength and low ductility (Table 9).

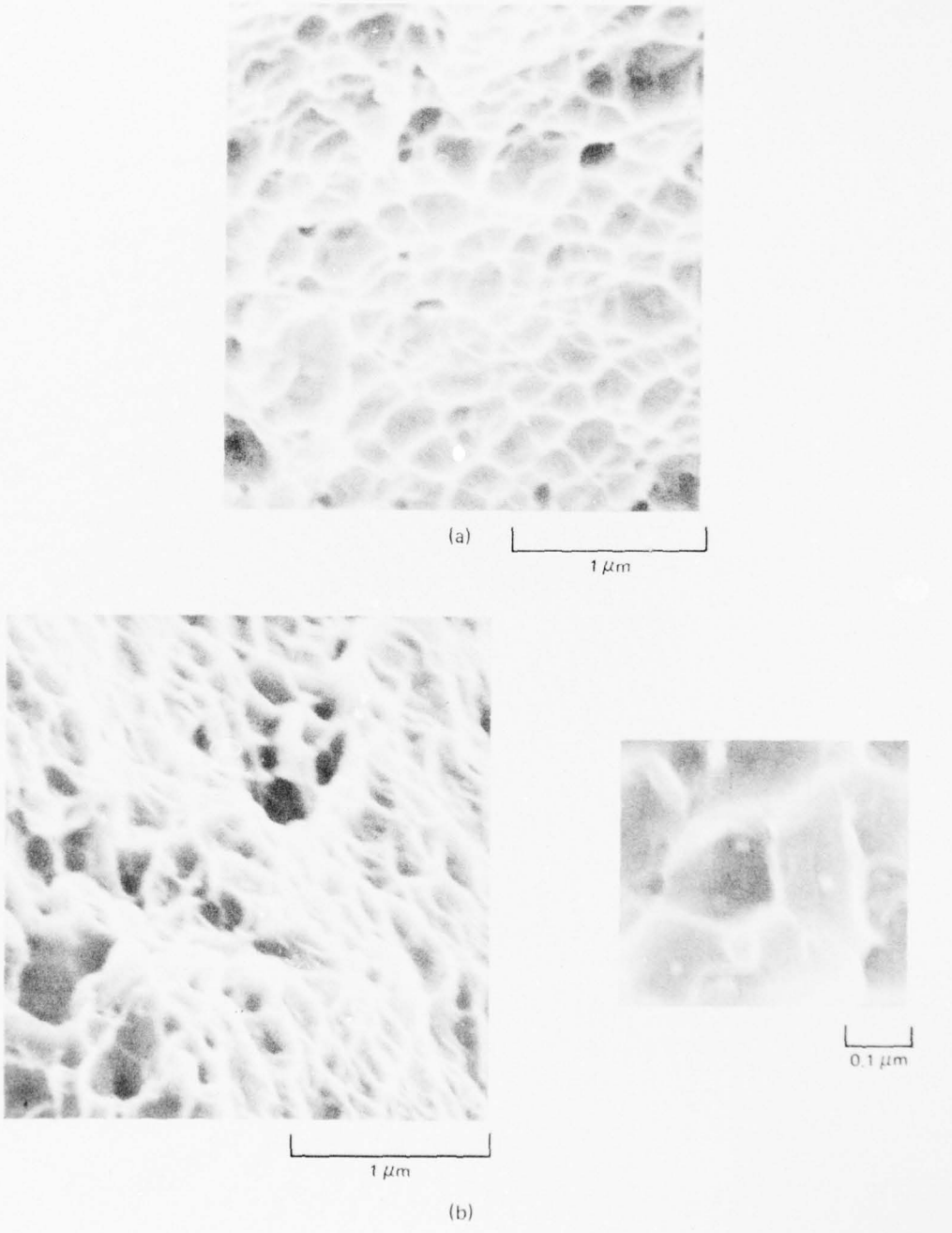

Figure 35. Fractographs of beta-annealed alloys tested in tension at room temperature; (a) Ti-6Al-4V reference alloy and (b) Ti-6Al-4V-0.10 Er.

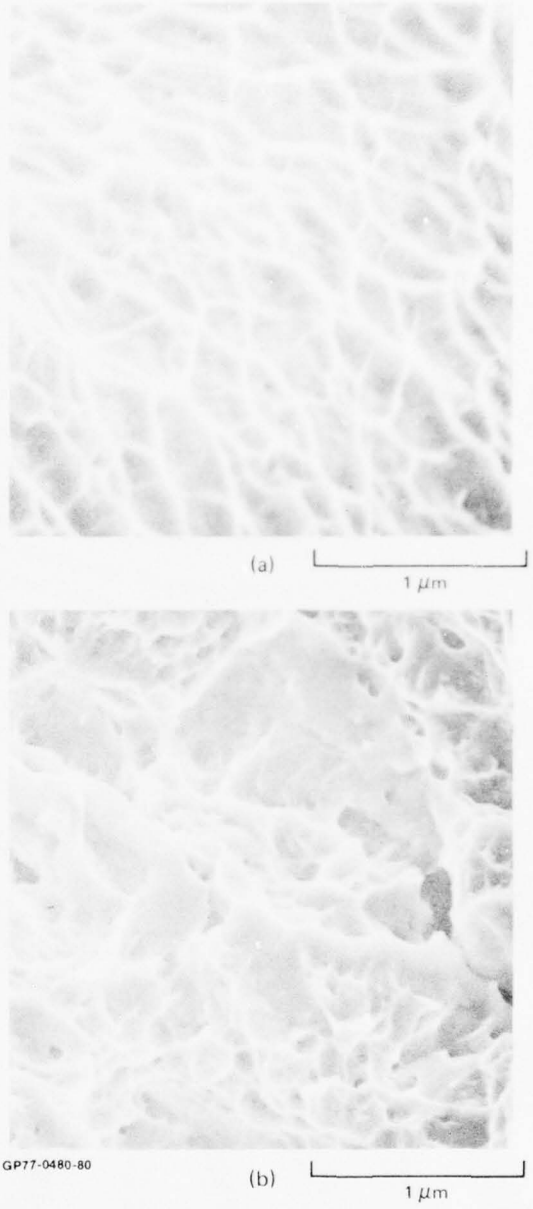

Figure 36. Fractographs of Ti-6Al-4V-0.10Er specimens tested in tension at room temperature; (a) beta annealed and (b) alpha-beta annealed.

(a)

1 μm

GP77-0480-81

(b)

1 μm

Figure 37. Deformation substructures at 3% strain in beta-annealed and water-quenched (a) Ti-6Al-4V reference alloy and (b) Ti-6Al-4V-0.10Er (heat treatment A, Figure 14).

Upon being aged at α-β temperatures, the martensitic α' decomposes by the nucleation and growth of β in α'. Simultaneously, α' approaches the equilibrium composition of α. The dislocation arrangement in a deformed alloy having the tempered martensitic structure is shown in Figure 38; beta precipitates exhibiting fringe contrast can be seen at several places. The slip length seems to be limited to the individual α plates as seen from bowed dislocation segments within the plates and lack of slip continuity across the boundaries. The alloys possessing the tempered martensite structure exhibit a high strength because of the β precipitation strengthening effect and the small slip length governed by the fine scale α-plates; the ductility, however, is low.

Figure 39 shows dislocation substructure in an α-β annealed alloy. Extensive slip activity in α grains results in a tangled dislocation structure in the α phase. The transformed-β grains exhibit extensive twinning. Figures 40a and 40b show details of dislocation activity in α phase, and Figures 40c and 40d are dark-field micrographs showing dislocation activity in the β phase. The higher ductility observed in the α-β annealed alloys is consistent with the extensive slip activity in the α alloys seen in Figures 39 and 40.

The influence of dispersoids on dislocation movement during the initial stages of deformation is shown in Figure 41. Dislocations overcome the dispersed-phase particles by the Orowan bypass[9] and Hirsch cross-slip[10] mechanisms. Figure 41 shows the formation of Orowan loops and prismatic loops around the dispersoids in the initial stages of deformation. The formation of these loops is governed by the size and spacing of the dispersoids. The dislocation arrangement in a heavily deformed α-β annealed Ti-6Al-4V-0.050Y alloy is shown in Figure 42. The dislocation structure consists of tangled dislocations in the α phase. The dominant effect of the dispersoids is to homogenize the slip and refine the substructure formed during deformation. Consequently the presence of dispersoids results in an increased ductility in all α-β annealed alloys (Table 9).

GP77-0480-82

1 μm

Figure 38. Deformation substructure at 3% strain in beta-annealed, water-quenched, and aged Ti-6Al-4V (heat treatment B, Figure 14).

GP77-0480-83

1 μm

Figure 39. Dislocation substructure in alpha-beta annealed (heat treatment E, Figure 14) Ti-6Al-4V deformed in tension at room temperature.

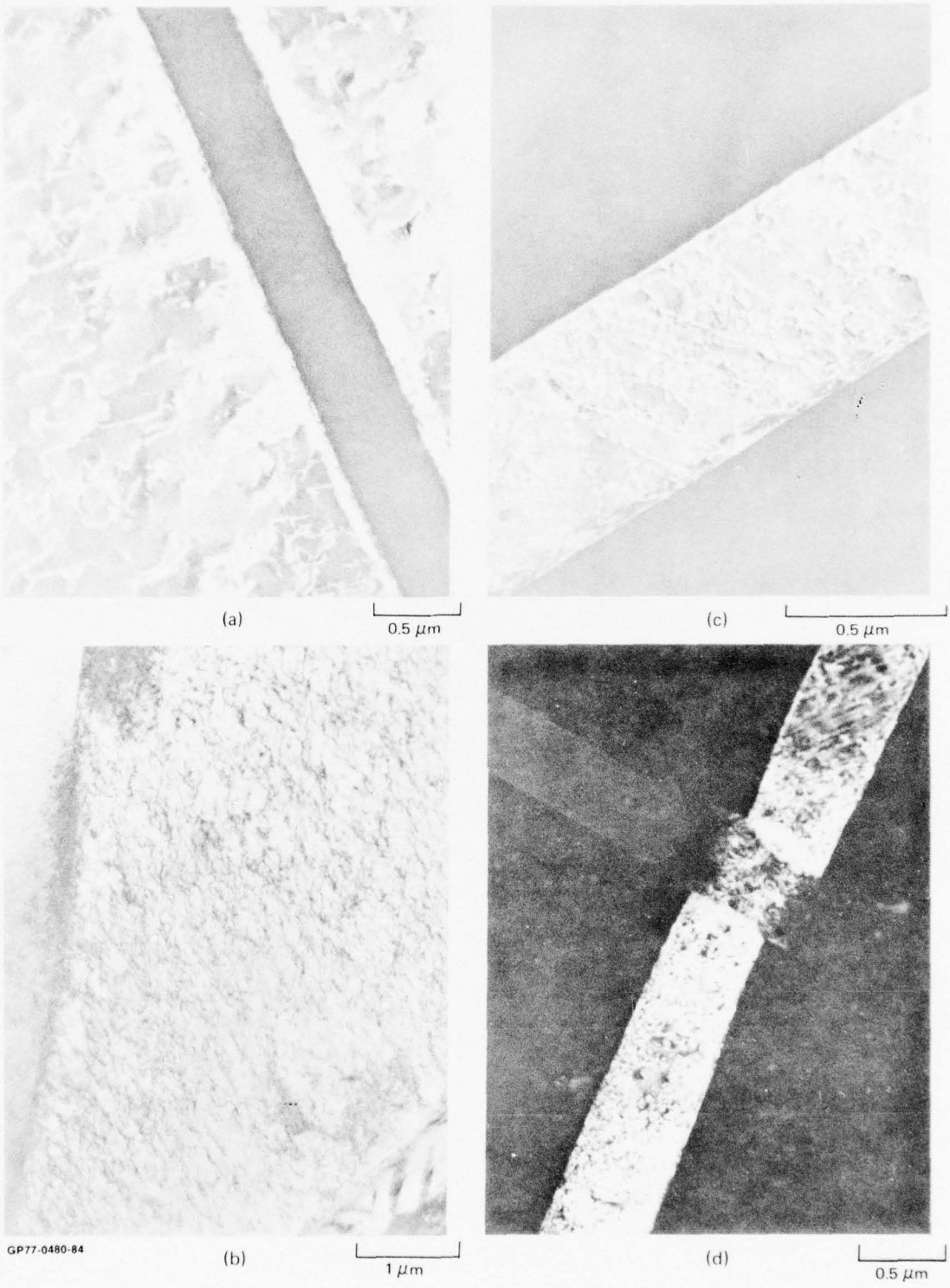

Figure 40. Dislocation activity in (a,b) alpha phase and (c,d) beta phase of alpha-beta annealed (heat treatment E, Figure 14) Ti-6Al-4V deformed in tension at room temperature.

GP77-0480-85

250 nm

Figure 41. Formation of Orowan and prismatic loops at dispersoids during the initial deformation of Ti-6Al-4V.

Figure 42. Dislocation substructure in alpha-beta annealed (heat treatment E, Figure 14) Ti-6Al-4V-0.050Y deformed in tension at room temperature.

6. CONCLUSIONS

The addition of small concentrations (< 1 wt%) of metallic Y or Er to Ti-6Al-4V results in a uniform dispersion of small (< 70 nm diam) second-phase precipitates in the alloy matrix. Both Er and Y effect grain-refinement and microstructural homogeneity in as-cast Ti-6Al-4V and retard grain growth during annealing at temperatures above the β-transus temperature.

The addition of small concentrations of mischmetal to Ti-6Al-4V results in a dispersion of particles that probably are oxides and aluminides. Although mischmetal produces grain-refinement, it is less than that effected by Er or Y.

Yttrium and erbium, in concentrations > 0.1 wt%, slightly lower the β-transus temperature of Ti-6Al-4V, but mischmetal in concentrations $\leq$ 0.08 wt% does not significantly alter the β-transus temperature. Yttrium and erbium act as β-phase stabilizers, and mischmetal is an α-phase stabilizer in Ti-6Al-4V.

The rolling pressures required for hot-rolling Ti-6Al-4V-Y and Ti-6Al-4V-MM alloys are less than those required for standard Ti-6Al-4V. (Rolling pressures were not measured for Ti-6Al-4V-Er alloys.) Edge-cracking during rolling for Y concentrations $\leq$ 0.05 wt% and Er concentrations $\leq$ 0.1 wt% is less than for standard Ti-6Al-4V.

The transverse tensile properties of Ti-6Al-4V are not adversely affected by Y and Er concentrations $\leq$0.1 wt%. Alloys containing 0.02-0.05 wt% Y or 0.1 wt% Er exhibit excellent transverse ductility and no appreciable loss in strength.

Yttrium and erbium, by their refinement of β-grains and retardation of β-grain growth, improve the ductility of β-annealed Ti-6Al-4V. A good combination of high strength and ductility of β-annealed alloys is obtained for Y and Er concentrations $\leq$ 0.1 wt%. Mischmetal significantly reduces the yield stress of Ti-6Al-4V.

For α-β annealed alloys, the yield stress increases linearly with volume fraction of transformed-β. Er and Y increase the ductility but slightly lower the yield stress of α-β annealed Ti-6Al-4V. The yield stress of Ti-6Al-4V-Y and Ti-6Al-4V-Er alloys is more nearly equal to that of standard Ti-6Al-4V for larger volume-fractions of equiaxed-α, for which second-phase dispersion strengthening is a significant factor.

For all annealing conditions and cooling rates, Ti-6Al-4V-Y and Ti-6Al-4V-Er alloys in comparison with standard Ti-6Al-4V exhibit a ductility enhancement resulting from slip homogenization by the rare-earth dispersoids.

The slight reduction of yield stress in Ti-6Al-4V-Y and Ti-6Al-4V alloys is likely caused by lower interstitial-oxygen concentrations in these alloys because of oxygen-scavenging by the rare-earth dispersoids. This effect can be neutralized by adjusting the oxygen content of the starting material.

Desired combinations of microstructural refinement, high room-temperature strength, and high ductility can be achieved by appropriate heat-treatment of Ti-6Al-4V-0.02Y, Ti-6Al-4V-0.05Y, and Ti-6Al-4V-0.1Er. The grain-refinement and grain-growth suppression by small concentrations of Y and Er are expected to significantly improve the high-temperature formability and creep behavior of Ti-6Al-4V. The fracture toughness and high-temperature properties of rare-earth-modified Ti-6Al-4V will be investigated as the next phase of this program.

REFERENCES

1. B. B. Rath, R. J. Lederich, and J. E. O'Neal, Recrystallization and Grain Growth in Ti-Rare Earth Alloys, ASM-AIME Materials Science Symposium, Cincinnati, OH, November 1975.
2. B. B. Rath, R. J. Lederich, and J. E. O'Neal, The Effects of Rare-Earth Additions on the Grain Refinement of Ti, in Grain Boundaries in in Engineering Materials, ed. by J. L. Walter, J. H. Westbrook, and D. A. Woodford (Claitors Publ. Div., Baton Rouge, LA, 1975), p. 39.
3. B. B. Rath, J. E. O'Neal, and R. J. Lederich, Grain Refinement in Ti-Er Alloys, in Proc. Electron Microscopy Soc. Am., ed. by C. J. Arceneaux, (Claitors Publ. Div., Baton Rouge, LA, 1974), p. 522.
4. Summaries of phase diagrams for the Ce-Ti, Er-Ti, La-Ti, and Ti-Y binary systems are given in: R. P. Elliot, Constitution of Binary Alloys, First Supplement (McGraw-Hill, New York, NY, 1965); F. A. Shunk, Constitution of Binary Alloys, Second Supplement (McGraw-Hill, New York, N. Y., 1969).
5. M. J. Buczek, G. S. Hall, S. R. Seagle, and H. B. Bomberger, Grain Refinement of Titanium Alloys, AFML-TR-74-255, November 1974.
6. K. A. Gschneidner, Jr., N. Kippenhan, and O. D. McMasters, Thermochemistry of the Rare Earths, Report IS-RIC-6, Rare Earth Information Center, Iowa State Univ., Ames, IA, 1973.
7. C. S. Smith, Grains, Phases, and Interfaces: An Interpretation of Microstructure, Trans. AIME 175, 15 (1948).
8. G. Welsch, G. Lützering, K. Gazioglu, and W. Bunk, Deformation Characteristics of Age Hardened Ti-6Al-4V, Met. Trans. 8A, 169 (1977).
9. E. Orowan, in Symposium on Internal Stresses in Metals and Alloys (Institute of Metals, London, 1948), p. 451.
10. P. B. Hirsch, The Interpretation of the Slip Pattern in Terms of Dislocation Movements, J. Inst. Metals 8b, 7 (1957).

APPENDIX A. ROOM-TEMPERATURE TENSILE PROPERTIES OF Ti-6Al-4V-RE ALLOYS

Tables A1-A28 list the room-temperature tensile properties for the Ti-6Al-4V reference, Ti-6Al-4V-Y, Ti-6Al-4V-Er, and Ti-6Al-4V-MM alloys that were cast, forged, rolled, and annealed in accordance with the schedule shown in Figure 1. Each of Tables A1-A12 lists the properties of a single alloy composition subjected to four different heat treatments. Tables A13-A28 list the same data as Tables A1-A12, but each of Tables A13-A28 lists the properties for a given heat treatment of all the alloy compositions. As indicated in Figure 1, each β-anneal and α-β anneal was followed by a 2-h anneal at 705°C.

TABLE A1. ROOM-TEMPERATURE TENSILE PROPERTIES OF Ti-6Al-4V REFERENCE ALLOY

Annealing temperature	Annealing time (min)	Elastic modulus (GPa)	Yield stress at 0.2% offset (MPa)	Ultimate tensile stress (MPa)	Fracture stress (MPa)	Uniform elongation (%)	Total elongation (%)
$T_\beta - 56^oC = 954^oC$	15	136	965	1005	860	5.5	14.4
	30	142	1010	1050	870	4.9	14.2
	60	118	950	1030	885	4.7	12.0
	180	138	970	1055	930	4.6	10.2
$T_\beta - 28^oC = 982^oC$	15	129	970	1050	915	3.7	10.0
	30	126	1020	1085	930	5.1	14.9
	60	131	950	1025	910	4.8	12.3
	180	120	985	1060	970	3.8	9.2
$T_\beta + 28^oC = 1038^oC$	5	138	1045	1125	990	2.5	12.0
	15	150	1085	1165	1105	2.4	9.2
	30	147	1085	1040	1110	2.2	7.2
	60	138	1070	1155	1140	1.9	3.2
$T_\beta + 56^oC = 1066^oC$	5	130	1020	1105	990	3.8	12.1
	15	141	1090	1170	1155	2.6	5.8
	30	170	1090	1145	1120	3.2	7.8
	60	128	1105	1165	1160	2.4	4.8

GP77-0480-10

TABLE A2. ROOM-TEMPERATURE TENSILE PROPERTIES OF Ti-6Al-4V-0.020Y

Annealing temperature	Annealing time (min)	Elastic modulus (GPa)	Yield stress at 0.2% offset (MPa)	Ultimate tensile stress (MPa)	Fracture stress (MPa)	Uniform elongation (%)	Total elongation (%)
$T_\beta - 56^oC = 954^oC$	15	137	945	985	840	5.0	13.0
	30	134	950	990	835	5.0	12.5
	60	158	885	975	950	5.9	13.8
	180	125	920	995	855	3.9	10.4
$T_\beta - 28^oC = 982^oC$	15	140	965	1010	835	4.3	12.1
	30	128	970	1040	925	3.7	8.3
	60	142	970	1040	930	3.8	8.3
	180	121	1005	1075	915	3.3	10.8
$T_\beta + 28^oC = 1038^oC$	5	148	990	1060	940	3.6	10.9
	15	154	1040	1110	1000	3.4	9.9
	30	128	1000	1055	945	4.5	11.1
	60	150	1030	1090	1000	3.0	9.2
$T_\beta + 56^oC = 1066^oC$	5	144	1035	1090	980	4.0	10.3
	15	158	1015	1095	1040	3.8	9.9
	30	170	1035	1105	1065	3.8	9.4
	60	150	1070	1130	1015	3.6	8.4

GP77-0480-11

TABLE A3. ROOM-TEMPERATURE TENSILE PROPERTIES OF Ti-6Al-4V-0.050Y

Annealing temperature	Annealing time (min)	Elastic modulus (GPa)	Yield stress at 0.2% offset (MPa)	Ultimate tensile stress (MPa)	Fracture stress (MPa)	Uniform elongation (%)	Total elongation (%)
$T_\beta - 56^oC = 932^oC$	15	124	825	905	780	4.4	9.3
	30	128	860	945	780	5.8	14.6
	60	150	885	935	845	6.1	15.2
	180	126	860	950	825	3.7	8.5
$T_\beta - 28^oC = 960^oC$	15	127	855	960	805	5.1	11.2
	30	134	905	980	815	5.1	12.2
	60	138	905	995	865	5.0	11.5
	180	136	930	1005	870	4.4	10.4
$T_\beta + 28^oC = 1016^oC$	5					3.8	10.5
	15	152	1025	1085	950	3.0	9.0
	30	165	980	1095	975	4.1	11.1
	60	165	990	1090	975	4.4	11.4
$T_\beta + 56^oC = 1044^oC$	5	154	1000	1070	930	4.5	12.3
	15	138	1005	1070	940	4.1	12.1
	30	150	1045	1100	970	4.0	11.7
	60	128	975	1050	895	3.4	12.2

GP77-0480-12

TABLE A4. ROOM-TEMPERATURE TENSILE PROPERTIES OF Ti-6Al-4V-0.10Y

Annealing temperature	Annealing time (min)	Elastic modulus (GPa)	Yield stress at 0.2% offset (MPa)	Ultimate tensile stress (MPa)	Fracture stress (MPa)	Uniform elongation (%)	Total elongation (%)
$T_\beta - 56^oC = 932^oC$	15	129	870	940	760	6.0	13.5
	30	135	920	980	815	5.7	12.7
	60	135	910	1000	840	5.3	13.7
	180	125	900	975	810	4.8	13.3
$T_\beta - 28^oC = 960^oC$	15	126	880	965	820	5.2	12.3
	30	147	990	1030	865	5.1	12.4
	60	142	930	1015	890	5.1	13.8
	180	130	920	1010	880	3.9	10.9
$T_\beta + 28^oC = 1016^oC$	5	148	960	1060	940	3.3	10.0
	15	124	1030	1090	980	3.9	10.4
	30	135	1030	1115	1005	4.3	11.3
	60	158	1025	1110	1010	3.3	9.2
$T_\beta + 56^oC = 1044^oC$	5	148	1020	1090	955	3.9	12.0
	15	136	1005	1070	925	3.8	13.0
	30	151	1015	1075	955	3.7	10.6
	60	142	1030	1100	975	4.0	11.5

GP77-0480-13

TABLE A5. ROOM-TEMPERATURE TENSILE PROPERTIES OF Ti-6Al-4V-0.30Y

Annealing temperature	Annealing time (min)	Elastic modulus (GPa)	Yield stress at 0.2% offset (MPa)	Ultimate tensile stress (MPa)	Fracture stress (MPa)	Uniform elongation (%)	Total elongation (%)
$T_\beta - 56^oC = 932^oC$	15	140	900	940	790	5.7	13.2
	30	139	885	950	810	6.0	13.0
	60	124	935	965	830	6.0	13.4
	180	136	905	970	835	4.8	10.0
$T_\beta - 28^oC = 960^oC$	15	128	930	965	825	3.5	10.5
	30	142	1000	1040	900	4.9	12.3
	60	135	960	1045	900	4.9	12.5
	180	142	1000	1060	945	4.7	11.3
$T_\beta + 28^oC = 1016^oC$	5	143	1010	1080	950	3.8	11.5
	15	156	1045	1105	960	3.4	9.8
	30	168	1045	1120	960	3.9	11.1
	60	142	1090	1145	1020	3.6	10.6
$T_\beta + 56^oC = 1044^oC$	5	148	1030	1105	965	3.4	10.2
	15	150	1020	1115	970	4.3	12.5
	30	162	1050	1120	960	4.2	14.2
	60	140	1035	1100	970	2.8	8.5

GP77-0480-14

TABLE A6. ROOM-TEMPERATURE TENSILE PROPERTIES OF Ti-6Al-4V-0.010MM

Annealing temperature	Annealing time (min)	Elastic modulus (GPa)	Yield stress at 0.2% offset (MPa)	Ultimate tensile stress (MPa)	Fracture stress (MPa)	Uniform elongation (%)	Total elongation (%)
$T_\beta - 56^oC = 932^oC$	15	123	845	920	795	6.1	12.9
	30	126	905	945	800	6.8	14.4
	60	128	855	940	810	5.8	12.0
	180	145	875	950	825	5.4	11.0
$T_\beta - 28^oC = 960^oC$	15	133	870	935	815	5.7	11.7
	30	128	905	970	830	6.1	12.5
	60	150	900	995	875	4.7	9.8
	180	126	955	1020	895	4.7	10.8
$T_\beta + 28^oC = 1016^oC$	5	150	945	1030	945	3.9	9.1
	15	144	1030	1095	1040	3.3	8.2
	30	134	1030	1090	990	3.2	8.3
	60	144	1020	1080	1005	2.9	7.3
$T_\beta + 56^oC = 1044^oC$	5	159	970	1065	965	4.0	10.7
	15	158	1005	1075	1035	3.8	8.3
	30	156	1010	1060	1020	3.3	8.0
	60	147	995	1075	1020	3.0	8.8

GP77-0480-15

TABLE A7. ROOM-TEMPERATURE TENSILE PROPERTIES OF Ti-6Al-4V-0.030MM

Annealing temperature	Annealing time (min)	Elastic modulus (GPa)	Yield stress at 0.2% offset (MPa)	Ultimate tensile stress (MPa)	Fracture stress (MPa)	Uniform elongation (%)	Total elongation (%)
$T_\beta - 56^oC = 932^oC$	15	128	840	900	770	4.8	12.9
	30	134	915	950	815	5.9	12.9
	60	142	890	930	780	6.2	14.1
	180	127	815	925	815	6.1	12.8
$T_\beta - 28^oC = 960^oC$	15	127	855	940	820	5.1	10.8
	30	140	845	950	840	6.3	12.3
	60	137	920	980	830	5.8	13.3
	180	123	900	960	865	5.7	12.2
$T_\beta + 28^oC = 1016^oC$	5	141	985	1055	1000	5.0	9.5
	15	150	1015	1055	990	3.8	9.1
	30	146	1040	1090	1030	4.1	9.1
	60	136	985	1050	995	2.1	5.3
$T_\beta + 56^oC = 1044^oC$	5	134	1015	1085	980	3.0	8.8
	15	150	1025	1080	1040	4.3	9.5
	30	129	1005	1070	1030	3.3	8.0
	60	141	1025	1070	1045	3.3	6.3

GP77-0480-16

TABLE A8. ROOM-TEMPERATURE TENSILE PROPERTIES OF Ti-6Al-4V-0.080MM

Annealing temperature	Annealing time (min)	Elastic modulus (GPa)	Yield stress at 0.2% offset (MPa)	Ultimate tensile stress (MPa)	Fracture stress (MPa)	Uniform elongation (%)	Total elongation (%)
$T_\beta - 56^oC = 932^oC$	15	137	890	930	825	6.4	13.3
	30	147	925	970	935	6.8	14.2
	60	132	925	970	870	6.1	12.8
	180	133	870	955	855	6.3	13.8
$T_\beta - 28^oC = 960^oC$	15	133	920	970	845	5.6	13.5
	30	124	950	1000	885	5.1	11.6
	60	119	890	985	910	6.0	13.1
	180	143	915	990	890	5.4	11.9
$T_\beta + 28^oC = 1016^oC$	5	120	1015	1070	1035	3.5	7.7
	15	153	1005	1090	1050	3.0	6.8
	30	150	1035	1105	1055	4.3	9.9
	60	154	1050	1110	1095	4.2	9.4
$T_\beta + 56^oC = 1044^oC$	5	144	1020	1090	1030	3.8	8.7
	15	141	1020	1085	1050	3.7	8.3
	30	158	1020	1085	1055	3.9	8.6
	60	142	1000	1055	1045	3.3	6.6

GP77-0480-17

TABLE A9. ROOM-TEMPERATURE TENSILE PROPERTIES OF Ti-6Al-4V-0.10Er

Annealing temperature	Annealing time (min)	Elastic modulus (GPa)	Yield stress at 0.2% offset (MPa)	Ultimate tensile stress (MPa)	Fracture stress (MPa)	Uniform elongation (%)	Total elongation (%)
$T_\beta - 56^oC = 948^oC$	15	139	930	995	815	5.5	16.1
	30	168	950	1010	830	5.2	14.8
	60	154	975	1025	830	4.9	14.8
	180	145	955	1005	835	4.4	13.0
$T_\beta - 28^oC = 976^oC$	15	133	985	1030	830	4.3	12.8
	30	130	1010	1060	850	4.2	13.8
	60	147	1030	1085	865	4.1	15.2
	180	140	1020	1080	860	3.5	14.0
$T_\beta + 28^oC = 1032^oC$	5	135	1015	1075	925	3.4	11.8
	15	138	1060	1125	1000	3.7	11.0
	30	132	1055	1115	995	3.5	9.6
	60	134	1045	1120	1015	3.5	9.9
$T_\beta + 56^oC = 1060^oC$	5	149	1020	1105	970	3.7	11.2
	15	138	1045	1105	985	3.7	10.7
	30	142	1080	1150	1020	3.3	11.4
	60	143	1055	1125	1095	4.2	8.6

GP77-0480-18

TABLE A10. ROOM-TEMPERATURE TENSILE PROPERTIES OF Ti-6Al-4V-0.30Er

Annealing temperature	Annealing time (min)	Elastic modulus (GPa)	Yield stress at 0.2% offset (MPa)	Ultimate tensile stress (MPa)	Fracture stress (MPa)	Uniform elongation (%)	Total elongation (%)
$T_\beta - 56^oC = 926^oC$	15	103	870	910	760	5.1	14.0
	30	106	860	915	735	5.5	15.7
	60	102	850	900	740	4.7	13.6
	180	113	885	935	810	4.7	12.1
$T_\beta - 28^oC = 954^oC$	15	109	965	1020	820	4.3	12.2
	30	108	960	1015	840	4.6	13.3
	60	103	940	1000	825	4.6	13.4
	180	107	985	1040	–	–	2.6
$T_\beta + 28^oC = 1010^oC$	5	132	1005	1075	910	3.5	12.2
	15	132	1005	1075	925	3.3	10.5
	30	135	1015	1105	960	3.5	12.0
	60	130	975	1040	870	3.8	11.9
$T_\beta + 56^oC = 1038^oC$	5	132	955	1040	880	3.7	10.8
	15	138	975	1045	895	3.5	10.6
	30	142	985	1070	930	3.5	10.2
	60	165	1005	1095	950	3.7	12.1

GP77-0480-19

TABLE A11. ROOM-TEMPERATURE TENSILE PROPERTIES OF Ti-6Al-4V-0.80Er (INGOT 27)

Annealing temperature	Annealing time (min)	Elastic modulus (GPa)	Yield stress at 0.2% offset (MPa)	Ultimate tensile stress (MPa)	Fracture stress (MPa)	Uniform elongation (%)	Total elongation (%)
$T_\beta - 56^oC = 926^oC$	15	144	855	965	760	4.9	13.2
	30						
	60	131	865	925	780	4.9	12.1
	180	125	840	900	765	5.1	12.6
$T_\beta - 28^oC = 954^oC$	15	133	955	1005	825	4.8	12.0
	30						
	60	129	935	985	860	4.0	8.6
	180	139	935	995	850	3.2	9.2
$T_\beta + 28^oC = 1010^oC$	5						
	15	135	970	1050	910	4.3	10.8
	30						
	60	165	980	1080	930	3.8	10.2
$T_\beta + 56^oC = 1038^oC$	5	139	965	1055	925	4.5	10.7
	15						
	30	146	960	1045	910	3.6	10.5
	60	147	945	1010	875	3.1	9.6

GP77-0480-20

TABLE A12. ROOM-TEMPERATURE TENSILE PROPERTIES OF Ti-6Al-4V-0.80Er (INGOT 29)

Annealing temperature	Annealing time (min)	Elastic modulus (GPa)	Yield stress at 0.2% offset (MPa)	Ultimate tensile stress (MPa)	Fracture stress (MPa)	Uniform elongation (%)	Total elongation (%)
$T_\beta - 56^oC = 926^oC$	15	129	875	905	720	5.9	14.2
	30	138	880	910	755	5.6	13.6
	60	150	890	915	780	5.4	11.7
	180	123	885	920	795	5.0	11.8
$T_\beta - 28^oC = 954^oC$	15	140	970	1015	860	3.9	10.3
	30	140	930	980	840	4.6	11.7
	60	142	965	1015	870	3.8	10.2
	180	140	970	1020	905	4.2	11.4
$T_\beta + 28^oC = 1010^oC$	5	148	980	1060	960	3.6	10.4
	15	144	1000	1070	955	3.9	10.3
	30	147	1010	1080	970	3.4	9.7
	60	164	1000	1095	940	4.1	11.8
$T_\beta + 56^oC = 1038^oC$	5	158	955	1065	940	4.2	11.3
	15	140	1015	1085	1035	3.7	9.2
	30	148	1030	1070	970	3.4	8.7
	60	150	1040	1110	990	3.2	9.7

GP77-0480-21

TABLE A13. ROOM-TEMPERATURE TENSILE PROPERTIES OF Ti-6Al-4V-RE ALLOYS ANNEALED AT T_β – 56°C FOR 15 min

Alloy composition	Annealing temperature, T_β – 56°C (°C)	Elastic modulus (GPa)	Yield stress at 0.2% offset (MPa)	Ultimate tensile stress (MPa)	Fracture stress (MPa)	Uniform elongation (%)	Total elongation (%)
Ti-6Al-4V	954	136	965	1005	860	5.5	14.4
Ti-6Al-4V-0.020Y	954	137	945	985	840	5.0	13.0
Ti-6Al-4V-0.050Y	932	124	825	905	780	4.4	9.3
Ti-6Al-4V-0.10Y	932	129	870	940	760	6.0	13.5
Ti-6Al-4V-0.30Y	932	140	900	940	790	5.7	13.2
Ti-6Al-4V-0.010MM	932	123	845	920	795	6.1	12.9
Ti-6Al-4V-0.030MM	932	128	840	900	770	4.8	12.9
Ti-6Al-4V-0.080MM	932	137	890	930	825	6.4	13.3
Ti-6Al-4V-0.10Er	948	139	930	995	815	5.5	16.1
Ti-6Al-4V-0.30Er	926	103	870	910	760	5.1	14.0
Ti-6Al-4V-0.80Er (Ingot 27)	926	144	855	965	760	4.9	13.2
Ti-6Al-4V-0.80Er (Ingot 29)	926	129	875	905	720	5.9	14.2

GP77-0480-22

TABLE A14. ROOM-TEMPERATURE TENSILE PROPERTIES OF Ti-6Al-4V-RE ALLOYS ANNEALED AT T_β – 56°C FOR 30 min

Alloy composition	Annealing temperature, T_β – 56°C (°C)	Elastic modulus (GPa)	Yield stress at 0.2% offset (MPa)	Ultimate tensile stress (MPa)	Fracture stress (MPa)	Uniform elongation (%)	Total elongation (%)
Ti-6Al-4V	954	142	1010	1050	870	4.9	14.2
Ti-6Al-4V-0.020Y	954	134	950	990	835	5.0	12.5
Ti-6Al-4V-0.050Y	932	128	860	945	780	5.8	14.6
Ti-6Al-4V-0.10Y	932	135	920	980	815	5.7	12.7
Ti-6Al-4V-0.30Y	932	139	885	950	810	6.0	13.0
Ti-6Al-4V-0.010MM	932	126	905	945	800	6.8	14.4
Ti-6Al-4V-0.030MM	932	134	915	950	815	5.9	12.9
Ti-6Al-4V-0.080MM	932	147	925	970	935	6.8	14.2
Ti-6Al-4V-0.10Er	948	168	950	1010	830	5.2	14.8
Ti-6Al-4V-0.30Er	926	106	860	915	735	5.5	15.7
Ti-6Al-4V-0.80Er (Ingot 27)	926						
Ti-6Al-4V-0.80Er (Ingot 29)	926	138	880	910	755	5.6	13.6

GP77-0480-23

TABLE A15. ROOM-TEMPERATURE TENSILE PROPERTIES OF Ti-6Al-4V-RE ALLOYS ANNEALED AT $T_\beta - 56^oC$ FOR 60 min

Alloy composition	Annealing temperature, $T_\beta - 56^oC$ (^oC)	Elastic modulus (GPa)	Yield stress at 0.2% offset (MPa)	Ultimate tensile stress (MPa)	Fracture stress (MPa)	Uniform elongation (%)	Total elongation (%)
Ti-6Al-4V	954	118	950	1030	885	4.7	12.0
Ti-6Al-4V-0.020Y	954	158	885	975	950	5.9	13.8
Ti-6Al-4V-0.050Y	932	150	885	935	845	6.1	15.2
Ti-6Al-4V-0.10Y	932	135	910	1000	840	5.3	13.7
Ti-6Al-4V-0.30Y	932	124	935	965	830	6.0	13.4
Ti-6Al-4V-0.010MM	932	128	855	940	810	5.8	12.0
Ti-6Al-4V-0.030MM	932	142	890	930	780	6.2	14.1
Ti-6Al-4V-0.080MM	932	132	925	970	870	6.1	12.8
Ti-6Al-4V-0.10Er	948	154	975	1025	830	4.9	14.8
Ti-6Al-4V-0.30Er	926	102	850	900	740	4.7	13.6
Ti-6Al-4V-0.80Er (Ingot 27)	926	131	865	925	780	4.9	12.1
Ti-6Al-4V-0.80Er (Ingot 29)	926	150	890	915	780	5.4	11.7

GP77-0480-24

TABLE A16. ROOM-TEMPERATURE TENSILE PROPERTIES OF Ti-6Al-4V-RE ALLOYS ANNEALED AT $T_\beta - 56^oC$ FOR 180 min

Alloy composition	Annealing temperature, $T_\beta - 56^oC$ (^oC)	Elastic modulus (GPa)	Yield stress at 0.2% offset (MPa)	Ultimate tensile stress (MPa)	Fracture stress (MPa)	Uniform elongation (%)	Total elongation (%)
Ti-6Al-4V	954	138	970	1055	930	4.6	10.2
Ti-6Al-4V-0.020Y	954	125	920	995	855	3.9	10.4
Ti-6Al-4V-0.050Y	932	136	860	950	825	3.7	8.5
Ti-6Al-4V-0.10Y	932	125	900	975	810	4.8	13.3
Ti-6Al-4V-0.30Y	932	136	905	970	835	4.8	10.0
Ti-6Al-4V-0.010MM	932	145	875	950	825	5.4	11.0
Ti-6Al-4V-0.030MM	932	127	815	925	815	6.1	12.8
Ti-6Al-4V-0.080MM	932	133	870	955	855	6.3	13.8
Ti-6Al-4V-0.10Er	948	145	955	1005	835	4.4	13.0
Ti-6Al-4V-0.30Er	926	113	885	935	810	4.7	12.1
Ti-6Al-4V-0.80Er (Ingot 27)	926	125	840	900	765	5.1	12.6
Ti-6Al-4V-0.80Er (Ingot 29)	926	123	885	920	795	5.0	11.8

GP77-0480-25

TABLE A17. ROOM-TEMPERATURE TENSILE PROPERTIES OF Ti-6Al-4V-RE ALLOYS ANNEALED AT $T_\beta - 28^oC$ FOR 15 min

Alloy composition	Annealing temperature, $T_\beta - 28^oC$ (°C)	Elastic modulus (GPa)	Yield stress at 0.2% offset (MPa)	Ultimate tensile stress (MPa)	Fracture stress (MPa)	Uniform elongation (%)	Total elongation (%)
Ti-6Al-4V	982	129	970	1050	915	3.7	10.0
Ti-6Al-4V-0.020Y	982	140	965	1010	835	4.3	12.1
Ti-6Al-4V-0.050Y	960	127	855	960	805	5.1	11.2
Ti-6Al-4V-0.10Y	960	126	880	965	820	5.2	12.3
Ti-6Al-4V-0.30Y	960	128	930	965	825	3.5	10.5
Ti-6Al-4V-0.010MM	960	133	870	935	815	5.7	11.7
Ti-6Al-4V-0.030MM	960	127	855	940	820	5.1	10.8
Ti-6Al-4V-0.080MM	960	133	920	970	845	5.6	13.5
Ti-6Al-4V-0.10Er	976	133	985	1030	830	4.3	12.8
Ti-6Al-4V-0.30Er	954	109	965	1020	820	4.3	12.2
Ti-6Al-4V-0.80Er (Ingot 27)	954	133	955	1005	825	4.8	12.0
Ti-6Al-4V-0.80Er (Ingot 29)	954	140	970	1015	860	3.9	10.3

GP77-0480-26

TABLE A18. ROOM-TEMPERATURE TENSILE PROPERTIES OF Ti-6Al-4V-RE ALLOYS ANNEALED AT $T_\beta - 28^oC$ FOR 30 min

Alloy composition	Annealing temperature, $T_\beta - 28^oC$ (°C)	Elastic modulus (GPa)	Yield stress at 0.2% offset (MPa)	Ultimate tensile stress (MPa)	Fracture stress (MPa)	Uniform elongation (%)	Total elongation (%)
Ti-6Al-4V	982	126	1020	1085	930	5.1	14.9
Ti-6Al-4V-0.020Y	982	128	970	1040	925	3.7	8.3
Ti-6Al-4V-0.050Y	960	134	905	980	815	5.1	12.2
Ti-6Al-4V-0.10Y	960	147	990	1030	865	5.1	12.4
Ti-6Al-4V-0.30Y	960	142	1000	1040	900	4.9	12.3
Ti-6Al-4V-0.010MM	960	128	905	970	830	6.1	12.5
Ti-6Al-4V-0.030MM	960	140	845	950	840	6.3	12.3
Ti-6Al-4V-0.080MM	960	124	950	1000	885	5.1	11.6
Ti-6Al-4V-0.10Er	976	130	1010	1060	850	4.2	13.8
Ti-6Al-4V-0.30Er	954	108	960	1015	840	4.6	13.3
Ti-6Al-4V-0.80Er (Ingot 27)	954						
Ti-6Al-4V-0.80Er (Ingot 29)	954	140	930	980	840	4.6	11.7

GP77-0480-27

TABLE A19. ROOM-TEMPERATURE TENSILE PROPERTIES OF Ti-6Al-4V-RE ALLOYS ANNEALED AT $T_\beta - 28^oC$ FOR 60 min

Alloy composition	Annealing temperature, $T_\beta - 28^oC$ (°C)	Elastic modulus (GPa)	Yield stress at 0.2% offset (MPa)	Ultimate tensile stress (MPa)	Fracture stress (MPa)	Uniform elongation (%)	Total elongation (%)
Ti-6Al-4V	982	131	950	1025	910	4.8	12.3
Ti-6Al-4V-0.020Y	982	142	970	1040	930	3.8	8.3
Ti-6Al-4V-0.050Y	960	138	905	995	865	5.0	11.5
Ti-6Al-4V-0.10Y	960	142	930	1015	890	5.1	13.8
Ti-6Al-4V-0.30Y	960	135	960	1045	900	4.9	12.5
Ti-6Al-4V-0.010MM	960	150	900	995	875	4.7	9.8
Ti-6Al-4V-0.030MM	960	137	920	980	830	5.8	13.3
Ti-6Al-4V-0.080MM	960	119	980	985	910	6.0	13.1
Ti-6Al-4V-0.10Er	976	147	1030	1085	865	4.1	15.2
Ti-6Al-4V-0.30Er	954	103	940	1000	825	4.6	13.4
Ti-6Al-4V-0.80Er (Ingot 27)	954	129	935	985	860	4.0	8.6
Ti-6Al-4V-0.80Er (Ingot 29)	954	142	965	1015	870	3.8	10.2

GP77-0480-28

TABLE A20. ROOM-TEMPERATURE TENSILE PROPERTIES OF Ti-6Al-4V-RE ALLOYS ANNEALED AT $T_\beta - 28^oC$ FOR 180 min

Alloy composition	Annealing temperature, $T_\beta - 28^oC$ (°C)	Elastic modulus (GPa)	Yield stress at 0.2% offset (MPa)	Ultimate tensile stress (MPa)	Fracture stress (MPa)	Uniform elongation (%)	Total elongation (%)
Ti-6Al-4V	982	120	985	1060	970	3.8	9.2
Ti-6Al-4V-0.020Y	982	121	1005	1075	915	3.3	10.8
Ti-6Al-4V-0.050Y	960	136	930	1005	870	4.4	10.4
Ti-6Al-4V-0.10Y	960	130	920	1010	880	3.9	10.9
Ti-6Al-4V-0.30Y	960	142	1000	1060	945	4.7	11.3
Ti-6Al-4V-0.010MM	960	126	955	1020	895	4.7	10.8
Ti-6Al-4V-0.030MM	960	123	900	960	865	5.7	12.2
Ti-6Al-4V-0.080MM	960	143	915	990	890	5.4	11.9
Ti-6Al-4V-0.10Er	976	140	1020	1080	860	3.5	14.0
Ti-6Al-4V-0.30Er	954	107	985	1040			2.6
Ti-6Al-4V-0.80Er (Ingot 27)	954	139	935	995	850	3.2	9.2
Ti-6Al-4V-0.80Er (Ingot 29)	954	140	970	1020	905	4.2	11.4

AD-A044 235 MCDONNELL DOUGLAS RESEARCH LABS ST LOUIS MO F/G 11/6
INFLUENCE OF RARE-EARTH ADDITIONS ON PROPERTIES OF TITANIUM ALL--ETC(U)
MAY 77 C R WHITSETT, S M SASTRY, J E O'NEAL N00014-76-C-0626
UNCLASSIFIED MDC-Q10627 NL

2 OF 2
AD
A044235

END
DATE FILMED
10-77
DDC

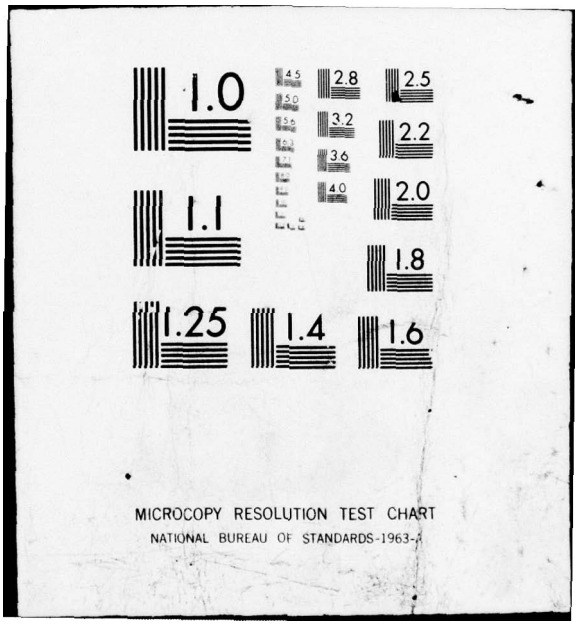
1.0
1.1
1.25
1.4
1.6
1.8
2.0
2.2
2.5
2.8
3.2
3.6
4.0
4.5
5.0
5.6
MICROCOPY RESOLUTION TEST CHART
NATIONAL BUREAU OF STANDARDS-1963-A

TABLE A21. ROOM-TEMPERATURE TENSILE PROPERTIES OF Ti-6Al-4V-RE ALLOYS ANNEALED AT T_β + 28°C FOR 5 min

Alloy composition	Annealing temperature, T_β + 28°C (°C)	Elastic modulus (GPa)	Yield stress at 0.2% offset (MPa)	Ultimate tensile stress (MPa)	Fracture stress (MPa)	Uniform elongation (%)	Total elongation (%)
Ti-6Al-4V	1038	138	1045	1125	990	2.5	12.0
Ti-6Al-4V-0.020Y	1038	148	990	1060	940	3.6	10.9
Ti-6Al-4V-0.050Y	1016					3.8	10.5
Ti-6Al-4V-0.10Y	1016	148	960	1060	940	3.3	10.0
Ti-6Al-4V-0.30Y	1016	143	1010	1080	950	3.8	11.5
Ti-6Al-4V-0.010MM	1016	150	945	1030	945	3.9	9.1
Ti-6Al-4V-0.030MM	1016	141	985	1055	1000	5.0	9.5
Ti-6Al-4V-0.080MM	1016	120	1015	1070	1035	3.5	7.7
Ti-6Al-4V-0.10Er	1032	135	1015	1075	925	3.4	11.8
Ti-6Al-4V-0.30Er	1016	132	1005	1075	910	3.5	12.2
Ti-6Al-4V-0.80Er (Ingot 27)	1010						
Ti-6Al-4V-0.80Er (Ingot 29)	1010	148	980	1060	960	3.6	10.4

GP77-0480-30

TABLE A22. ROOM-TEMPERATURE TENSILE PROPERTIES OF Ti-6Al-4V-RE ALLOYS ANNEALED AT T_β + 28°C FOR 15 min

Alloy composition	Annealing temperature, T_β + 28°C (°C)	Elastic modulus (GPa)	Yield stress at 0.2% offset (MPa)	Ultimate tensile stress (MPa)	Fracture stress (MPa)	Uniform elongation (%)	Total elongation (%)
Ti-6Al-4V	1038	150	1085	1165	1105	2.4	9.2
Ti-6Al-4V-0.020Y	1038	154	1040	1110	1000	3.4	9.9
Ti-6Al-4V-0.050Y	1016	152	1025	1085	950	3.0	9.0
Ti-6Al-4V-0.10Y	1016	124	1030	1090	980	3.9	10.4
Ti-6Al-4V-0.30Y	1016	156	1045	1105	960	3.4	9.8
Ti-6Al-4V-0.010MM	1016	144	1030	1095	1040	3.3	8.2
Ti-6Al-4V-0.030MM	1016	150	1015	1055	990	3.8	9.1
Ti-6Al-4V-0.080MM	1016	153	1005	1090	1050	3.0	6.8
Ti-6Al-4V-0.10Er	1032	138	1060	1125	1000	3.7	11.0
Ti-6Al-4V-0.30Er	1016	132	1005	1075	925	3.3	10.5
Ti-6Al-4V-0.80Er (Ingot 27)	1010	135	970	1050	910	4.3	10.8
Ti-6Al-4V-0.80Er (Ingot 29)	1010	144	1000	1070	955	3.9	10.3

GP77-0480-31

TABLE A23. ROOM-TEMPERATURE TENSILE PROPERTIES OF Ti-6Al-4V-RE ALLOYS ANNEALED AT T_β + 28°C FOR 30 min

Alloy composition	Annealing temperature, T_β + 28°C (°C)	Elastic modulus (GPa)	Yield stress at 0.2% offset (MPa)	Ultimate tensile stress (MPa)	Fracture stress (MPa)	Uniform elongation (%)	Total elongation (%)
Ti-6Al-4V	1038	147	1085	1040	1110	2.2	7.2
Ti-6Al-4V-0.020Y	1038	128	1000	1055	945	4.5	11.1
Ti-6Al-4V-0.050Y	1016	165	980	1095	975	4.1	11.1
Ti-6Al-4V-0.10Y	1016	135	1030	1115	1005	4.3	11.3
Ti-6Al-4V-0.30Y	1016	168	1045	1120	960	3.9	11.1
Ti-6Al-4V-0.010MM	1016	134	1030	1090	990	3.2	8.3
Ti-6Al-4V-0.030MM	1016	146	1040	1090	1030	4.1	9.1
Ti-6Al-4V-0.080MM	1016	150	1035	1105	1055	4.3	9.9
Ti-6Al-4V-0.10Er	1032	132	1055	1115	995	3.5	9.6
Ti-6Al-4V-0.30Er	1016	135	1015	1105	960	3.5	12.0
Ti-6Al-4V-0.80Er (Ingot 27)	1010						
Ti-6Al-4V-0.80Er (Ingot 29)	1010	147	1010	1080	970	3.4	9.7

GP77-0480-32

TABLE A24. ROOM-TEMPERATURE TENSILE PROPERTIES OF Ti-6Al-4V-RE ALLOYS ANNEALED AT T_β + 28°C FOR 60 min

Alloy composition	Annealing temperature, T_β + 28°C (°C)	Elastic modulus (GPa)	Yield stress at 0.2% offset (MPa)	Ultimate tensile stress (MPa)	Fracture stress (MPa)	Uniform elongation (%)	Total elongation (%)
Ti-6Al-4V	1038	138	1070	1155	1140	1.9	3.2
Ti-6Al-4V-0.020Y	1038	150	1030	1090	1000	3.0	9.2
Ti-6Al-4V-0.050Y	1016	165	990	1090	975	4.4	11.4
Ti-6Al-4V-0.10Y	1016	158	1025	1110	1010	3.3	9.2
Ti-6Al-4V-0.30Y	1016	142	1090	1145	1020	3.6	10.6
Ti-6Al-4V-0.010MM	1016	144	1020	1080	1005	2.9	7.3
Ti-6Al-4V-0.030MM	1016	136	985	1050	995	2.1	5.3
Ti-6Al-4V-0.080MM	1016	154	1050	1110	1095	4.2	9.4
Ti-6Al-4V-0.10Er	1032	134	1045	1120	1015	3.5	9.9
Ti-6Al-4V-0.30Er	1016	130	975	1040	870	3.8	11.9
Ti-6Al-4V-0.80Er (Ingot 27)	1010	165	980	1080	930	3.8	10.2
Ti-6Al-4V 0.80Er (Ingot 29)	1010	164	1000	1095	940	4.1	11.8

GP77-0480-33

TABLE A25. ROOM-TEMPERATURE TENSILE PROPERTIES OF Ti-6Al-4V-RE ALLOYS ANNEALED AT T_β + 56°C FOR 5 min

Alloy composition	Annealing temperature, T_β + 56°C (°C)	Elastic modulus (GPa)	Yield stress at 0.2% offset (MPa)	Ultimate tensile stress (MPa)	Fracture stress (MPa)	Uniform elongation (%)	Total elongation (%)
Ti-6Al-4V	1066	130	1020	1105	990	3.8	12.1
Ti-6Al-4V-0.020Y	1066	144	1035	1090	980	4.0	10.3
Ti-6Al-4V-0.050Y	1044	154	1000	1070	930	4.5	12.3
Ti-6Al-4V-0.10Y	1044	148	1020	1090	955	3.9	12.0
Ti-6Al-4V-0.30Y	1044	148	1030	1105	965	3.4	10.2
Ti-6Al-4V-0.010MM	1044	159	970	1065	965	4.0	10.7
Ti-6Al-4V-0.030MM	1044	134	1015	1085	980	3.0	8.8
Ti-6Al-4V-0.080MM	1044	144	1020	1090	1030	3.8	8.7
Ti-6Al-4V-0.10Er	1060	149	1020	1105	970	3.7	11.2
Ti-6Al-4V-0.30Er	1044	132	955	1010	880	3.7	10.8
Ti-6Al-4V-0.80Er (Ingot 27)	1038	139	965	1055	925	4.5	10.7
Ti-6Al-4V-0.80Er (Ingot 29)	1038	158	955	1065	940	4.2	11.3

GP77-0480-34

TABLE A26. ROOM-TEMPERATURE TENSILE PROPERTIES OF Ti-6Al-4V-RE ALLOYS ANNEALED AT T_β + 56°C FOR 15 min

Alloy composition	Annealing temperature, T_β + 56°C (°C)	Elastic modulus (GPa)	Yield stress at 0.2% offset (MPa)	Ultimate tensile stress (MPa)	Fracture stress (MPa)	Uniform elongation (%)	Total elongation (%)
Ti-6Al-4V	1066	141	1090	1170	1155	2.6	5.8
Ti-6Al-4V-0.020Y	1066	158	1015	1095	1040	3.8	9.9
Ti-6Al-4V-0.050Y	1044	138	1005	1070	940	4.1	12.1
Ti-6Al-4V-0.10Y	1044	136	1005	1070	925	3.8	13.0
Ti-6Al-4V-0.30Y	1044	150	1020	1115	970	4.3	12.5
Ti-6Al-4V-0.010MM	1044	158	1005	1075	1035	3.8	8.3
Ti-6Al-4V-0.030MM	1044	150	1025	1080	1040	4.3	9.5
Ti-6Al-4V-0.080MM	1044	141	1020	1085	1050	3.7	8.3
Ti-6Al-4V-0.10Er	1060	138	1045	1105	985	3.7	10.7
Ti-6Al-4V-0.30Er	1044	138	975	1045	895	3.5	10.6
Ti-6Al-4V-0.80Er (Ingot 27)	1038						
Ti-6Al-4V-0.80Er (Ingot 29)	1038	140	1015	1085	1035	3.7	9.2

GP77-0480-35

TABLE A27. ROOM-TEMPERATURE TENSILE PROPERTIES OF Ti-6Al-4V-RE ALLOYS ANNEALED AT T_β + 56°C FOR 30 min

Alloy composition	Annealing temperature, T_β + 56°C (°C)	Elastic modulus (GPa)	Yield stress at 0.2% offset (MPa)	Ultimate tensile stress (MPa)	Fracture stress (MPa)	Uniform elongation (%)	Total elongation (%)
Ti-6Al-4V	1066	170	1090	1145	1120	3.2	7.8
Ti-6Al-4V-0.020Y	1066	170	1035	1105	1065	3.8	9.4
Ti-6Al-4V-0.050Y	1044	150	1045	1100	970	4.0	11.7
Ti-6Al-4V-0.10Y	1044	151	1015	1075	955	3.7	10.6
Ti-6Al-4V-0.30Y	1044	162	1050	1120	960	4.2	14.2
Ti-6Al-4V-0.010MM	1044	156	1010	1060	1020	3.3	8.0
Ti-6Al-4V-0.030MM	1044	129	1005	1070	1030	3.3	8.0
Ti-6Al-4V-0.080MM	1044	158	1020	1085	1055	3.9	8.6
Ti-6Al-4V-0.10Er	1060	142	1080	1150	1020	3.3	11.4
Ti-6Al-4V-0.30Er	1044	142	985	1070	930	3.5	10.2
Ti-6Al-4V-0.80Er (Ingot 27)	1038	146	960	1045	910	3.6	10.5
Ti-6Al-4V-0.80Er (Ingot 29)	1038	148	1030	1070	970	3.4	8.7

GP77-0480-36

TABLE A28. ROOM-TEMPERATURE TENSILE PROPERTIES OF Ti-6Al-4V-RE ALLOYS ANNEALED AT T_β + 56°C FOR 60 min

Alloy composition	Annealing temperature, T_β + 56°C (°C)	Elastic modulus (GPa)	Yield stress at 0.2% offset (MPa)	Ultimate tensile stress (MPa)	Fracture stress (MPa)	Uniform elongation (%)	Total elongation (%)
Ti-6Al-4V	1066	128	1105	1165	1160	2.4	4.8
Ti-6Al-4V-0.020Y	1066	150	1070	1130	1015	3.6	8.4
Ti-6Al-4V-0.050Y	1044	128	975	1050	895	3.4	12.2
Ti-6Al-4V-0.10Y	1044	142	1030	1100	975	4.0	11.5
Ti-6Al-4V-0.30Y	1044	140	1035	1100	970	2.8	8.5
Ti-6Al-4V-0.010MM	1044	147	995	1075	1020	3.0	8.8
Ti-6Al-4V-0.030MM	1044	141	1025	1070	1045	3.3	6.3
Ti-6Al-4V-0.080MM	1044	142	1000	1055	1045	3.3	6.6
Ti-6Al-4V-0.10Er	1060	143	1055	1125	1095	4.2	8.6
Ti-6Al-4V-0.30Er	1044	165	1005	1095	950	3.7	12.1
Ti-6Al-4V-0.80Er (Ingot 27)	1038	147	945	1010	875	3.1	9.6
Ti-6Al-4V-0.80Er (Ingot 29)	1038	150	1040	1110	990	3.2	9.7

GP77-0480-37

DISTRIBUTION

	Copies
Defense Documentation Center Cameron Station Alexandria, Virginia 22314	12
Office of Naval Research Department of the Navy Attn: Code 471	1
Code 102	1
Code 470	1
Commanding Officer Office of Naval Research Branch Office 495 Summer Street Boston, Massachusetts 02210	1
Commanding Officer Office of Naval Research Branch Office 536 South Clark Street Chicago, Illinois 60605	1
Office of Naval Research San Francisco Area Office 760 Market Street, Room 447 San Francisco, California 94102 Attn: Dr. P. A. Miller	1
Naval Research Laboratory Washington, D. C. 20390 Attn: Code 6000	1
Code 6100	1
Code 6300	1
Code 6400	1
Code 2627	1
Naval Air Development Center Code 302 Warminster, Pennsylvania 18974 Attn: Mr. F. S. Williams	1
Naval Air Propulsion Test Center Trenton, New Jersey 08628 Attn: Library	1
Naval Construction Batallion Civil Engineering Laboratory Port Hueneme, California 93043 Attn: Materials Division	1
Naval Electronics Laboratory Center San Diego, California 92152 Attn: Electron Materials Sciences Division	1
Naval Missile Center Materials Consultant Code 3312-1 Point Mugu, California 93041	1
Commanding Officer Naval Surface Weapons Center White Oak Laboratory Silver Spring, Maryland 20910 Attn: Library	1
David W. Taylor Naval Ship R&D Center Materials Department Annapolis, Maryland 21402	1
Naval Undersea Center San Diego, California 92132 Attn: Library	1
Naval Underwater System Center Newport, Rhode Island 02840 Attn: Library	1
Naval Weapons Center China Lake, California 93555 Attn: Library	1
Naval Postgraduate School Monterey, California 93940 Attn: Mechanical Engineering Dept.	1
Naval Air Systems Command Washington, D. C. 20360 Attn: Code 52031	1
Code 52032	1
Code 320	1

	Copies
Naval Sea System Command Washington, D. C. 20362 Attn: Code 035	1
Naval Facilities Engineering Command Alexandria, Virginia 22331 Attn: Code 03	1
Scientific Advisor Commandant of the Marine Corps Washington, D. C. 20380 Attn: Code AX	1
Naval Ship Engineering Center Department of the Navy CTR BG #2 3700 East-West Highway Prince Georges Plaza Hyattsville, Maryland 20782 Attn: Engineering Materials and Services Office, Code 6101	1
Army Research Office Box CM, Duke Station Durham, North Carolina 27706 Attn: Metallurgy & Ceramics Division	1
Army Materials and Mechanics Research Center Watertown, Massachusetts 02172 Attn: Res. Programs Office (AMXMR-P)	1
Air Force Office of Scientific Research Bldg. 410 Bolling Air Force Base Washington, D. C. 20332 Attn: Chemical Science Directorate	1
Electronics and Solid State Sciences Directorate	1
Air Force Materials Lab (LA) Wright-Patterson AFB Dayton, Ohio 45433	1
NASA Headquarters Washington, D. C. 20546 Attn: Code RRM	1
NASA Lewis Research Center 21000 Brookpark Road Cleveland, Ohio 44135 Attn: Library	1
National Bureau of Standards Washington, D. C. 20234 Attn: Metallurgy Division	1
Inorganic Materials Division	1
Defense Metals and Ceramics Information Center Battelle Memorial Institute 505 King Avenue Columbus, Ohio 43201	1
Director Ordnance Research Laboratory P.O. Box 30 State College, PA 16801	1
Director Applied Physics Laboratory University of Washington 1013 Northeast Fortieth Street Seattle, Washington 98105	1
Metals and Ceramics Division Oak Ridge National Laboratory P.O. Box X Oak Ridge, Tennessee 37380	1
Los Alamos Scientific Laboratory P.O. Box 1663 Los Alamos, New Mexico 87544 Attn: Report Librarian	1
Argonne National Laboratory Metallurgy Division P.O. Box 229 Lemont, Illinois 60439	1

	Copies
Brookhaven National Laboratory Technical Information Division Upton, Long Island New York 11973 Attn: Research Library	1
Library Building 50 Room 134 Lawrence Radiation Laboratory Berkeley, California	1
Dr. G. S. Ansell Dean of the School of Engineering Rensselaer Polytechnic Institute Troy, New York 02181	1
Professor H. K. Birnbaum University of Illinois Department of Metallurgy Urbana, IL 61801	1
Dr. E. M. Breinan United Technologies Research Center East Hartford, CT 06108	1
Professor H. D. Brody University of Pittsburgh School of Engineering Pittsburgh, PA 15213	1
Professor J. B. Cohen Northwestern University Department of Material Sciences Evanston, IL 60201	1
Professor M. Cohen Massachusetts Institute of Technology Department of Metallurgy Cambridge, MA 02139	1
Professor B. C. Giessen Northeastern University Department of Chemistry Boston, MA 02115	1
Dr. G. T. Hahn Battelle Memorial Institute Department of Metallurgy 505 King Avenue Columbus, OH 43201	1
Dr. David G. Howden Battelle Memorial Institute Columbus Laboratories 505 King Avenue Columbus, OH 43201	1
Professor C. E. Jackson Ohio State University Dept. of Welding Engineering 190 West 19th Avenue Columbus, OH 43210	1
Dr. L. A. Johnson General Electric Company P.O. Box 8 Corporate Research and Development Schnectady, NY 12301	1
Professor D. A. Koss Michigan Technological University College of Engineering Houghton, MI 49931	1
Professor A. Lawley Drexel University Dept. of Metallurgical Engineering Philadelphia, PA 19104	1
Dr. H. Margolin Polytechnic Institute of New York 333 Jay Street Brooklyn, NY 11201	1
Professor K. Masubuchi Massachusetts Institute of Technology Department of Ocean Engineering Cambridge, MA 02139	1
Dr. H. I. McHenry National Bureau of Standards Institute for Basic Standards Boulder, CO 80302	1
Professor J. W. Morris, Jr. University of California College of Engineering Berkeley, CA 94720	1

	Copies
Professor Ono University of California Materials Department Los Angeles, CA 90024	1
Dr. M. Pakstys General Dynamics Electric Boat Division Eastern Point Road Groton, CT 06340	1
Dr. Neil E. Paton Rockwell International Science Center 1049 Camino Dos Rios P.O. Box 1085 Thousand Oaks, CA 91360	1
Mr. A. Pollack David Taylor Naval Ship Research and Development Center Annapolis, MD 21402	1
Dr. Karl M. Prewo United Technologies Laboratories United Technologies Corporation East Hartford, CT 06108	1
Professor W. F. Savage Rensselaer Polytechnic Institute School of Engineering Troy, NY 12181	1
Dr. C. Shaw Rockwell International Science Center 1049 Camino Dos Rios P.O. Box 1085 Thousand Oaks, CA 91360	1
Professor O. D. Sherby Stanford University Materials Sciences Division Stanford, CA 94300	1
Dr. E. A. Starke, Jr. Georgia Institute of Technology School of Chemical Engineering Atlanta, GA 30332	1
Professor David Turnbull Harvard University Division of Engineering and Applied Physics Cambridge, MA 02139	1
Dr. F. E. Wawner University of Virginia School of Engineering and Applied Science Charlottesville, VA 22901	1
Dr. Charles R. Whitsett McDonnell Douglas Research Laboratories McDonnell Douglas Corporation Saint Louis, MO 63166	1
Dr. J. C. Williams Carnegie-Mellon University Department of Metallurgy and Materials Sciences Schenley Park Pittsburgh, PA 15213	1
Professor H. G. F. Wilsdorf University of Virginia Charlottesville, VA 22903	1
Dr. M. A. Wright University of Tennessee Space Institute Tullahoma, TN 37388	1
Mr. Larry Clark Bldg. 653/Room 325 Air Force Materials Laboratory Wright-Patterson AFB, OH 45433	1
Mr. C. S. Kortovich Section Manager Materials Research Department TRW Inc. 23555 Euclid Avenue Cleveland, OH 44117	1
Professor M. E. Paulaitis Department of Chemical Engineering University of Delaware Newark, Delaware 19711	1